On the role of pigment-pigment and pigment-protein interaction in regulating excitation energy and electron transfer in photosynthesis

Vorgelegt von
MSc
Albert Collins Nganou Assonkeng
aus Kamerun

Vor der Fakultät II – Mathematik und Naturwissenschaften
der Technischen Universität Berlin
zur Erlangung des akademischen Grades
Doktor der Naturwissenschaften
Dr. rer. nat.
Genehmigte Dissertation

Promotionsausschuss

Vorsitzender:	Prof. Dr. Mario Dähne
Berichter:	Prof. Dr. H. J. Eichler
Berichter:	PD Dr. Martin Mkandawire
Berichter:	Prof. Dr. habil. Ulrike Woggon
Berichter:	Prof. Dr. Rienk van Grondelle

Tag der wissenschaftlichen Aussprache: 19.12.2011

Berlin 2012
D 83

Acknowledgments

This thesis with the title "**On the role of pigment-pigment and pigment-protein interaction in regulating excitation energy and electron transfer in photosynthesis"** is based on studies conducted between 22 October 2008 and 2 June 2011 at the Institute of Optics and Atomic Physics in the Berlin University of Technology (TU Berlin). This work and my precedent study on DNA conductance and CNT have been supported by the DAAD.

I would like to express my sincere gratitude to all the people who contributed in different ways to the success of this work. Here, I would like to state only a few because they are so numberours: Firstly, I am indebted to Prof. Hans Joachim Eichler, who gave me the opportunity to conduct the research in the field of cyanobacteria in his laboratory. Despite the working conditions which were far below the expectation of a PhD candidate, this work would not have been possible without this opportunity. Secondly, I thank Prof. Renger who contributed to the architecture of the proposal.

A special acknowledgement is addressed to H. Lokstein, Schmilinsky, Sabine Kussin, Monika Weß, Liron David, Prof:s Noam Adir, Martin Mkandawire, Heiko Lokstein and Rienk Van Grondelle for sample preparations as well as rich and constructive discussions on the topic. Thanks go to Prof. Pieper for inviting me to University of Tartu through the Dora Program as well as Avri Freiberg. I do not forget Cris (your help with the spectrometer was very helpful), Prof. Woggon and all the members of our group. Thanks to Nicolai Grosse for his strong interest and proof reading of the manuscript.

I am greatly indebted to the Dean of our faculty, Prof. Thomsen. Without his strong engagement in favour of morality and ethic in science, this work would have probably not been published. I believe all students of the faculty II shall be proud to have him as Dean.

Further I would like to express my gratitude to Prof. Pouhè for wise advice. I wish also to thank my colleagues who have supported me, especially Dr. Margus Rästep, Moritz Grehn and Franz

Joseph Schmit for their patience during my training on different laser systems. Finally, I wish to say thanks to my family and friends.

Finally, this work is entirely my origin. I have made every effort where possible to provide timely and accurate details in the content as well as acknowledge any information borrowed from other works. Nevertheless, mistakes may occur and I assume entirely responsibility.

Dedication

I would like to dedicate this work to my loving parents for their unconditional support, wishes, fortitude, understanding, help and guidance in every walk of life.

Abstract

The pathways of excitation energy transfer (EET) to photosynthetic reaction centres inside phycobiliprotein antenna system of *Acaryochloris Marina* (*A. marina*) were studied using time resolved absorption difference spectroscopy with a resolution time of 200 fs. The results revealed a new pathway of 14 ps inside the phycocyanin spectral band in addition to the previously known EET-equilibration pathway of all phycocyanins to allophycocyanin. This EET funnelling is faster than the previous kinetic found in phycobilisomes of 17 ps inside the phycocyanin (spectral range 600-630 nm) to allophycocyanin (640-650 nm). In addition, we present the result that excitonic coupling does not contribute to the EET inside the phycobiliprotein antenna system at room temperature. Anisotropy of the EET pathway was calculated to determine the contribution of excitonic coupling, which originated from the strong interaction between adjacent chromophores. This band is located between 624 nm to the final emitter 675 nm.

In order to compare the results with those of the cyanobacterium containing phycobilisome and to address the functional role of the linker protein, further femtosecond flash induced transient absorption changes were monitored. This was done to obtain a time-resolved view of the excitation energy transfer in intact phycobilisomes of *Thermosynechococcus vulcanus* (*T. vulcanus*) having different linker proteins at room temperature. Ultrafast excitation energy transfer in phycobilisomes occurs along the phycocyanin rod shaped domain to the allophycocyanin core domain in two channels (i.e. 890 fs and 17 ps). The phycocyanin is assembly in the form of a rod of two PC hexamers separated by a distinct linker protein along the symmetry axis of the hexameric units, and an additional rod–core linker. In comparison to the absorbance of the phycobiliprotein antenna system of *A. marina*, the presence of the rod-core linker induces a 5 nm red shift on the rod spectrum. The kinetic component of 890 fs indicates that the presence of the linker proteins induces ultrafast EET inside the phycobilisome (PBS). Thus, we suggest that the PBP rod structure (with APC in the rod involving less pigment) of *A. marina* is not the reason of the ultrafast EET in comparison to the phycobilisomes. Furthermore, the absorbance of the phycocyanin rod (PC rod) sub-domain of phycobilisomes and PBP indicate

that the high-energy sub-aggregate state of the PBP is likely to be influenced by different conformations.

Further comparative study at low temperature by spectral hole burning (SHB) and fluorescence narrowing (FLN) revealed the existence of the inhomogeneous broadened distribution of local vibrational mode along the PBP antenna system of *A. marina*. In addition to the inhomogeneous broadened distribution of pure electronic frequencies in the spectra of the PBP antenna system, the presence of a blue shifted delocalized satellite hole along the rod is originated from different vibrations.

The low amount of local vibrational frequencies in the PBS *T. vulcanus* leads to a high strength of pigment coupling which enhanced the ultrafast energy transfer. Thus, it is a coupling with the downhill energy transfer of the upper state towards a lower state. Additional information through FLN and SHB reveal the existence of new pigment absorbing at 635 nm in the PBP rod and 645 nm in the PBS as well as some similarity and difference on the terminal emitter spectral band. The similarity leads to an identification of two different pigments absorbing between 660 – 665 nm and 670 nm. The 660 – 665 nm pigment is an allophycocyanin (APC) pigments indentified by a 40 cm^{-1} energy gap between α_{84} and β_{84}, while the difference between the first vibrational mode and the red shift of wing supports the suggestion of a different APC gene. Due to the wavelength of the latter, it might be the apcB of the L_{CM}. A further difference leads to excitonic contribution on the all-spectral band of the PBS *T. vulcanus* instead of the 624 nm to the final emitter 675 nm in the PBP of it case.

In addition to the excitation energy transfer in cyanobacteria, time resolved absorption changes in the light harvesting complex II of higher plants (LHC II) were monitored. Aggregation state size was controlled by specific ß-DM concentration. The equilibrium time in each aggregation state was complemented by findings from the literature. Some information sources are listed as follows:

- The aggregation state was observed where dependence of the relative maximum of the absorption state in time domain.
- No significant change in the excited states was observed

Further femto-second transient absorption spectroscopy at room temperature (RT) was applied to investigate the charge transfer process. This was done by photo-exciting ligand chlorine dendrone (PaCD) in different concentrated solutions of oxidant horse heart cytochrome c (Hccox) at 620 nm. After the HccoxPaCD was photo-excited, a delayed-bleach recovery signal at 550 nm was observed. This was due to the charge transfer from the excited state of the donor ligand PaCD to the acceptor state within about 30 ps. In the longer wavelength region above 620 nm, an excited state absorption signal originating from the PaCD was observed while a flash induced transient absorption signal was also observed at 667 nm. This was due to the excitation energy transfer (EET) produced from the 620 nm excitation to the 667 nm. The latter was followed by a red shift bleaching at 667 nm. The detailed analysis of the red shift bleaching at 667 nm indicates the quenching of excess EET originating from the ligand excited state band.

TABLE OF CONTENTS

Tables

Figures

Acronyms and Abbreviations

A. marina	*Acaryachloris marina*
T. vulcanus	*Thermosynechococcus vulcanus*
BBO	beta barium borate
E	First order electric-field
EE	Second order electric-field
EEE	Third order electric-field
EET	Excitation energy transfer
ET	Electron transfer
HOMO	Highest energy occupied molecular orbital
LHC II	Light harvesting complex II
LUMO	Lowest unoccupied molecular orbital
$NADP^+$	Nicotinamide adenine dinucleotide phosphate
NADPH	Nicotinamide adenine dinucleotide phosphate-oxidase
OPA	Optical parametric amplifier
PSI	Photosystem I
PSII	Photosystem II
RC	Reaction centre

1 Introduction

The mechanism of converting light energy into chemical energy and storing the absorbed energy in form of sugar is a complex process optimized by life on Earth billions of years ago. Detailed understanding of this process is of fundamental importance to developing new technologies that mimic photosynthetic organisms. Although the fundamental principles of photosynthesis are known, there are many open questions concerning the specifics of photochemical processes occurring between light absorption and sugar creation. Furthermore, mechanisms that control and regulate photosynthetic processes are not fully understood.

The primary process of photosynthesis takes place in biochemical nanomachines, which are called photosystems. Photosystems of higher plants and cyanobacteria are divided into photosystem I and II (Chen, 2005; Govindjee, 2001; Witt, 2004). These nanomachines are found in the thylakoid membrane located in chloroplasts in higher plants. Here, light driven photosynthetic reaction centres are embedded in the thylakoid membrane. In addition, photosystem I (PS I) and photosystem II (PS II) contain light harvesting antenna systems. A schematic view of the component parts of photosystem II is summarised in figure 1.1. Details regarding PSII in higher plants are found in the given references.

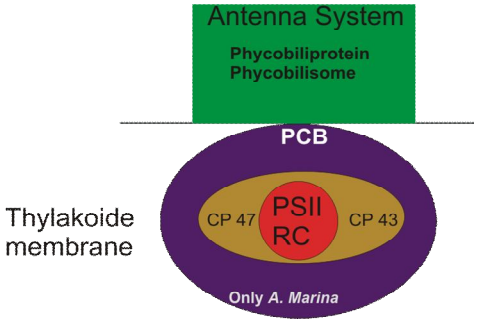

Figure 1.1 Model of the organization of the Photosystem II in some cyanobacteria: antenna system and reaction centre (RC), while CP47 and CP43 are found in all photosynthetic organisms. The membrane intrinsic PCB antenna is found in *A. marina* only.

1.1 Background and problem setting

Proteins that form PS II and antenna systems bind several types of chromophores like chlorophylls, carotenoids and phycocyanobilin. These pigment molecules are specifically arranged and stationed in pigment protein complexes having a typical size of several ten kDa. The main function of most pigments in the antennae is to absorb and transfer light energy to specific chlorophyll pairs in the reaction centres (RC) of the photosystems. In these reaction centres, charge separation and the primary electron transfer steps take place. PS I and II are functionally connected in line by a linear electron chain that enables the reduction of NADP+ to NADPH and ADP to ATP. The connection between these photosystems PS I and PS II, and reaction centre functions are not in the scope of this work, which focuses on excited state energy transfer (EET) in the PSII antenna complexes.

In addition to their highly optimized light harvesting function, pigment protein complexes have important regulatory functions i.e. they adapt the photosynthetic apparatus to variable light conditions and prevent the organism from photo-damage. Spectral and functional properties of pigments bound to the protein matrix have been suggested to depend on different parameters (Renger, 1999):

i The chemical nature of the pigment;

ii The strength of the pigment-pigment coupling (electronic- coupling); and

iii The mode of pigment-protein interaction (electron-vibration coupling).

In principle, two types of coupling can be distinguished: EET and electron transfer (ET). The first process takes place mainly in photosynthetic antennae; the second is preferably found in the RC but is also of interest in antenna systems in cases of closely separated pigments. Depending on the strength of pigment-pigment interaction (which mainly depends on the inter-pigment distance, the mutual orientation and the nature of the intervening medium), different EET-mechanisms exist. The experimental methods have to be suitable for the analysis of the given strength of electronic and electron-vibrational coupling of interacting molecules.

In a fundamental approach, Fermi's Golden rule (May, 2005) can be used to describe the EET dynamics.

In case of long distances between the coupled pigments, the transfer can be described with the Förster dipole-dipole interaction mechanism. Förster-resonance energy transfer (FRET) describes the EET mechanisms in the limiting case of weak coupling (May, 2005). Here the electronic structure of the participating pigments remains virtually unaffected by the interaction, and the excited states are localized on one of the pigments. Then, the excitation is transferred from the donor (D) to the acceptor (A) pigment via an incoherent hopping type process. This occurs when the centre-to-centre distance between the pigments are larger than the pigment dimension (Renger, 1992). Förster EET originates from Coulomb interaction of the dipole moments without exchange of electrons between the interacting pigments.

When the distance between neighbouring pigments is less than 10 Å, excitonic interactions can occur due to strong coupling between closely spaced pigments. The wave functions of donor and acceptor orbits overlap and form a common molecule orbit that can be described as a linear combination of the locally excited states. As a result, excitation energy is delocalised over the two pigments. This can be considered as one super molecule due to the overlap (dimer). This interaction leads to a splitting of the energy levels in contrast to non-interacting molecules. The extended exciton splitting and oscillator strength of the transition depends on the distance between the pigments, the oscillator strength of transition of isolated monomers and the mutual orientation of the dipole moments within the dimer (Tetenkin, 2003).

Whereas the above excitonic coupling distance is verified in case of chlorophyll in the antenna complexes, it has been shown to fail in case of strong excitonic coupling between bilichromophores α_{84} and β_{84} (MacColl, 2004). Thus, the strength of the dipole moment between these chromophores in allophycocyanin induced the formation of delocalised exciton along them.

In the case of a short distance between the pigments, the interaction can be described by the Dexter exchange mechanism. Electron exchange between donor and acceptor occurs due to overlap of electronic wave functions at close distance. When the donor is in an electronically excited state, an unpaired electron is in the so-called LUMO-state (Lowest unoccupied molecule orbital). This electron is transferred to the LUMO of the acceptor pigment and simultaneously an electron of opposite spin from the HOMO (Highest occupied molecule orbital) of the acceptor is transmitted to the HOMO of the donor. The net result is the same as for the Förster type EET, but the process is quite different. In the Dexter case, the transfer rate decays exponentially with the donor-acceptor distance (Dexter, 1953) and the energy

transfer is therefore a very fast process at close pigment separations. In addition, Dexter transfer can also occur between triplet states, which are not allowed in FRET because the electron is generally excited in the singlet state only.

If more than two pigment molecules are present within a pigment protein complex and involved in the dynamics, investigations of the energy transfer become very difficult. The reason for that is that a different simultaneous EET processes are spectrally close, and in addition, aggregates of strongly coupled pigments can be formed (Scholes, 2001).

From this brief introduction, it is obvious that detailed description and understanding of optical properties, EET processes that occur in pigment-protein complexes containing numerous pigments, and charge transfer in artificial photosynthetic process is highly complex and challenging.

1.2 Aims of the study

The main aim of the study reported in this thesis was the investigation of the pigment coupling in the PBP antenna system of *A. marina* and the PBS antenna system of *Thermosynechococcus vulcanus*. In particular, to determine whether the so called linker protein really contributes to the tuning of the EET in the outer antenna system; as well as to determine if there are yet more energy channelling pathways in *A. marina* that may have not been discovered and therefore elucidate the mechanism and process involved. Another aim of this work was to investigate EET in light harvesting complex two (LHC II) of higher plants where the question of EET dependence on the aggregate size will be addressed, as well as the photo-protection mechanisms.

These aims are based on the following background. To harvest light in the spectral range where the absorption of chlorophyll is low, *T. vulcanus* and *A. marina* use different architectures of a special phycobiliprotein as outer antenna system located on the thylakoid membrane (Adir, 2005; Adir et al., 2001; Chen et al., 2009; Chen et al., 2010; Schliep et al., 2010). The biliprotein antenna system of *T. vulcanus* is organized as phycobilisome (PBS). The PBS consists of core substructures and peripheral rods that are arranged in hemidiscoidal fashion around that core. The core of most hemidiscoidal phycobilisomes is composed of three cylindrical subassemblies (Adir, 2005). However, other morphological types of PBS, like those composed of hemiellipsoidal, bundle-shaped, and bloc-shaped, can also be found in

cyanobacteria (Wehrmeyer, 1983a). The biliprotein antenna systems of A. *marina* are organized as single rod-shaped structures of phycobiliprotein (PBP) (Chen, 2009; Hu, 1999).

Recently, the assembly of the PBS rod domains has been shown to consist of a stack of two PC hexamers embedded by linker $L_R^{8,6}$, L_R, L_{RC} (David, 2011).

In *A. marina* PBP rod, the presence of the structural linker polypeptide has not yet been clearly demonstrated. Reported kinetic components in the PBS as well as the rod PBP of *A. marina* have been obtained from fractions of PBS where the linkers were absent, thus resulting in a slow lifetime component. In the present work, the PBS samples from *T. vulcanus* which were used contain different linkers as shown by David (David, 2011). The linker, especially the L_R in the axis of symmetry might change the coupling between β_{84} phycocyanobilin chromophores in adjacent hexamers. The L_{RC}, which connects the rod hexamer of phycocyanobilin (PC) to the trimeric assembly disc of allophycocyanin (APC), might induce different coupling pathways between PC and APC.

Thus, questions arise as to whether these linkers really contribute to the tuning of the EET in the outer antenna system, by changing the coupling between chromophores in adjacent sub-compounds.

Additional question arise when comparing the EET between the PBP rod antenna system of *A. marina* and the PBS of other cyanobacteria. For instance, is the EET kinetic of 3 ps from PC to APC found in PBP of the *A. marina* by (Theiss et al., 2011; Theiss et al., 2008) the fastest PC to APC that can exist in the cyanobacteria?

- Is the 3 ps component a specific phenomenon in *A. marina* due to the adaptation of A. marina to its living habitat?
- It is reported in chapter 3 of this thesis, that in a buffer with low ionic strength (a) the 3 ps component is disrupted, (b) the 14 ps component amplitude diminishes and (c) its minimum is located on the β_{84} maximum absorption in PC. Which pathway does the EET use in that case?
- Can another pathway exist in addition to the 3 ps component found in the PBP in buffer with high ionic strength?

MacColl (MacColl, 2004) suggests an excitonic coupling of the chromophores β84 and α84 in APC. He also discusses the redshift observed in the absorbance of APC from 620 nm to 650 nm. This coupling between chromophores β_{84} and $\alpha_8$4 has been shown by Edington (Edington, 1995) to contribute in energy transfer in APC. The same coupling can be found in PC between the same chromophores. Can the coupling between β84 and α84 in PC contribute to EET via an excitonic delocalisation as shown in APC? This latter question remains an open issue in the rod of all PBS. Finally, this work reports a new insight into artificial photosynthesis based on the donor acceptor model Chlorine Dendron – horse hearth cytochrome c (Hcc).

1.3 Study approach

The approach used in the study reported in this thesis has cross-disciplinarily approach. It involved application of advanced physics principles to understand physicochemical processes in a biological system. Thus, laboratory studies involving *ex vivo* studies were used to unveil intrinsic process of photosynthesis that makes most cyanobacteria to be one of most efficient phototropic organism. Light harvesting nanomachines of the cyanobacteria are extracted and investigated using the femtosecond transient absorption technique, where a fraction of the pigments inside the sample is promoted to an excited state by a pump beam in femtosecond range. Then, the absorption changes are absorbed at different wavelengths by probing the sample with a probe beam at specific wavelengths. The probe beam has an adjustable delay (fs to ns) with respect to the pump beam. The polarisation of the excitation beam is set to 54.7°, while for anisotropy measurement the excitation beam is set to parallel as well as perpendicular with respect to the probe beam. Specific methods and procedure are listed in each chapter.

1.4 Thesis outline

This thesis is presented in seven stand-alone chapter, where each chapter reports a completed study. This first chapter introduce the research question, and outlines the objectives of the study, which followed by providing the outlines of this document. The second chapter reports the procedure and techniques involved in the construction of the instrument instrumentation and setup of two-colour pump probe technique used in the study. The third chapter deals with the new EET pathway in the PBP of *A. marina*. The fourth chapter reports a comparative

study between the PBP antenna system of *A. marina* and the PBS of *Thermosynechoccus vulcanus*. Here, special emphasis is devoted to the functional role of the linker polypeptide in tuning the excitation energy transfer (EET). Chapter five deals with EET in LHC II, by analyzing the aggregate state size dependence in EET. Chapter 6 is devoted to mimicking an artificial photosynthetic system and a general conclusion is reported in chapter 7.

2 Femtosecond laser system and pump-probe

In this chapter, the central equipment used in the study is detailed from its theoretical principle of functioning to the set up of specific experiments.

2.1 Theoretical background

Electromagnetic waves can be described by a time and space dependent electric field. This light is described in the framework of linear optics (Midwinter, 1973) when the light-matter interaction drives the properties of the matter that do not depend on the intensity of light. Thus, the interaction of light and matter can be characterized by a set of parameters, which depend only on the nature of the medium such as index of refraction, the absorption and reflection coefficients and the orientation of the medium with respect to light polarization. In fact, absorption and reflection can be calculated from the complex index of refraction. This linear optical approach fails if the interaction of short-pulses with high peak powers is described. In this case, the optical parameters become functions of the intensity of the impinging light (Diels, 2006). The intensity dependence of the material response is usually described by nonlinear optics, according to the polynomial expansion of the macroscopic polarization of a medium when it is illuminated with an electric field (E).

In our experiment the 800 nm output of a femtosecond laser is converted to the visible spectral range by an optical parametric amplifier (OPA). To achieve the generation of such pulses we use a commercial system, the *spectra physics* Tsunami, for femtosecond pulse generation and the Spitfire for its amplification. simplified overview of the system is presented in figure 2.1. Further details on the topic can be obtained from Diels (2006) and Shen (Shen, 1984).

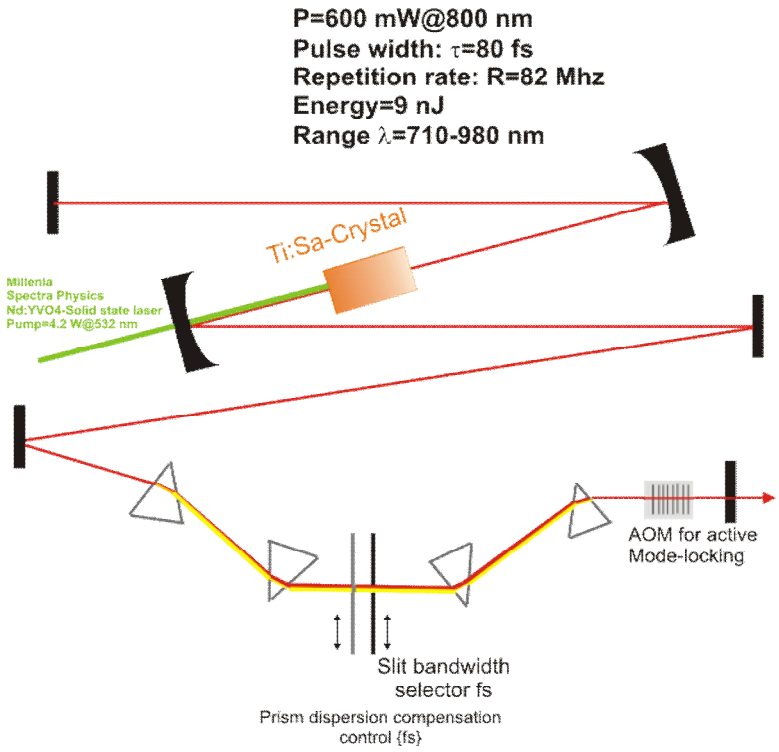

Figure 2.1: Tsunami resonator

Figure 2.1 shows the nonlinear crystal pumped by the solid-state laser Nd:YVO4 at 532 nm. The emission pulse passes many times inside the resonator where the self-mode locking is established at 800 nm. The dispersion of the group velocity induced by the multipass through the resonator is compensated by four prisms. At the position of the slit, the prism has dispersed the beam into different wavelengths therefore the wavelength can be selected by moving the slit. The pulse is therefore directed to the amplifier for amplification where it is chirped as described in figure 2.2.

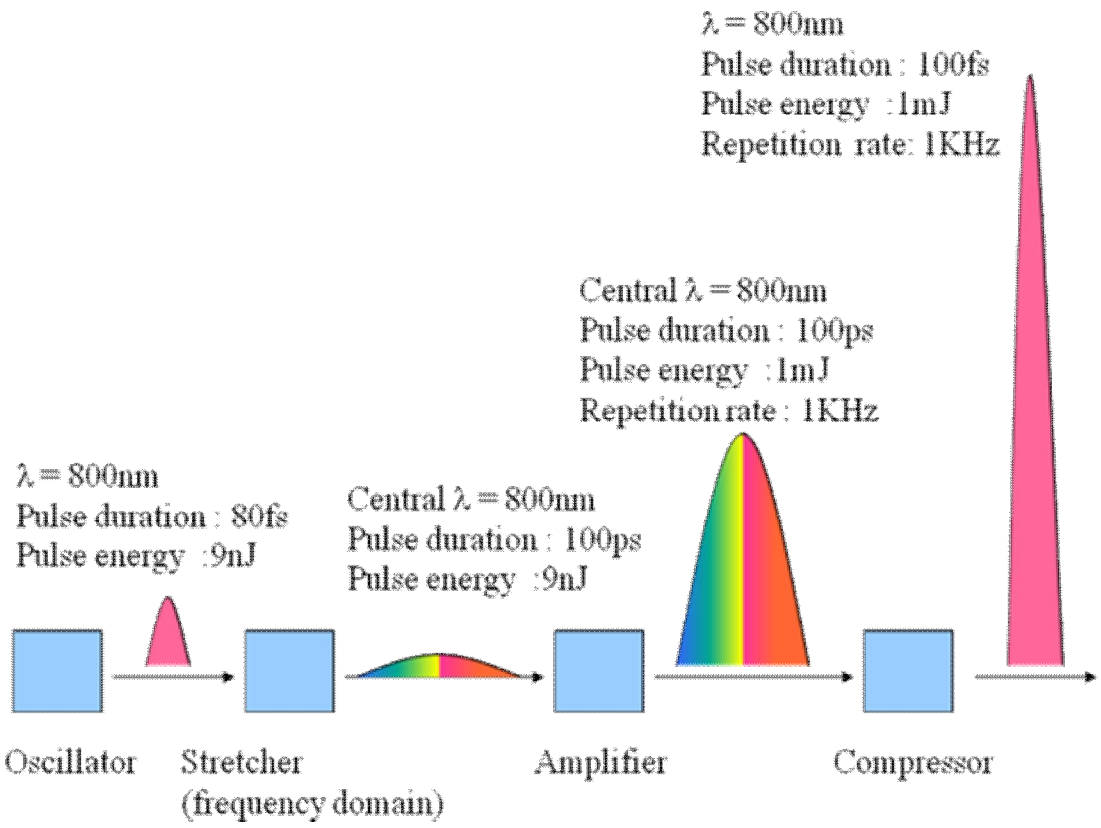

Figure 2.2: Chirped pulse amplification to avoid damage of optical components

The amplification process of the chirped pulse is the main role of the *spitfire*. Firstly an energy conserving stretch of the pulse duration is performed. The gathered high-energy pulse from the oscillator is compressed afterwards as figure 2.2 shows.

The pulse is chirped to avoid damage to optical components when the amplification occurs in the Spitfire laser system as shown in Fig 2.3. There are two main factors, that can affect chirped pulse amplification of fs pulses, described in the spectra physic manual and (Jovanovic, 2010): the overall band pass of the system, and the spectral phase aberrations that interfere with the production of Fourier transform-limited pulses. The band pass of the optical system can be limited by the spatial size of optical components within the stretcher and compressor, as well as spectral limiting components in the regenerative amplifier. Because of the multi-pass nature of the amplifier, small variations in spectral transmission can result in significant spectral modulations in the amplified pulse.

The spectral phase of ultra short optical pulses is typically described by considering a power series expansion of the frequency dependent phase (Rullière, 2003). In this case, the quadratic

term in the phase is primarily responsible for the stretching and compressing of the pulse. The residual cubic and quadratic phase terms (and higher order terms) limit the temporal fidelity of the recompressed pulse.

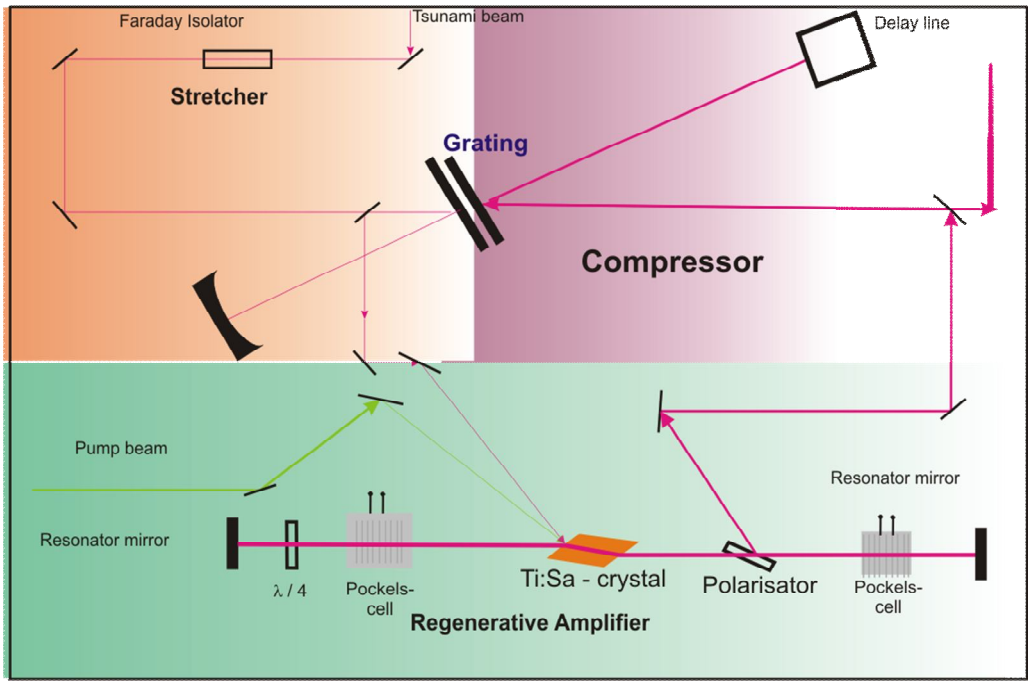

Figure 2.3: Spitfire operating system. Output λ = 800 nm; pulse duration < 200 fs; pulse energy = 1 mJ

Figure 2.3 displays a beam pathway for the amplification process inside the *Spitfire* laser system. The Faraday isolator is used to avoid sending a pulse back to the Tsunami. The stretcher stretches the pulse in time before it is directed to the resonator for amplification. After amplification, the pulse is recompressed. In the perfectly matched system, each term in the phase expansion of the compressor has the same magnitude but opposite sign of the stretcher. There is generally some higher order phase error introduced by imaging aberrations in the optics of the stretcher.

Most stretcher designs perform fairly well as long as material dispersion is not introduced. When material, such as the Ti:Sa amplifier, is introduced between the stretcher and compressor as we can see in the spitfire design, the phase of the stretched pulse is modified by the inherent dispersion of the various materials. This includes a significant quadratic phase term as well as some cubic phase. In order to produce a short pulse, the compressor must now be adjusted to compensate for the phase of the stretcher plus the phase of the material.

These usually only results in some percent change in the length of the compressor. The problem comes from the fact that lengthening the compressor does not compensate for the higher order phase terms of the material. The high-energy output pulse of the spitfire is used to pump the optical parametric amplifier (OPA) (see figure 2.4) below for short pulse generation in the visible spectral range in our case.

2.2 Optical parametric amplification

Optical parametric amplification is a special case of difference-frequency generation. It well know that in difference-frequency generation the photon with the highest frequency is split into two photons with lower frequencies, where the energy taken away from the highest energy pulse beam is converts into the two beams of lower frequency. This process is used as an amplifier. A weak signal is made to interact with a strong one (high frequency pump beam), and the obtained result of this interaction is the difference frequency known as the idler. Consequently, the original signal is amplified. If the idler and the signal are passed through the missing crystal again within the proper phase, both are again amplified. (Nelet, 2007).

The 800 nm output from spitfire is first split in two parts, where the first 4% is directed to a sapphire plate for the white light generation, which will be the seed for the first stage amplification in the 3 mm BBO crystal. The second part is split in two parts where the first 10 % will be incident in time and space with the seed in the BBO crystal, signal and idler and pump are phase matched. With the help of a filter, the short wavelength is removed and the weak idler is returned to the same BBO with the rest of the 800 nm pump for the amplification process.

One photon with angular frequency w_2 is destroyed while two photons are created. One of the new photons has the signal frequency $w_1=w_{(n1+1)}$ and the other has the new frequency $w_3=w_{(n3+1)}$, such that $w_2=w_1+w_3$ (Rullière, 2003). This process leads to an increase in the signal photon flux and therefore the amplification of the signal beam. The OPA system can be tuned in wavelength, by rotating the orientation of the nonlinear crystal and thereby changing the phase-matching condition.

After signal amplification, the residual 800 nm is trapped-off to be used to drive for white light generation in the custom-built pump–probe setup. The infrared signal is therefore

submitted to second harmonic generation to convert the infrared signal to the visible spectral range by passing through two successive slim BBO crystals, linearly positioned.

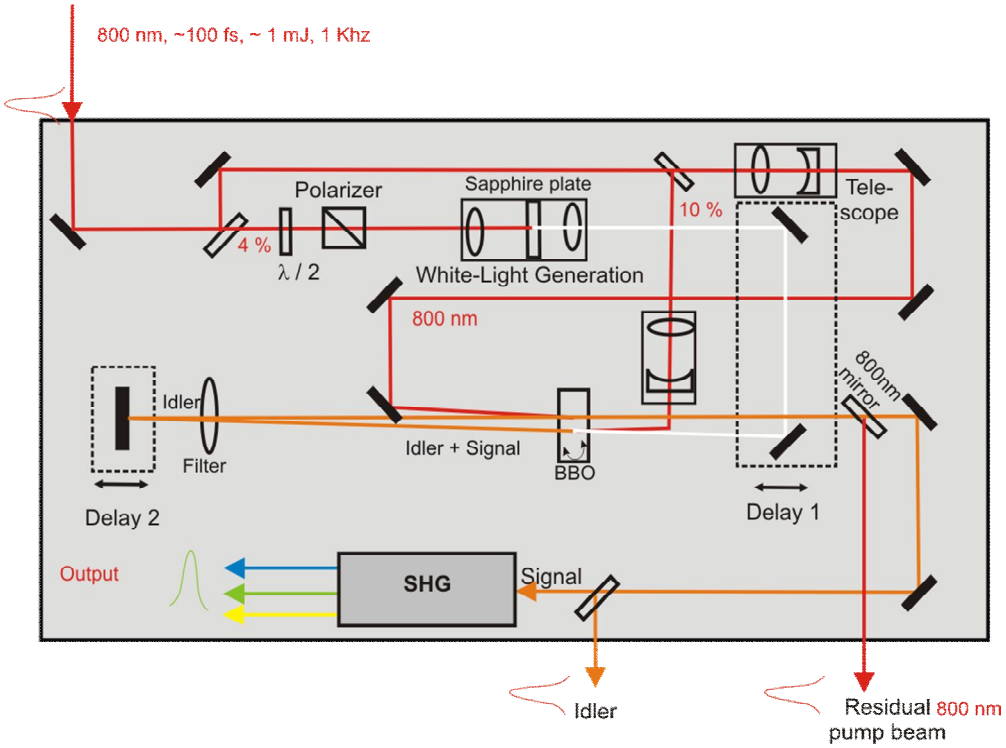

Figure 2.4: Optical parametric amplification system[1] (Theiss, 2006)

2.3 Pump-probe experiment

The pump-probe and fluorescence techniques are the most widely used of ultrafast spectroscopic tools. In this section, we will focus on pump-probe. It requires two synchronized laser pulses of duration shorter than the dynamic event being studied and of the appropriate wavelength. The general principle common to all types of pump-probe technique is schematically shown in (figure 2.5). The sample initially in equilibrium is optically excited into unoccupied states with a higher energy laser pulse, called the pump. Once excited, the sample relaxes back to the equilibrium states with the characteristic relaxation time according to the pigment in the sample. A probe pulse with variable time-delay with respect to the

[1] A principle of OPA is well described in The Principles of Nonlinear Optics. Book from Y.R. Shen, or in Prof. Webber lecture notes at the Technical University Berlin ..., the German description can be obtained in Theiss thesis 2006.

pump pulse monitors the absorption changes in the relaxing system. Photons gated by the probe pulse reflect the actual state of the system at the time of the probe pulse arrival. By scanning the time delay τbetween pump and probe pulses one, can monitors ultrafast events occurring in the relaxation dynamics of the system, even with a slow detector.

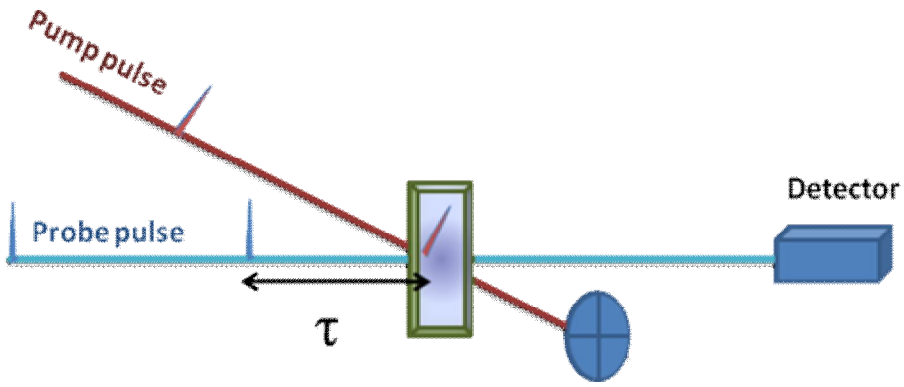

Figure 2.5: General scheme of pump - probe technique

Let us assume that the relaxation of the system back to the equilibrium is described by the function ψ(t) after the excitation with the delta-like pump pulse δ(t). The actual response of the system Θ(t) is described by the following convolution with the pump pulse's temporal intensity profile F_{pump}(t)(Lobo, 2002; Weiner,1995):

$$\Theta(t) = \psi(t) \times F_{pump}(t) = \int_{-\infty}^{+\infty} \psi(x).F_{pump}(t-x)dx \tag{2.3}$$

The measured signal m(t) gated by the time delayed probe pulse with the temporal intensity profile F_{pump}(t) can be written as convolution in the form (Lobo, 2002; Weiner,1995):

$$m(t) = \Theta(t) \times F_{probe}(t) = \int_{-\infty}^{+\infty} \Theta(x).F_{probe}(t-x)dx \tag{2.5}$$

Let us assume that pump and probe intensity pulse profiles are delta-like functions. Therefore, the measured signal m(t) equals the relaxation function of the system ψ(t). It means that we measure the relaxation of the system without any influence of pumping and probing pulses. The other limiting case is when the relaxation function of the system ψ(t) is a delta-like function. The measured signal m(t) now equals a cross-correlation of the pump and

probe pulses. This case allows one to monitor the cross-correlation signal when the pump duration is considerably larger than relaxation time of the system.

To avoid the sample being influenced by the probe pulse, one measures the photons directly gated with the time delayed probe pulse under the assumption that the intensity of the probe pulse is smaller than that of the pump pulse. Experimentally the following observables can be monitored:

- Absorption, transmission, reflection, diffraction, polarization of the probe pulse photons.
- Nonlinear effects like second harmonic generation (SHG) of the probe photons.
- fluorescence photons gated with the probe photon
- photocurrent due to photo-excited electrons by the probe pulse photons
- Photoelectrons emitted by the probe pulse photons

In the experimental setup, after re-compression of the regenerative amplifier output, transform limited pulses of 1 mJ energy and 100 fs duration are obtained. The main portion of the beam is used to pump a collinear optical parametric amplifier (OPA) to generate excitation pulses for the experiments in the visible spectral range. In this way, femtosecond pulses of 130 fs FWHM between 400 nm and 2500 nm and energies of some ten micro joules with a repetition rate of 1 kHz can be achieved. The spectrum of the pump pulses was centred at a desired wavelength according to the maximum absorption of the pigment. The probe beam was obtained by generating a white light by focusing a residual 800 nm from the OPA inside a 1 cm optical path length flow cell, which contains D_2O. The white light was directed to a single grating pulse shaper analogous to that described by (Weiner, 2000)[2] where a 15 nm bandwidth of a specific wavelength of the white was send out in the focal plane of the pulse shaper. The pulse shaper had a time resolution around 200 fs. The probe pulse can reach 15 nJ per pulse.

[2] More detailed characterization of the pump-probe set is well described by Weiner (2009) in his book ultrafast optic.

The probe and pump beams were superimposed in the sample at an angle of 5°. In two colours pump-probe setup, the collection of data $\Delta A(\lambda,\tau)$ allows us to follow the kinetic trace for each wavelength. For a better overview of the kinetic trace, another stage of data analysis called decay associated spectra (DAS) can be used. Here, all the recorded trace signals for each wavelength are globally fitted by a multi-exponential decay function. The obtained kinetics expresses the decay of the relaxation process inside the system. The relative polarization of the beams is set to the ideal angle of 54.7° to avoid unwanted misleading kinetics in the transient spectra caused by depolarization effects in the sample between the arrivals of pump and probe pulse. The transmitted probe beam and another 10 % of the probe beam that was trapped off prior to the sample acted as a reference beam, which was directed, to two matched silicon photodiodes. Using a variable attenuator, the intensity of both beams illuminating the photodiodes was set to identical values when the pump beam was blocked. The monitoring of the pump induced changes in the transmission of the sample. This was made possible by synchronously chopping the pump and probe beam at different frequencies with a mechanical chopper, which was phase-locked to the SR 510 Lock–in amplifier. The translation stage of 1 ns and the Lock–in amplifier were controlled by a computer for data acquisition.

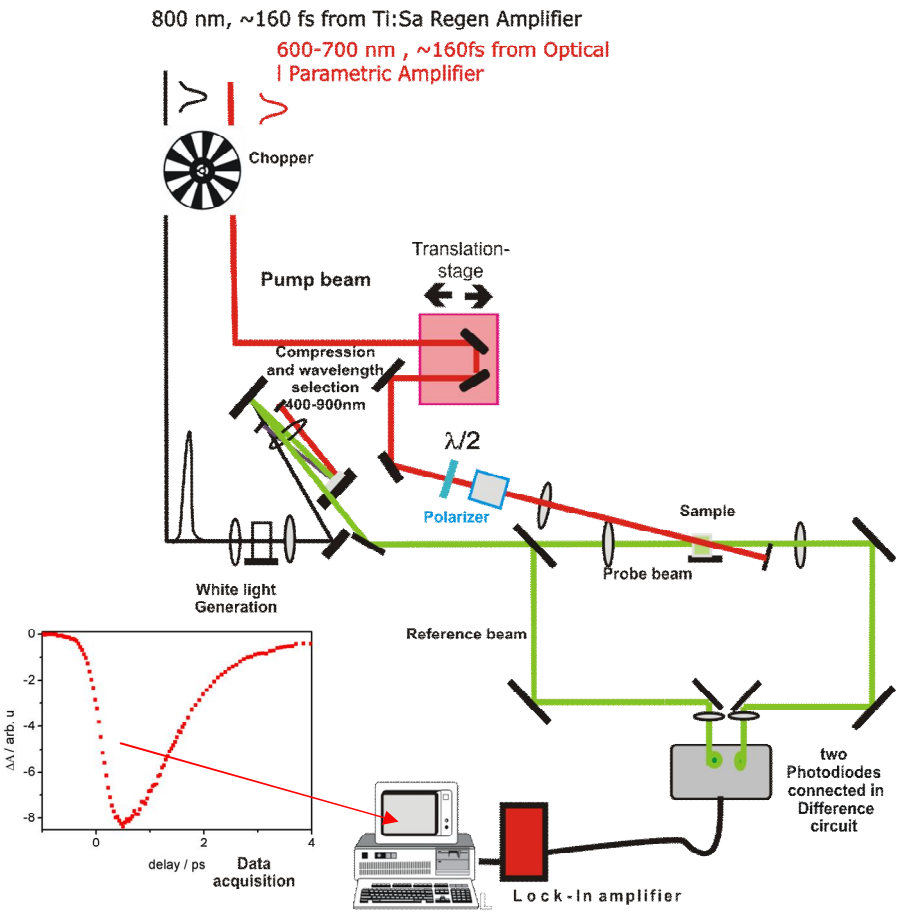

Figure 2.6 Two colour pump–probe setup[3]

[3] The setup was improved with the help of Alexander Achstein and Moritz Grehn, I am very grateful for that.

3 Excitation energy transfer in PBP antenna system of *Acaryochloris marina*

In phototrophic organisms, sunlight is absorbed by the light harvesting complexes containing pigments such as chlorophyll, carotenoids and phycocyanobiliprotein (PBP). The generated excited states are then funnelled by excitation energy transfer (EET) to the photosynthetic reaction centres (RCs) where they induce charge separation followed by secondary electron transfer. The latter leads to oxidation of water, and the formation of the energy rich compounds ATP and NADPH, which are used in the Calvin Cycle to synthesize organic compounds.

3.1 Introduction

Changes in ecosystems have forced some phototrophic organisms to develop efficient light harvesting mechanisms and adapt to certain light conditions. One is the cyanobacterium Acaryochloris marina (*A. marina*) which has chlorophyll d (*Chl d*) as dominant photosynthetic pigment (Miyashita, 1996). All known oxygenic photosynthetic organism except *A. marina* and the new cyanobacterium containing chlorophyll (*Chl f)* (Chen, 2010) contain *Chl a* in the core complexes antenna system RC of photosystem II (PSII) and photosystem I (PSI). Thus, *Chl a* was assumed to be the primary electron donor in the reaction centre of PSII which provides a high redox potential for the water splitting reaction. The *Chl d* in methanol has a Q_y band at 697 nm, which is red-shifted by 32 nm from the *Chl* a Q_y band at 665 nm (Larkum, 2005). In whole cells of *A. marina*, it is observed at around 714-718 nm (Miyashita, 1996). This allows *A. marina* to utilize the red light above 700 nm and to live in environments where the intensity of light is drastically reduced due to absorption by other organisms containing *Chl a* as the major photosynthetic pigment. However it has been shown by Akiyama that *A. marina* also contains low amount of *Chl a* (Akiyama, 2001) depending on the growth condition. The dominant Chl d exhibits a lower redox potential than *Chl a*. Thus, the adaptation of *A. marina* to different ecosystems emphasizes the question of the pigment organization and the mechanism, which might govern the EET in this organism.

To harvest light in the spectral range where the absorption of chlorophyll is low, *A. marina* uses a special phycobiliprotein as an outer antenna system (Hu, 1999). This PBP is located on

the *thylakoid* membrane, where it has been suggested to be structurally composed of four stacked hexameric discs (Hu, 1999). Three of the hexamers contain only phycocyanin (PC), while the fourth is a hetero-hexamer containing PC and allophycocyanin (APC) (see figure 3.1). The hexamer and heterohexamer are structurally organized by an assembly of two trimers through a C_3 symmetry (Adir, 2005).

In comparison to *A. marina*, the phycobilisomes (PBS) of other cyanobacteria are assembled in a different form. One of them is the hemidiscoidal organisation as a six rod-shaped form, which is connected to the APC core complex by a linker rod - core (see figure 3.1). Each rod-shaped structure is a stack of PC hexamers. Depending on the growth condition, they can also contain phycoerythrin (MacColl, 1998). The structural arrangement is such that the lowest energy aggregate state is located at the bottom of the stack for a downhill EET. Therefore, the APC is situated closest to the thylakoid membrane. Then the linker connects the APC to the thylakoid membrane. The PBS is connected to the thylakoid membrane through two linker proteins containing an APC compound: the apcE and apcB, which are the terminal emitters. However, the functional role and the pigment composition of the linker membrane connecting the PBP rod of *A. marina* to the thylakoid membrane remains an open issue (Hu, 1999). Another question related to difference between *A. marina* and common cyanobacteria containing *Chl a* is the presence of prochlorophyte Chl binding (PCB) protein complex, which binds *Chl d* and is structurally analogous to CP43 and enhances the efficiency of light collection (Chen, 2005). This PCB light harvesting complex is commonly found in cyanobacteria lacking phycobiliproteins (Post, 1994). How does this PCB influence the EET in the photosynthesis RC?

The main absorption bands of the PBS and PBP aggregates are listed in table 3.1. This comparison between PBS and PBP does not contain the PE, which has its absorption maximum at 560-575 nm. Table 3.1 reveals that the hexameric PC aggregates have almost the same maximum inside PBS and PBP while the APC aggregate is 10 nm blue-shifted in PBP of *A. marina* in comparison to the PBS antenna system. The second contrast with PBS is the absence of the linker protein information in the PBP data present in the literature (MacColl, 1998).

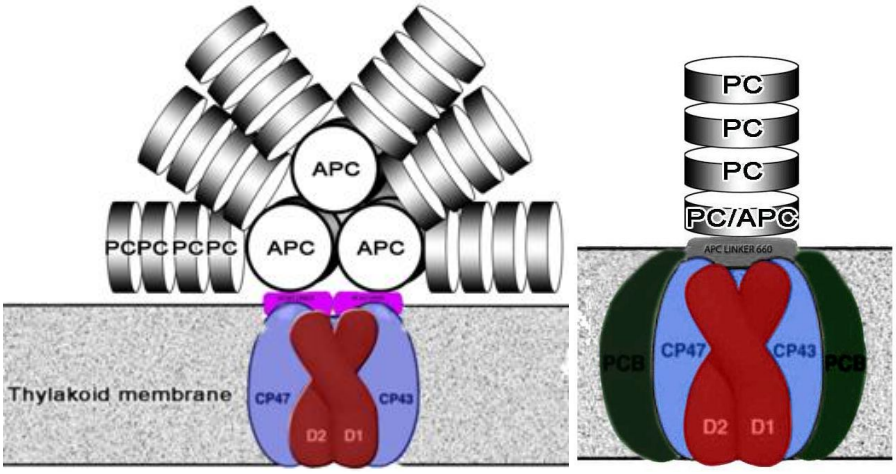

Figure 3.1: Conceptual model of (a) tricylindrical hemidiscoidal phycobilisome antenna system revealing the two bottom cylinders attached to the thylakoid membrane, and the third APC cylinder located on top of the two; and (b) rod shaped PBP antenna system of *A. marina* composed of four hexameric discs where three are homohexamers of PC and the bottom one (PC/APC) is an heterohexamer composed of a PC trimer and an APC trimer. The APC is the bottom of the heterohexamer disc where the rod antenna is attached to the thylakoid membrane through a linker membrane. The PCB is portrayed around the CP47, CP43 and D1/D2 in RC (Zouni, 2001; Chen, 2005; MacColl, 1998; Theiss, 2011).

Inside the assembly of trimeric structure of PC and APC, each monomeric sub-unit is composed of an α and β polypeptide chain, which binds a so-called bilin or phycocyanobilin. Each polypeptide (PC and APC) has a tetrapyrrole chromophore chemically bound to the cysteine position 84. In addition, PC has a β tetrapyrrole chromophore chemically bound to the cysteine position 155 (MacColl, 1998). The absorption of the PC chromophore β_{155} is located around 600 – 602 nm while the one for α84 is located around 624 nm, not far away from β84 which is located at around 626 – 628 nm (Debreczeny, 1993). At room temperature, the monomeric PC (β_{155}, β_{84}, α_{84}) has an absorption maximum at 617 nm while the mutant PC (β_{84}, α_{84}) and PC (β_{84}) are respectively at 625 nm and 630 nm. Consequently, the chromophore $\beta_{84,}$ which is closed to the C_3 symmetry axis (Adir, 2005; Debreczeny, 1993) may absorb at the low energy level of PC. In view of the above similarities and differences, this chapter reports investigations using a time resolved absorption change at room temperature with a resolution time of 200 fs, and anisotropy calculations from the data obtained by polarisation measurements on the PBP of *A. marina*. The results show amongst other things, the existence of a new pathway for excitation energy transfer inside the PBP antenna system of *A. marina*. These experiments were motivated by several questions related

to the existence of an additional EET pathway in the PC spectral band as well as the contribution of excitonic coupling; the ultrafast red-shift in time resolved multicolour pump-probe absorption of difference spectra inside the PBP antenna system of *A. marina* (Theiss, 2008), and the suggestion of its occurrence through the inter-exciton state relaxation (Edington, 1995).

Table 3. 1 Comparison of the maxima absorption of the phycobilins chromophores between phycobilisome aggregate and the PBP antenna system of *A. marina* the question mark denotes unknown absorption bands of certain sub-aggregates

Aggregate States	**Chromophores**	**Absorbance Maximum (nm) PBS**	**Sub-aggregate States**	**absorbance Maximum (nm) *(A. marina)***
CPC	$\alpha_{84}\beta_{84}\beta_{155}$	616	monomer	?
CPC	$(\alpha_{84}\beta_{84}\beta_{155})_3$	-	trimer	614[1]
CPC	$(\alpha_{84}\beta_{84}\beta_{155})_6$	-	hexamer	614 – 618[1]
APC	$\alpha_{84}\beta_{84}$	615[3]	monomer	?
APC	$(\alpha_{84}\beta_{84})_3$	650[3]	trimer	640[1]
CPC	α_{84}	624[2]	monomer	?
CPC	β_{84}	628[2]	monomer	?
CPC	β_{155}	600[2]	monomer	?
APCE	α, β	660[4]	-	?
APCB	α, β	670[5]	-	?

1. (Hu, 1999)
2. (Debreczeny, 1993)
3. (Andrei, 1994)
4. (Zhao, 2004)
5. (Lundell, 1981)

3.2 Spectral properties of intact and disrupted PBP antenna systems

An extremely interesting aspect of the cyanobacteria research is the observation of the EET kinetic component dependent on the surrounding medium. There were a variety of early key contributions in such studies. Gantt (Gantt, 1979) observed the dissociation of the PBS due to drastically reduced amounts of phosphate inside the buffer which affected the ionic strength which influenced the PBS stability. This was mainly observed for the compounds, which are functional at a lower energy level in the PBS.

Studies of chromophore coupling by Holzwarth (Holzwarth, 1987) showed that with increasing amounts of phosphate in the buffer, the aggregation state of the PBP monomers or trimers changed to a higher proportion of hexameric structures. Therefore, the PBP of A. marina without of a phosphate buffer should be affected in terms of its assembly. The comparison of kinetics between the PBP antenna complexes of *A. marina* with phosphate and depleted phosphate inside the buffer will help us to get more insight into the kinetics of the efficient EET in the antenna system.

We will assume the "PBP antenna complexes of *A. marina* in buffer with phosphate" to be intact (due to the high ionic strength) and those without phosphate inside the buffer to be disrupted (due to the low ionic strength). The following questions will be addressed:

(a) Can the reduced ionic strength lead to the disruption of the fast kinetic component instead of the appearance of the slower kinetic component, when the EET from PC to APC occurs?

(b) Which model can best describe the intact and the disrupted antenna system?

To answer these questions, I performed a comparative study of the absorbance, time resolved absorption change and decay associated spectra from the absorption changes between intact and disrupted PBP antenna system of the cyanobacterium *A. marina*.

3.3 Absorbance of the intact, disrupted PBP antenna complex of *A. marina* and the Phycobilisome antenna complex of Thermosynechococcus elongates

Prior to the current work, the fastest energy transfer kinetics observed in *Thermosynechoccus elongates* was 17 ps inside PC. Consequently, we compared the absorbance in the PBP antenna complex of *A. marina* with the phycobilisomes of *Thermosynechoccus elongatus*. Figure 3.2 (a) presents the normalized absorbance spectra of the isolated Phycobilisome (PBS) of Thermosynechoccus elongatus and the PBP antenna system of *A. marina* in different buffers at room temperature. The PBS exhibit a difference profile at short spectral range which is likely due to the presence of phycoerythrin (MacColl, 1998), and perhaps to the protein conformation change, because different conformations of the protein exist at this spectral range that might influence the absorption shape independently to the temperature. There were also differences in the APC absorption wavelength, which may have been induced by the presence of more APC and linker core membrane in the PBS when compared to the rod PBP antenna system of *A. marina*. A pronounced difference appears in the short spectral range where the disrupted antenna exhibits a broader spectrum, which could be attributed to the reduction in size of the antenna system in absence of the phosphate in buffer. The broadening can be explained due to the dissociation into aggregate pieces (Gantt, 1979; Sarcina, 2001). The latter case is also the cause of the slight difference observed in the red-shifted spectral range where the linker APC membrane is present (see chapter 4). The second derivative spectrum (right side) gives a comparison between the intact antenna absorption of *A. marina* and the PBS antenna of *T. elongatus*. A 10 nm red shift of the APC aggregate states in the rod is observed. In PBS, the absence of the shoulders may be due to its low amount during the isolation of the PBS. The existence of this linker membrane in the PBS has been discussed by (Lundell, 1981; Zhao, 2004) (see Chapter 4 for details). The second derivative of the absorbance maximum of the PBP antenna shows that the PC absorption maximum is around 618 nm and APC absorption maximum is at 640 nm (Hu, 1999). The absorption of the Linker APC membrane is discussed in Chapter 4. Intriguingly, both samples, the PBS of elongatus and the PBP of *A. marina* exhibit a minimum in the 2nd derivative absorption spectrum at 570 nm, which is not yet clearly assigned. Because the gene of phycoerythrocyanin with an absorption in this spectral has not been found in *A. marina*.

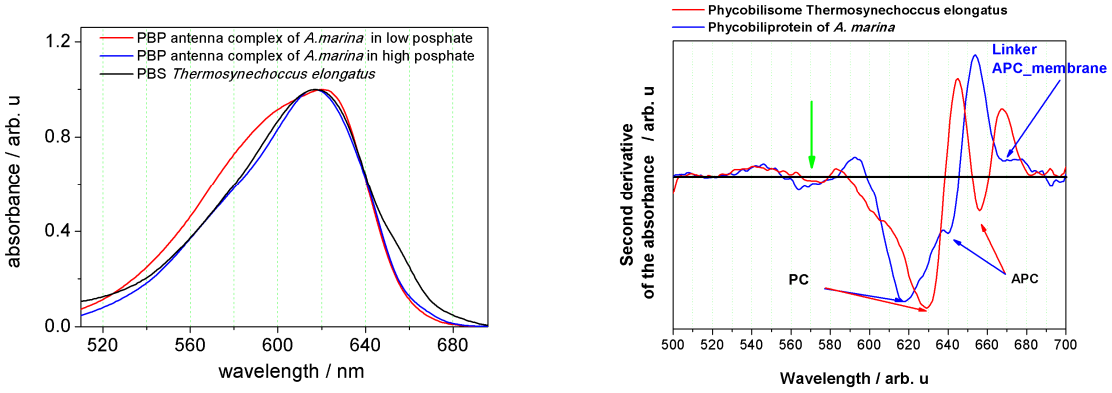

Figure 3.2: (a) Comparison of absorption spectra of the Phycobilisome of *Thermosynechocus elongatus* (black line), PBP antenna system of *A. marina* in high ionic strength (blue line) and depleted phosphate in buffer (red line) obtained at RT; and (b) Second derivative of the absorption spectrum at RT of the PBS antenna system of *Thermosynechocus elongatus* and the PBP antenna system of *A. marina* in phosphate buffer.

3.4 Femtosecond Time-resolved absorption changes of the intact antenna system of *A. marina*

In order to measure the EET in the PBP antenna system of *A. marina*, the samples were excited at 618 nm and time resolved absorption changes monitored at different probe wavelengths. The results are presented in figure 3.3. Bleaching occurs immediately during the excitation because of the ground state depletion. This is observed on the spectra by a fast bleaching (see 625 nm and 640 nm) and absorption rise (see 660 nm). This rising kinetic, due to the excitation, is followed by the recovery kinetic. Although not displayed here, the bleaching was observed in all of the PC spectral range, where the selected evolution of the 625 nm is presented. The bleaching of the spectrum at 640 nm spectral band is two times the one observed at 625 nm. Because the APC absorbs between 640 nm and 645 nm, this might be due to the energy transfer from PC at 625 nm to APC at 640 nm. The 660 nm component of the absorption change exhibits first a very fast rise; afterwards a delay in bleaching appears (figure 3.3). All the lower energy aggregates between 660-675 nm show a delayed bleaching of some other pigments as discussed in Chapter 4. Since the vibration of regular APC is shown to be different from that of the pigment absorbing resonantly at 660 nm (figure 4.10, Chapter 4), we suggest that the delayed bleaching is due to the energy transfer of different

sub-compounds at high energy level. While the rise absorption at 660 nm is mainly due to the excited state absorption of PC (ESA).

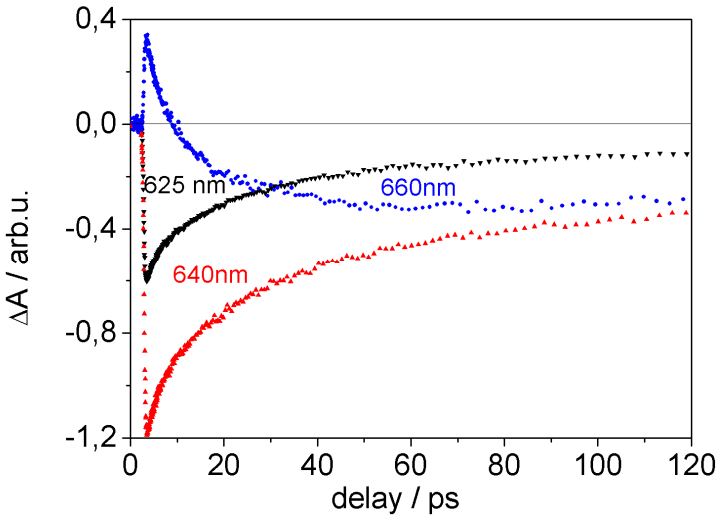

Figure 3.3: Photo-induced absorption change of three selected wavelength of the PBP antenna system of *A. marina* in the buffer containing phosphate after excitation at 618 nm. The absorption peaks at 625 nm, 640 nm and 660 nm represent the aggregate states of PC, APC and an unknown pigment absorbing at 660 nm (that we infer to be the linker APC). The PBP rod contains 73 bilin chromophores, and the PC contains 63 chromophores. Pulse energy 30 nJ.

3.5 Femtosecond Time-resolved Absorption Changes of the disrupted antenna system of *A. marina*

Figure 3.4 shows the time resolved absorption trace for the disrupted PBP antenna complex of *A. marina* after excitation at 618 nm. The changes of the absorption spectra were monitored at the same time scale as for the intact PBP for comparative purpose of the excited state lifetime. The observed bleaching assignment in the intact antenna at 625 nm of the PC and 640 nm of the APC is present in disrupted PBP. The bleaching at 640 nm in the intact PBP is due to an energy transfer from PC to APC. This latter effect remains within the disrupted PBP. However, the recovery kinetic slope of the PC and APC in comparison to that of the intact system presents a difference. A slower kinetic takes place instead of the fast slope observed in figure 3.3. Whereas the kinetics are affected, the energy is still at least partially funnelled to the APC after excitation at 618 nm. Further difference on the absorption

trace of the disrupted PBP in comparison to that of the intact PBP is the disappearance of the delayed bleaching.

The latter was observed in intact PBP by the absence of a negative course in the 660 nm spectrum. One probable explanation for the disruption of the energy transfer to the 660 nm pigment of the linker membrane is that the absence of phosphate has decreased the ionic strength that ensures the stability of the antenna system. It might be possible that the linker membrane either changed its spectral position where an overlap of the spectrum might occur with the donor, or that it is simply dissociated. According to the protein cofactors and all the manifold present in our system, the cause can be divers.

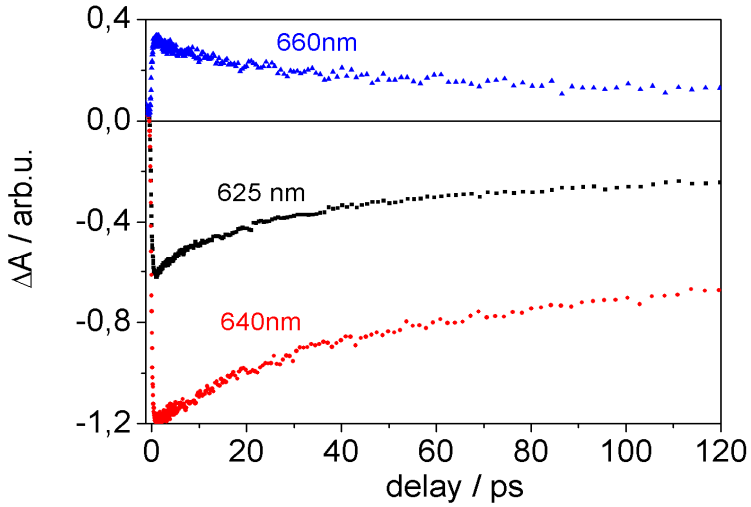

Figure 3.4: Photo-induced absorption changes of three selected wavelengths of the PBP antenna system of *A. marina* inside the buffer depleted of phosphate after excitation at 618 nm. The absorption peaks at 625 nm, 640 nm and 660 nm represent the aggregate states of PC, APC and the ESA of the PC, respectively.

To get more insight into the kinetic components of the intact and the disrupted antenna, we present the decay associated spectra (DAS) of the absorption changes, which were recorded at 10 nm intervals as a function of probe wavelength (see 3.5).

3.6 The decay associated spectra (DAS)

In order to obtain the kinetic components of the intact and the disrupted antenna system, the DAS were plotted for three lifetimes. For the PC, APC and 660 nm spectral ranges, spectral

properties of each of the amplitude lifetime components is shown for the intact and disrupted antenna system as DAS.

The DAS consists of a global analysis of the spectral dynamic of the excited states lifetime components found inside the sample in which a clear visualization of the system is obtained. When the wavelength-dependent form of the amplitude of each time constant rises from negative to positive, it can be interpreted as energy transfer, provided that the wavelength for zero crossing in the amplitude coincides with an absorbing pigment state as shown here below.

For each lifetime, we observe the evolution of the amplitude as a function of wavelength. The following results of global fit were performed by using a multi-exponential decay model:

$$\Delta A(\tau,\lambda) = \sum_{i=1}^{n} a_i(\lambda) e^{-\left(\frac{\tau}{\tau_i}\right)} \qquad (3.1)$$

The kinetics at different wavelength intervals were fitted together with the common values of the lifetime's τ_i as a linked parameter, and the wavelength dependent amplitude factor $a_i(\lambda_i)$ was set as a non-linked parameter. The best fit was obtained with three components with lifetimes τ_1 =3 ps, τ_2 =14 ps and τ_3 >200 ps (up to the resolution time of 1 ns). The obtained spectra show the evolution of the excited state lifetime, and open the pathway of the possible model which fit with the involved EET (Von Stokkum, 2004; Theiss, 2011), for review of the DAS. The figure 3.5 (a) shows the evolution of three lifetime components found inside the intact antenna.

(a) (b)

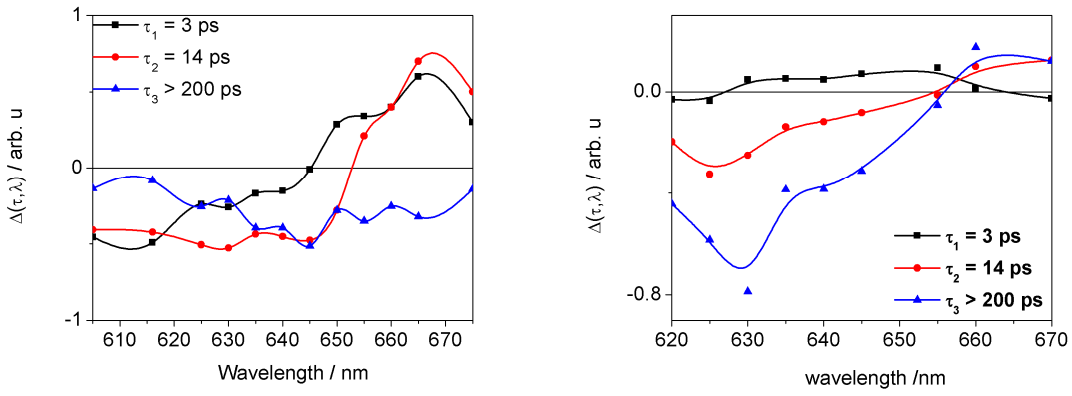

Figure 3.5: (a) Decay associated spectra (DAS) of photo-induced absorption change of the PBP antenna system of *A. marina* in phosphate buffer after excitation at 618 nm. The kinetic amplitude course is shown with 3 ps, 14 ps and a component more than 200 ps; and (b) DAS of photo-induced absorption change of the PBP antenna system of *A. marina* in buffer without phosphate after excitation at 618 nm. The kinetic amplitude course shows the disappearance of the 3 ps component, the reduced 14 ps component and the component more than 200 ps with pronounced minimum at 630 nm of the PC band.

The 3 ps component exhibits a negative spectrum in the interval range of 605-643 nm and a positive spectrum from 643 nm to 675 nm. The negative spectrum range of the 3 ps exhibits a minimum around 618 nm, which reflects the decay of excited state of PC. The positive spectrum range of the 3 ps on the figure 3.5 (a) might have the following different causes: It can be described as mainly coming from a decay of the excited state absorption (ESA) of PC, due to the decay of the ESA within 3 ps (Theiss, 2011). While between 643 nm and 655 nm, the amplitude has been suggested to be due to an increasing relative ground state bleaching of APC (Theiss, 2011) due to the EET from PC to APC. Because APC absorbs resonantly between 640 nm and 645 nm, a fraction of the excited population in PC might transfer the energy to APC in 3 ps. This explains the zero amplitude of the 3 ps between 640 nm and 645 nm.

The 3 ps kinetic component is shorter than the EET from the PC containing rods to the APC-core inside the PBS antenna system of typical cyanobacteria, which has been reported to occur within 17-18 ps (Sandström, 1988; Theiss, 2011; Zhang, 1997).

The 14 ps component in figure 3.5 (a) shows a negative spectrum range between 605-653 nm and a positive spectrum above 653 nm. It also exhibits a broad local minimum between 618-640 nm, where PC and APC have the maximum absorption. The positive spectrum shows higher amplitude than the 3 ps component and it exhibits a maximum at 670 nm. This increase in amplitude can, by analogy of the positive spectrum of 3 ps component between 643–655 nm, be attributed as increase ground state bleaching of the linker membrane around 660–670 nm due to EET from PC/APC to the linker. The characteristic of the 14 ps amplitude with a value of zero between 653 nm and 657 nm, where the linker membrane pigments absorb, may be due to energy transfer of different fractions of the excited state originated from PC and APC. By analogy to the terminal emitters in the phycobilisomes of other cyanobacteria (Lundell, 1983; Mimuro, 1986), we have suggested that the 660-675 nm

pigment could be a linker polypeptide containing different pigments (see Chapter 4) that connected the antenna rod PBP of the cyanobacterium *A. marina* to the thylakoid membrane (figure 3.2) and contributed to efficient energy transfer to Chl d (Petrasek, 2005). The same analogy leads to the 14 ps component found in the APC with linker AP_{665} of the PBS from the *Mastigocladus laminosus* by Holzwarth (Holzwarth, 1990), which raises the question of the particular structural assembly of the *A. marina* antenna system to PSII: how can the pigment in the linker membrane be assembled?

Due to the isolated antenna system used in this measurement, the EET to the PS II is interrupted. This will therefore lead to a long time scale decay of the excited state of the linker membrane. This lifetime exhibits a completely broad negative evolution in all spectral ranges and it is shown in figure 3.5 (a) as τ_3>200 ps.

The results presented in figure 3.5 (b) also show the evolution of three lifetime components found inside the disrupted antenna. The 3 ps, 14 ps and a kinetic component more than 200 ps are found.

The component of the 3 ps exhibits fluctuating amplitude close to zero. Therefore, it is likely to statistically average to zero. We suggest that the 3 ps component vanishes in buffer with low ionic strength.

The 14 ps component in the figure 3.5 (b) displays a negative spectrum from 620 nm to 653 nm and its spectrum is positive above 653 nm. It also exhibits a local minimum around 625 nm, which is near the absorption maximum of the PC, especially the phycobili chromophore α_{84}. Additional observation shows reduced amplitude of the 14 ps kinetic. The latter reduction in amplitude is pronounced in the APC regime around 640 nm. The above finding is an indication that the 14 ps kinetic is also an intrinsic part of the PC lifetime excited states. This 14 ps component can be the EET from PC to the terminal emitter linker membrane.

Finally, the evolution of the 14 ps kinetic component inside the disrupted antenna can support the conclusion that the excitation energy is not equilibrated between the entire PC hexamers and the main part of the APC inside the hetero-hexamer PC/APC within 14 ps. However, there is a fraction of excitation energy, which is directly transferred from PC to a residual linker that might be present. This finding is in line with the components of lifetime found inside CPC and APC in early reports, which had variations in the interval range of 10 – 18 ps (Gillbro, 1985; Zhang, 1997).

The τ_3>200 ps component exhibits a negative shape in the spectral range between 620 nm and 653 nm. The slight positive amplitude above 653 nm might also be attributed to zero as a disruption of the 3 ps. The minimum amplitude is located at 630 nm in the PC spectral range. Especially on the phycocyanobili chromophore β_{84} (figure 3.5 (b)). This may be the excited state lifetime of the PC. It has been found in other cyanobacteria to be in the ns range (Holzwarth, 1987); (Sandström, 1988). However, given the second minimum at 645 nm, it is likely that the APC state contribute to the long lifetime. Could this be the lifetime of the hetero-hexamer? How can we know that the 14 ps is due to an energy transfer to a residual linker? Because no delay in bleaching has been detected in the transient absorption spectra, and the slight positive evolution (over increasing wavelength) of the 14 ps component can either be supported by a residual linker absorbing at nearby location or to the APC.

We can conclude from our results, that the low ionic strength of the surrounding medium has strongly modified the electronic states of pigments in the whole antenna system. Because of this modification, a fraction of the PBP compound may remain in the linker membrane. However, further studies on the last hetero-hexamer are necessary to understand better the mechanism of these 14 ps components.

3.7 The anisotropy assignment

For estimating the coupling between pigments with strong spectral overlap as well as energy transfer between these pigments, polarisation measurements are performed. For more detail see (Lakowicz, 2006). The following non-deconvoluted anisotropy decay was measured and calculated from the direct trace of the absorption changes inside the intact and disrupted PBP antenna system of *A. marina*. Absorption changes were monitored separately with the polarization of the pump beam set parallel ($\Delta A||$) and perpendicular ($\Delta A\perp$) with respect to the polarised probe beam. In all the cases tested, the sum $\Delta A|| + 2*\Delta A\perp$ was found to be indistinguishable from that obtained with isotropic monitoring (with the pump beam polarization set at the optimum angle, 54.7°, with respect to that of the probe beam. The measurement is not shown). A λ/2- retarder at the pump laser wavelength was employed to modulate the pump beam plane of polarization from parallel to perpendicular with respect to the parallel polarization of the probe beam. The anisotropy was calculated using the following function:

$$r(\tau) = \frac{\Delta A\| - \Delta A_{\perp}}{\Delta A\| + 2\Delta A_{\perp}} \qquad (2)$$

The kinetics of the depolarization were fitted with a multi-exponential decay model:

$$A(\tau) = \sum_{i=1}^{n} a_i(\tau_i) e^{\left(-\frac{\tau}{\tau_i}\right)} \qquad (3)$$

The values of the depolarization time τ_i and the amplitude factor $a_i(\tau_i)$ were taken to be a free parameter. Three components with the depolarization time constant of $\tau 1$= 280 - 500 fs, $\tau 2$= 10 – 14 ps and $\tau 3$>200 ps were obtained (see figure 3.6; 3.7; 3.8; 3.9).

3.7 Absorption changes and anisotropy after excitation and probe at 618 nm of the intact antenna complex of *A. marina*

Figure 3.6 (a) presents results of the photo-induced absorption changes inside the intact antenna after parallel excitation and perpendicular excitation at 618 nm. In figure 3.6 (b) the anisotropy decay is displayed according to equation 2 with the maximum value at 0.38 (r(0)). This measured anisotropy value which is close to the theoretical maximum of 0.4 (Lakowicz, 2006) indicates that no saturation effect takes place at the employed excitation energies. That means there is no excitonic delocalisation over all the excited pigments. In the case of saturation effects as described, by Edington (1995) and MacColl (2004), the anisotropy value would be located between 0.5 - 0.7, and as a consequence the exciton would be delocalised along the pigments far from the highest absorption state of PC. Based on the available anisotropy data presented here, excitonic delocalisation over the PC pigments far from the PC low state does not occur. It means that only a small fraction of the ground state molecules is excited by each pulse. Three components of the depolarization have been identified as 450 fs, 10 ps and a kinetic of more than 200 ps kinetic. The 450 fs kinetic might be the kinetic induced by a strongly excitonic relaxation of the dipole moment of the excitonically coupling chromophores α_{84} and β_{84} (Debreczeny, 1993) in PC. Due to the 0.38 anisotropy value, we suggest that excitonic delocalisation does not take place over homo-hexamers. The 450 fs, which is not observed in the global analysis, seems to be trapped in the hexamer.

The 450 fs component is within the framework of (Sauer, 1988) who suggested a fast 370 fs component that was attributed to the relaxation between two excitonic states formed as the

result of the excitonic interaction between pigments in adjacent subunits of the PC trimers. The EET within the single PC monomer occurs on a longer timescale, caused by the comparatively larger distance between adjacent chromophores. The kinetic is also close to that found by (Gillbro, 1993) in trimeric PC units. Thus, the higher amplitude of the 450 fs might be taken as indicative of the trimer symmetry conservation as well as excitonic coupling between adjacent chromophores α_{84} and β_{84}.

The 10 ps of the anisotropy kinetics is in line with the 14 ps component found inside the PC spectral range with the DAS. This kinetic had been suggested by Holzwarth to occur inside single hexamers (Holzwarth, 1987). According to the presence of homo-hexamers units, and the maximum of the trimeric units in others species located around 617 nm (Debreczeny, 1993), we suggest that the 618 nm component might be located around the maximum of the PC trimeric unit in the PBP homo-hexamer. Thus, the depolarisation kinetic in trimer might occur in fair agreement within 10 ps. The non-negligible amplitude (13 %) of the kinetic of more than 200 ps is an indication that a partial depolarization effect takes place between weakly coupled pigments. This residual anisotropy is an indication that the energy component around 10 ps is transferred out of the trimer before a total depolarisation. This residual anisotropy can also be used as indication of the symmetry order.

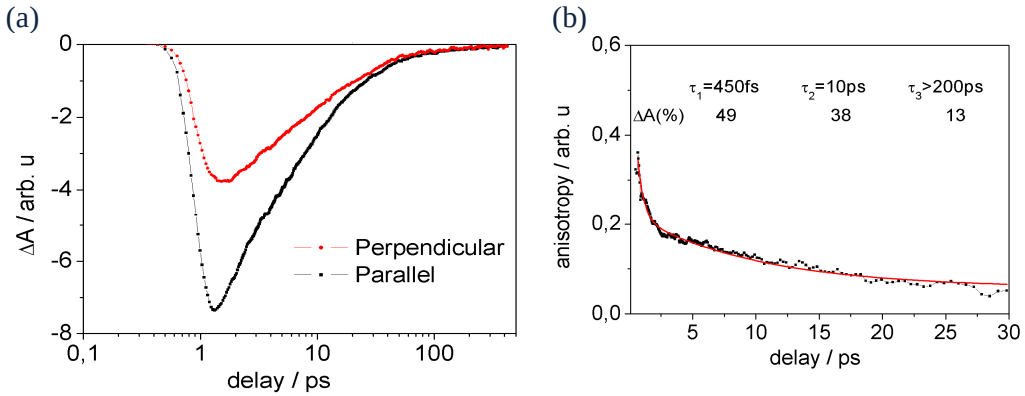

Figure 3.6: (a) Photo-induced absorption changes of the probe beam induced by pumping the PBP antenna system of *A. marina* at 618 nm in phosphate buffer at RT. The polarisation of the excitation beam is perpendicular (red) or parallel (black) to the polarization of the probe beam; and (b) Absorption anisotropy calculated from the decay kinetics measured for parallel and perpendicular polarization of the excitation beam at 618 nm relative to the probe beam at the same wavelength of the PBP antenna system of *A. marina* inside the buffer containing phosphate at RT. I_{pump}= 30 nJ.

3.8 Absorption changes and anisotropy after excitation and probe at 618 nm of the disrupted antenna complex of *A. marina*

Figure 3.7 (a) presents the photo-induced absorption changes inside the disrupted antenna after parallel excitation and perpendicular excitation at 618 nm. The recovery kinetic of the parallel and perpendicular excitation is slower than those of the intact antenna are as we expect from the overall absorption changes due to the disrupted antenna structure. The figure 3.7 (b) shows the anisotropy decay with a maximum value of 0.4. The delay scale is cut off after 30 ps to get a better view of the 14 ps component with regard to the noise. This measured anisotropy value, which is equal to the theoretical maximum of 0.4 supports the same conclusion as was addressed for the intact antenna: there is no delocalised exciton when the ionic strength is low. However, the decreased ionic strength did not affect the stability of the trimeric units. This can be observed from the high amount of 500 fs component. Comparing the 10 ps inside the intact antenna, we found 14 ps inside the disrupted antenna system. The amplitude of the 14 ps component is reduced compared to the 10 ps component which is found at the same wavelength inside the intact antenna (figure 3.6 (b) and 3.7 (b)). The high amplitude (40%) of the residual anisotropy supports two conclusions:

1. The 14 ps component propagation exits the hexameric units before total depolarisation. The bleaching after 14 ps might due to the contribution of the outer phycocyanobilin chromophore β_{155}. Furthermore, the build up of the ESA is slower.

2. In comparison to the intact antenna, there is more asymmetry in the disrupted antenna.

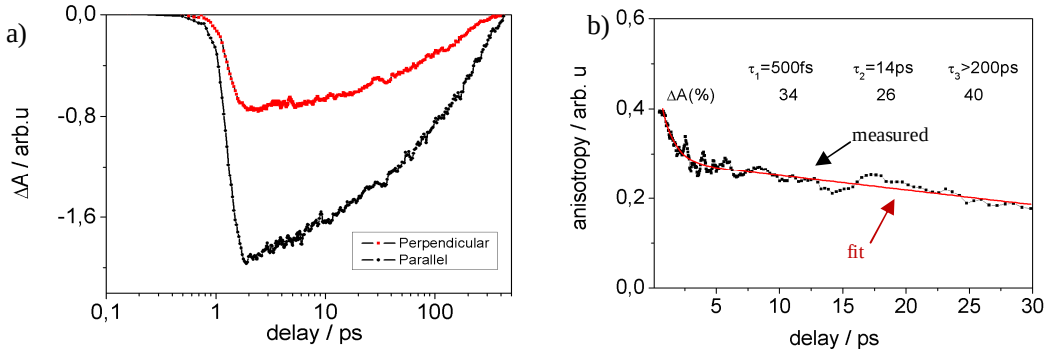

Figure 3.7: (a) Photo-induced absorption changes of the probe beam induced by pumping the PBP antenna system of *A. marina* in buffer without phosphate at RT. The polarisation of the excitation beam

is perpendicular (red) or parallel (black) to the polarization of the probe beam; and (b) Absorption anisotropy calculated from the decay kinetics measured for parallel and perpendicular polarization of the excitation beam at 618 nm relative of the probe beam at same wavelength of the PBP antenna system of *A. marina* in buffer without phosphate at RT.

3.9 Absorption changes and anisotropy after excitation at 618 nm and probe at 630 nm of the intact antenna complex of *A. marina*

Figure 3.8 (a) presents results of photo-induced absorption changes inside the intact antenna at 630 nm after parallel and perpendicular excitation at 618 nm. The 630 nm is the absorption state of the β_{84} chromophore, which is close to the low state of PC at 635 nm (see chapter 4). Figure 3.8 (b)[4] shows the anisotropy decay with a maximum value of 0.52. This measured initial anisotropy value is slightly higher than the theoretical maximum of 0.4 (Lakowicz, 2006) and lower than the expected value 0.7 of the excitonic delocalization along adjacent pigments. This indicates that saturation effects take place at the edge of the PC sub-band, especially near the low side of the PC assembly inside the PBP antenna system of *A. marina.* This value is close to the one found by Edington (Edington, 1995) in APC trimers. The smaller amplitude (2%) of the residual anisotropy is likely an indication that high symmetry of the closely overlapping spectral band pigments (α_{84}, β_{84}) is dominant. This might induce the contribution of the 400 fs component devoted to this excitonic coupling to be delocalized over the α_{84}, β_{84} and the low state of the PC (see chapter 4). Without any indication to the negligible value of the residual anisotropy in this system, and a lower value of residual anisotropy in other systems (Tleugabulova, 2004) we are proposing that the energy component of 10 ps is still transfer out of the hexamer. Furthermore, the ESA seems to be built up faster than at 618 nm.

[4] After 70 ps, there is a recovery kinetic between parallel and perpendicular polarisation, which induces more fluctuation due to the ESA of PC. I apply a cut off of 70 ps to remove those points.

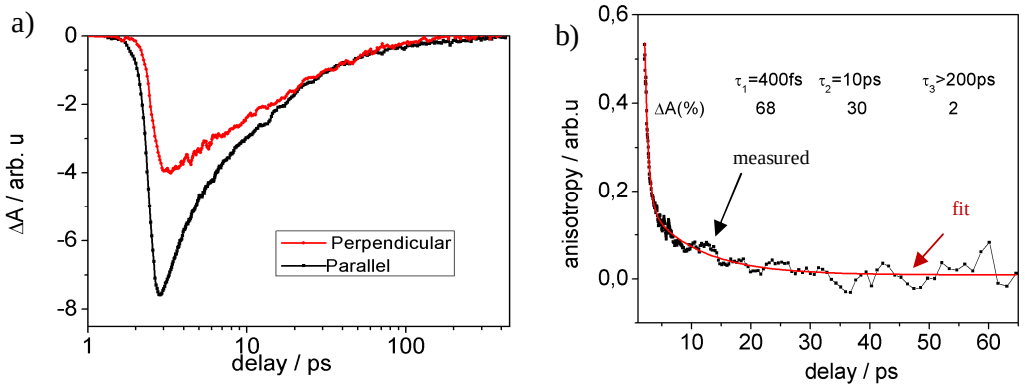

Figure 3.8 (a) Photo-induced absorption changes of the probe beam at 630 nm induced by pumping the PBP antenna system of *A. marina* at 618 nm in phosphate buffer at RT. The polarization of the excitation beam is perpendicular (red) or parallel (black) to the polarization of the probe beam; and (b) Absorption anisotropy calculated from the decay kinetics measured for parallel and perpendicular polarization of the excitation beam.

3.10 Absorption changes and anisotropy after excitation at 618 nm and probe at 630 nm of the disrupted antenna complex of *A. marina*

Figure 3.10 (a) shows the Photo-induced absorption changes at 630 nm inside the disrupted antenna after parallel excitation and perpendicular excitation at 618 nm. The recovery kinetic between parallel and perpendicular is slower. This supports the same conclusions as drawn for the disrupted antenna measured at 618 nm. Figure 3.10 (b) shows the anisotropy decay which is slightly under the maximum value of 0.4. This measured anisotropy value which is near to the theoretical maximum of 0.4 indicates that excitonic coupling energy transfer between adjacent chromophores especially chromophores α_{84} and β_{84} are not propagating out of the PC trimer. Three components of the depolarization have been identified: 280 fs, 14 ps and a kinetic of more than 200 ps. The 280 fs is likely due to the decrease of ionic strength, which has changed the coupling between the adjacent chromophores (α_{84}, β_{84}). We can suggest that the low electrostatic charge in the disrupted antenna changes the spatial position of close spectrally overlapping pigments. Thus, a stronger coupling takes place at the low state of the PC units between these pigments. Instead of the 10 ps inside the intact antenna, we found 14 ps inside the disrupted antenna as trimer depolarization kinetic. The amplitude of the 14 ps is reduced in comparison to that of the 10 ps component found at the same wavelength inside the intact antenna (figure 3.9 (b) and 3,10 (b)). The amplitude of the long

kinetic component (>200 ps) drastically increases in comparison with the component found inside the intact antenna at the same wavelength (figure 3.8 (b) and 3.9 (b)).That means the pigments at the edge of the hexamer have become more asymmetric. In comparison to the disrupted antenna measured at 618 nm, the amplitude of a kinetic component more than 200 ps is likely to be almost conserved. The change of the fast component from 400 fs to 280 fs might also be induced due to the coupling with the low state of PC (see Chapter 4). The high value of the residual anisotropy indicates that more asymmetry is present at low ionic strength. The 14 ps component is caused by the EET out of the hexamer before total depolarization.

These finding are in line with the long component found inside the DAS of the disrupted antenna (figure 3.5 (b)).

In low ionic strength, excitonic delocalisation did not contribute to the EET.

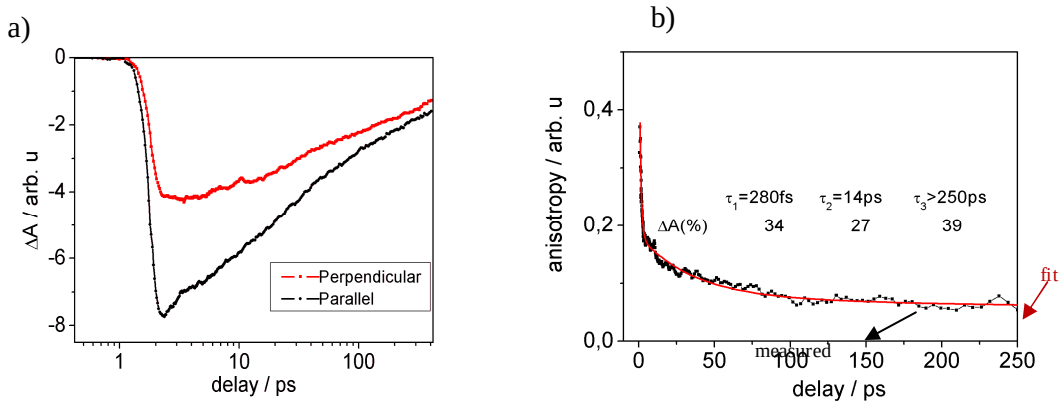

Figure 3.9: (a) Photo-induced absorption changes of the probe beam at 630 nm induced by pumping at 618 nm the PBP antenna system of *A. marina* having depleted phosphate inside the buffer at RT. The polarisation of the excitation beam is perpendicular (red) or parallel (black) to the polarization of the probe beam; and (b) Absorption anisotropy calculated from the decay kinetics measured for parallel and perpendicular polarization of the excitation.

4 Comparison of antenna system of *A. marina* and *Thermosynechococcus vulcanus*

Recently, the structure of a PBS rod domain has shown to be assembled by two PC hexamers embedded in linker protein $L_R^{8.7}$, L_R, L_{RC} (David, 2011). These isolated rods exhibit the low absorption state of PC located at 635 nm. However, no evidence of a linker has been presented between the APC core disc and the terminal rod hexamer. Consequently, the structural linker polypeptide of the stacking process in hexamer PC and the heterohexamer PC/APC of the PBP antenna system of *A. marina* cannot be asserted. Thus, questions arise as to whether the linker protein really contributes to the tuning of the EET in the outer antenna system. Additional questions arise when comparing the EET between the PBP antenna system of *A. marina* and the PBS of other cyanobacteria. For instance, is the EET kinetic of 3 ps from PC to APC as found in PBP by (Theiss, 2011) the fastest that can exist in the cyanobacteria containing *Chl a* as T. vulcanus? Can the 3 ps found in *A. marina* be generalized to other cyanobacteria or is it only a specific case due to adaptation of *A. marina* in its living habitat?

Motivated by the aforementioned similarity of the pigment composition (bilichromophore), and the evident difference in the assembly between the phycobilisome of *T. vulcanus* (PBS) and the PBP of *A. marina*, we present below a comparative study of these two cyanobacteria.

4.1 Comparison of the Absorbance Spectra at Room Temperature

In figure 4.1, we compare the absorbance at RT in PBP antenna complex of *A. marina* with the PBS of *T. vulcanus*. In collaboration with Noam Adir at the Schulich Faculty of Chemistry in Israel, the PBS of *T. vulcanus* are isolated in a sucrose gradient and appear as several bands. The band 1 and 3 are obtained in high phosphate strength, while the band 2 is extracted in low phosphate. The culture of the *T. vulcanus* and the fraction preparation of the ROD containing PC are describe by David (David, 2011). In this Section a comparison between the absorbance from band 1, 2, 3, ROD of *T. Vulcanus* and the PBP of *A. marina* was performed.

Evidence of a difference is observed in the absorbance spectra at 575 nm between all the PBS antenna systems and the PBP antenna system independently of the extraction band as well as the isolated ROD containing only PC. The 575 nm is still under investigation. Further differences are observed at the maximum absorption of the outer antenna system of these two cyanobacteria, where the maximum of the absorption of the PBS and ROD is around 5 nm red shifted compared to the PBP. This effect is perhaps induced by the presence of different linker proteins inside the ROD. Additionally, a more pronounced difference is observed in the red edge of the spectra and the spectral width, as the spectra of all PBS as well as the ROD, are broader than the absorption spectrum of the PBP of *A. marina*. Furthermore the PBS 1 (extracted at the band 1 of the sucrose gradient) present additional differences in the red with the PBS 2 and PBS 3.

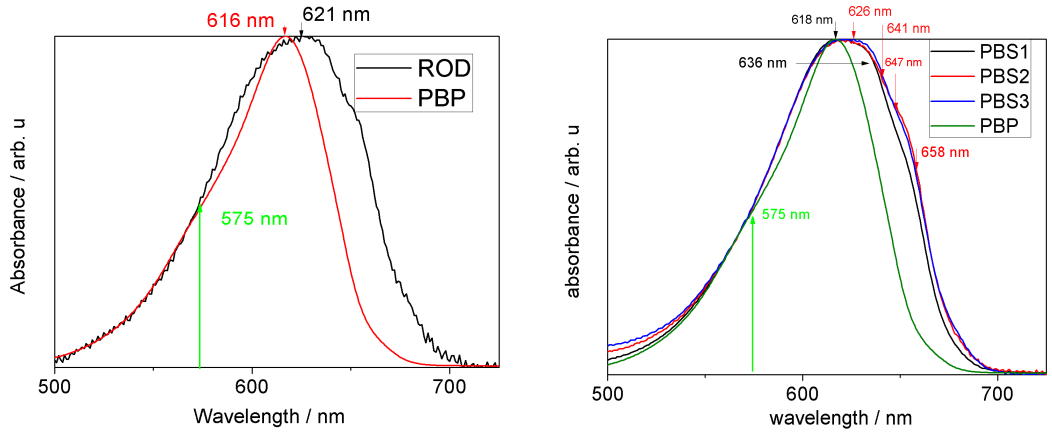

Figure 4.1: RT absorbance of the PBS antenna system of *T. vulcanus* extracted as different fractions by the sucrose gradient centrifugation (PBS1, PBS2, PBS3), the PBP antenna system of *A. marina* and comparison of the absorbance of the isolated rod of T. *vulcanus* with the PBP antenna system of *A. marina* (b). The spectral features are labelled by their peak wavelengths in nanometres.

Considering the comparison between the PBP and the ROD, the 575 nm shoulder might be induced by a motion of a denatured sub-protein or the interaction with different protein cofactors. However, the red shift appears with a broader spectrum in PBS as well as on the ROD. Thus, it might be induced by internal organisation of the PC sub-aggregate states through strong electrostatic interaction with different linkers. The presence of different linker polypeptide in the PC hexamer as well as in the APC core domain (David, 2011) might induce asymmetry in the axis of adjacent chromophores. That means, the β_{84} chromophores of adjacent PC hexamers are pushed out of their original pocket in PC trimer, because of their

strong electrostatic coupling with the L_R connected the adjacent PC hexamers. The result of this interaction with the linker might be the reason for the observed spectral shift.

4.2 Femtosecond time-resolved absorption changes

In order to measure the EET in the PBS antenna system of the *T. vulcanus*, in comparison to the PBP antenna system of *A. marina*, the samples were excited at 621 nm to monitor the time resolved absorption changes at different probe wavelengths. The changes in the absorption spectra were monitored at the same delay times. The results are presented in figure 4.2 for PBS and for PBP (see also figure 3.5 (a)). Figure 4.2 shows the bleaching which occurs immediately during the excitation as a result of the ground state depletion, which was observed in the spectra by a fast bleaching and concomitant rise at longer wavelength due to the ESA. These rising kinetics are followed by the recovery kinetics. The bleaching is observed in the whole spectral range of PC where the course of the 620 nm absorption change is presented. The bleaching of the spectra at 650 nm is mainly due to APC in the Core APC. The 670 nm and 680 nm kinetic components exhibit first a very fast rise term, followed by a delayed bleaching. All of the lower energy components between 670-685 nm show a delayed bleaching of two different pigments, since the absorption of APC is very weak in these spectral ranges (see figure 4.1 (b)). The successive bleaching observed between the PC and the APC band can either be an indication of the EET over the entire PC to the APC or a faster annihilation, which shall be further investigated. The rise term at 670 nm and 680 nm is mainly due to the ESA of PC, and the delayed bleaching is an indication to the existence of two different pigments. These pigments are APC E and APC B. They display fast relaxation kinetic originating from (α,β) chromophores (see table 4.1). This latter pigment at 680 nm might be the terminal emitter of the PBS.

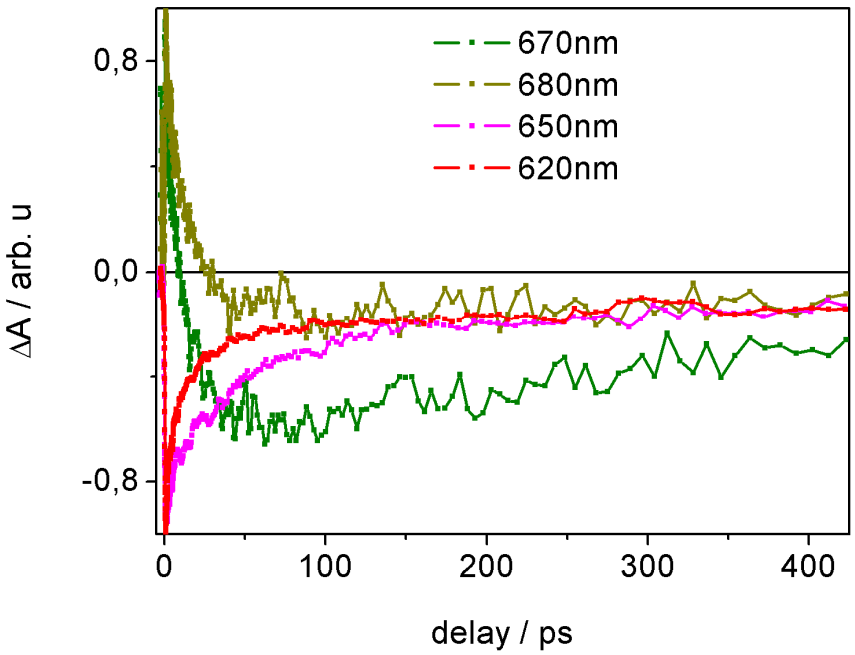

Figure 4.2: Photo-induced absorption change of four selected wavelength of the PBS antenna system of Thermosysechococcus vulcanus extracted at the band three of the sucrose gradient inside the buffer containing phosphate after excitation at 618 nm where the absorption peaks at 620 nm, 650 nm, 670 nm and 680 nm represent the aggregate states of PC, APC, linker pigment absorbing at 660 nm and 680 nm (that we suppose to be the linker APC_{LCM}.)

Our assignment of the photo-induced absorption changes inside the PBS antenna system of *T. vulcanus* is fortified by the same phenomena on the photo induced absorption changes of the PBP antenna system of *A. marina* after excitation at 618 nm which was shown in figure 3.5 (a). Where the successive bleaching of the PC spectral range (625 nm) to the APC spectral range (640 nm) occurs. The ESA of the PC appears concomitant with the delay bleaching at 660 nm as well as 670 nm (not shown on the figure). At 660 nm and 670 nm, the terminal emitter might be present, and the related linker core membrane for PBS is 10 nm red-shifted to the delay bleaching observed in the PBP of *A .marina*. This might be an indication that the structural connection of the PBP of *A. marina* and the PBS of *T. vulcanus* might be the same. However, the excited state decay of the pigments tied in the linker membrane displayed in Table 4.1 is an open issue, which needs further investigation.

Table 4.1 Comparison of the excited state decay of the terminal emitter in the PBS antenna system of *T.* Vulcanus PBS-1. There are obtained from the PBS 1 absorption change trace, which is not shown here.

Wavelength (nm) PBS 3	Relative amplitude (%) of the kinetics pathway		
	Channel 1 (430 fs)	Channel 2 (13 ps)	Channel 3 (>1 ns)
670	40	30	30
680	20	60	20

4.3 Decay associated spectra

In order to follow the kinetic components inside the PBS antenna system of the *T. Vulcanus,* (extracted as band 3 fraction by the sucrose gradient) along the spectral axis, the amplitudes of each kinetic pathway were plotted as a function of wavelength intervals according to the available data of the flash induced absorption changes as decay associated spectra (see chapter 3). For the sub-domain PC ROD, APC core and the polypeptide linker core membrane pigment with absorption between 660-680 nm, the evolution of the course kinetic is shown for the PBS antenna system of *T. vulcanus*.

In *T. vulcanus,* PBS the 888 fs component of the EET exhibits a negative spectrum in the interval range of 600-650 nm and a positive spectrum between 650-690 nm. The negative spectral range of the 888 fs component exhibits a minimum around 620 nm (which is in the PC band). This 888 fs component rises and displays a zero amplitude at 650 nm where the APC in the Core absorbs.

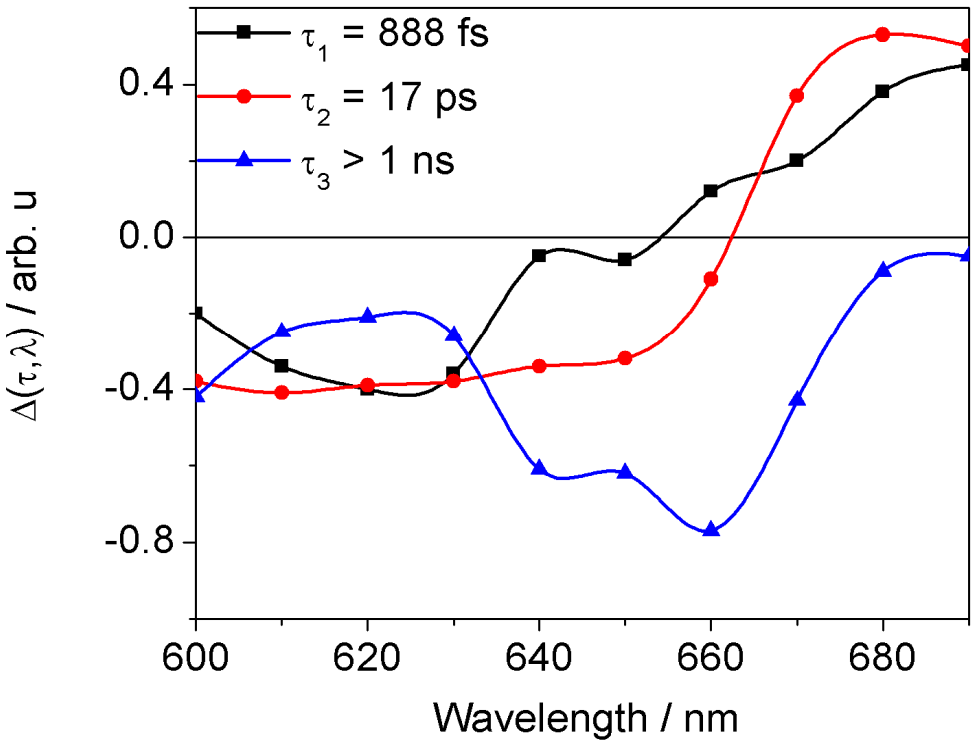

Figure 4 3: Decay associated difference spectra (DAS) of the photo-induced absorption changes of the PBS antenna system of *T. vulcanus*.

The positive spectral band of the 888 fs kinetic component seen in figure 4.3 can have two different sources. It can be described as increased ground state bleaching of the APC core due to EET from the ROD PC to the Core APC. However, the lower absorption of APC (see figure 4.1 (a)) above 660 nm led to a second interpretation that it originated either from the excited state absorption (ESA) of PC or APC. The concomitant maximum of the 888 fs at 670 nm could also originate from the overlap of the delayed bleaching spectrum of the pigment, which absorbs at 660 – 680 nm. Finally, the evolution of the 888 fs component supports the conclusion that the excitation energy can be equilibrated between the entire PC–hexamers ROD and the fraction of the APC core within 888 fs. However, further investigation on the excited state lifetime of the pigment is necessary to estimate the annihilation contribution in the fast component 888 fs.

A clear cut-off can be derived by the diagnostic of the residual anisotropy and the comparison of the amplitude variation in low ionic strength. The above 888 fs is shorter than the EET

from the PC containing rods to the APC-core inside the PBS antenna system of typical cyanobacteria without linker protein inside the ROD, which has been reported to occur within 17-18 ps (Sandström, 1988; Zhang, 1997). A kinetic component of 14 ps is found to be one of the EET channels between PC and APC inside the PBP antenna system of *A. marina* (see chapter 3). This 888 fs is even shorter than the 3 ps found inside the PBP of *A. marina*. Therefore, our measurements reveal that in *T. vulcanus*, which exhibits the linker protein in the ROD PC, a linker protein between the ROD PC and Core APC the EET is even faster between the PC and APC pigments than in the PBP of *A. marina*.

The 17 ps component of the EET in the figure 4.3 shows (as in the ultrafast 890 fs component) a negative spectrum between 600-660 nm and the positive spectrum above 660 nm. The positive spectrum shows higher amplitude than the 888 fs component and it exhibits a maximum at 670 nm. The amplitude of the 17 ps component displays a zero value at 660 nm of the APC E in the linker membrane. These characteristics suggest that the red shift 17 ps decay component at 660 nm reflects mainly an EET of the APC core to the pigment absorbing around 660 nm (APC E), which is the upper state of the core membrane linker (L_{CM}) that connects the APC core to the thylakoid membrane and acts as terminal emitter from the PBS to Chl a inside the RC of PS II. For a review of the phycobilisomes of other cyanobacteria, see (Lundell, 1983; Mimuro, 1986). This kinetic is slightly slower than the 14 ps kinetic component found by Holzwarth (Holzwarth, 1990) , and Theiss (Theiss, 2011) for PBP.

Due to the isolated antenna system used in this measurement, the EET to the PS II is interrupted. This is in fair agreement with the prolongation of the excited state lifetime. This lifetime exhibits a completely negative spectrum in the whole measured spectral range with a pronounced minimum at 660 nm, which is the non resolved lifetime of the pigment bound to L_{CM} and as shown in figure 4.3 for the component τ_3> 1 ns. It cannot be resolved with our setup. In short, the current work has demonstrated an ultrafast kinetic component of the EET along the ROD PC domain containing linker proteins to the APC core domain in the *T. Vulcanus* PBS antenna system, which has never been reported before. The value was as short as ~ 900 fs.

The experimental results above which were carried out at RT, deal with a simple relaxation model through intramolecular propagation of the EET in the liquid phase media where the degree of disorder is high. The absorption peak of homogeneous pigment in the protein

matrix is superimposed with inhomogeneous broadened spectra. The relaxation of pigments in the related phase does allow a view of the electronic transition. In order to obtain additional insight of the spectral position of pigments and the substructure between the PBS of *T. vulcanus* and PBP of *A. marina* as well as electron-vibrational coupling, the results of site-selective spectroscopy at low temperature are presented below. The decrease in temperature will quench the Brownian motion observed in liquid phase, which is replaced by a semi-ordered ice. In addition, the inhomogeneous distribution can be side-stepped by the selective analyses of the contribution of certain pigments by hole burning and fluorescence line narrowing.

4.4 Fluorescence Line Narrowing (FLN), Delta Fluorescence Line Narrowing (ΔFLN) and Hole Burning (HB)

We use FLN to overcome the inhomogeneous broadening (Inhomogeneous broadening deals with a high amount of disorder in the transition energy of individual pigments embedded in the protein matrix) (see figure 4.6). This experimental method is based on the collection of fluorescence from a single guest pigment by a narrow-band laser excitation at low temperatures. A fraction of the guest pigment (i.e. which absorbs near the narrow excitation line width) is excited. The selectivity of the excitation will induce a more narrow fluorescence than the inhomogeneous broadened ensemble. This principle is helpful for the characterisation of the vibrational frequencies of the ground and excited state. However, it is limited due to the concomitant excitation of the guest pigments absorbing at the zero-phonon line (ZPL), and through phonon-assisted transitions (also called phonon sideband (PSB)) of neighbouring chromophores which do not absorb resonantly with the excitation. Thus, the collected fluorescent intensity is composed of both real PSB (PSB of the homogeneous single-site fluorescence spectrum from the guest pigments whose ZPL is resonant with the excitation frequency) and pseudo-PSB (fluorescence from the neighbouring guest pigment excited through their PSB). This makes the analysis complicated. A further problem comes from the difficulty in evaluating the sharp ZPL and the broad pseudo-PSB, because of the contribution of the scattered excitation light.

These difficulties can be overcome by combining HB with FLN. The original idea behind this is to eliminate the pseudo-PSB by the difference between consecutive FLN collected signals. This latter called ΔFLN has been revised as an alternative method to estimate electron –

phonon coupling strength by measuring the ZPL and the PBS (Rätsep, 2003)(see figure 4.5 and 4.6).

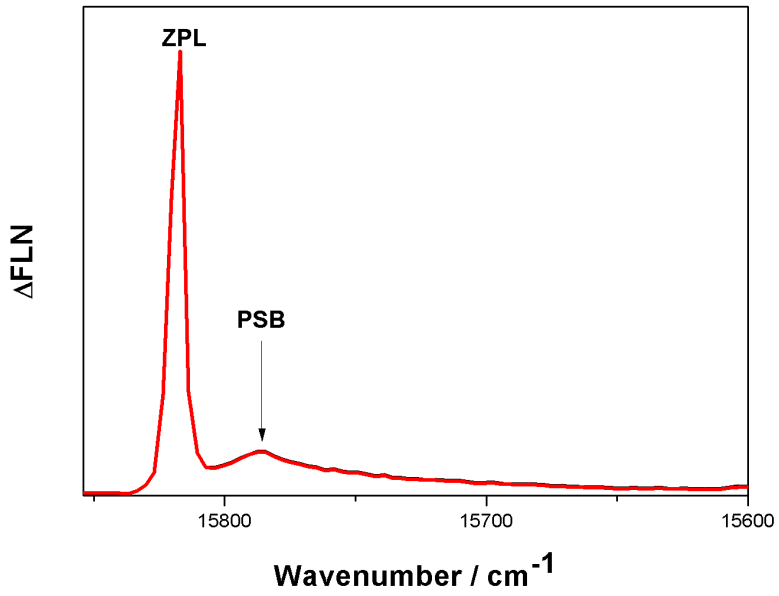

Figure 4.4: Example of delta FLN spectrum from the PBP of *A. marina*

Concerning spectral hole burning, excitation by a such narrow-band laser light will change the excited state population of the guest pigment in the protein matrix. This perturbation alters the guest pigments transition frequency and the site distribution function (SDF) at the excitation frequency, this will decrease the formation of a hole at the ZPL as well as in PSB. Antiholes will occur with an increase of the SDF. This latter has been suggested to be a pseudo-PSB (Rätsep, 2007).

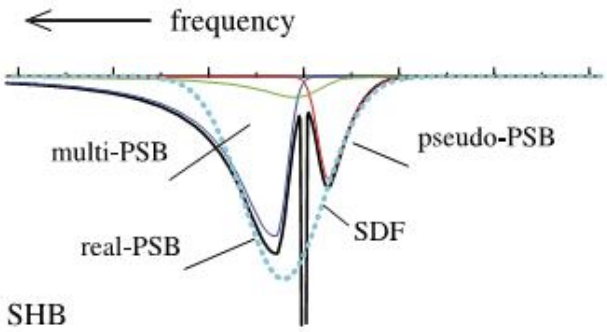

Figure 4 5 suggested model of spectra hole burning by Rätsep (Rätsep, 2007). The 0-0 electronic transition displays different component labelled in the figure.

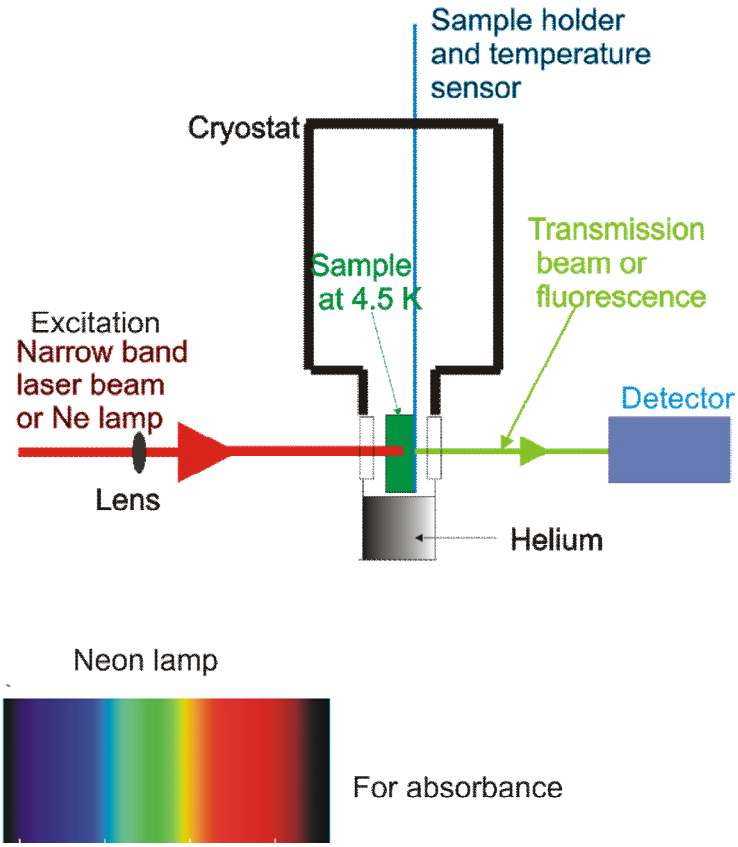

Figure 4. 6 Spectral hole burning setup. The sample is maintained just above the surface of liquid helium to ensure a temperature of 4.5 K. The detector is a spectrometer. The neon lamp is used to measure the absorbance before the excitation with a narrow laser beam, and after the excitation. The difference spectra give us a view of the excited state as describe in Fig.... The same setup was used for the FLN measurement, where the fluorescence induced by the narrow laser beam excitation is collected. The delta FLN is a fluorescence spectrum collected after consecutive burn fluency. The difference of the two FLN gives a delta FLN spectrum.

4.5 Insight the electronic structure of the phycobiliprotein of *Acaryochloris marina*

4.5.1 Fluorescence Line narrowing

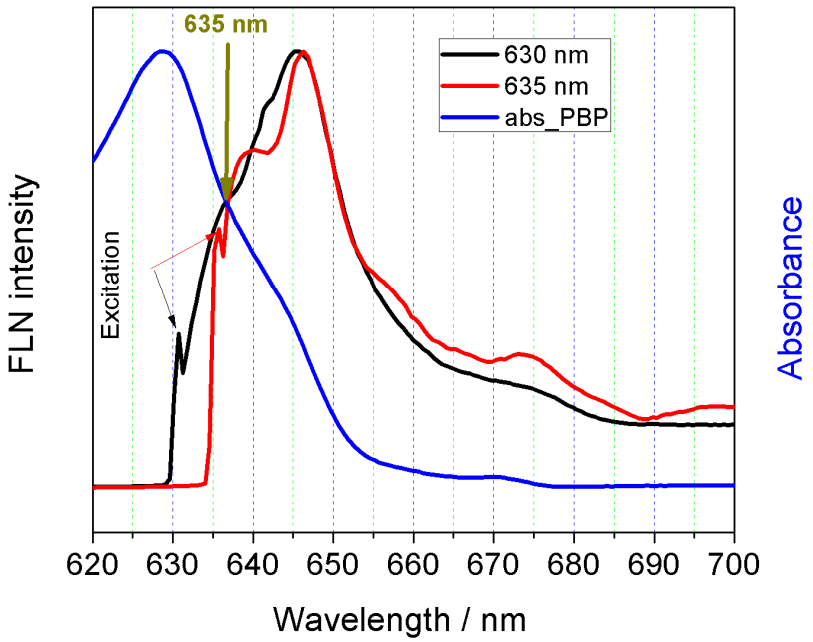

Figure 4 7 Comparison of the FLN spectra at 4.5 k of the PBP of *A. marina* after excitation at 630 nm (black shaped), 635 nm (red shaped), and the absorption spectra (blue shaped)[5].

In figure 4.7, the shape of the FLN spectrum obtained by excitation at 630 nm excitation displays a shoulder at 635 nm, while that obtained at 635 nm excitation shows a steep rise in comparison to the spectrum excited at 630 nm and a pronounced flat shoulder between 640 – 645 nm due to the energy transfer to the APC. Further differences can be seen at 655-700 nm where the FLN spectrum obtained after excitation at 635 nm shows site selective phonon sidebands, which are in homogeneously broadened in the spectrum after excitation at 630 nm. Because of the excitation at 630 nm, the bilichromophore β_{84} is excited. At 635 nm, selective vibrational sidebands become visible due to the resonant excitation of a red shifted chromophore.

[5] Note that experimental results displayed for figure 4.6 to 4.16 upon using were obtained the Hole burning setup at the Institute of Physics, the University of Tartu.

If there is a linker pigment, it is electrostatically bound to the red shifted chromophore at 635 nm. This will induce modes in vibration with the linker when an excitation occurs. That becomes visible if the 635 nm chromophore is solely excited. If the 630 nm excites this linker, vibration can also occur, but it will be different to that of the 635 nm. The hypothesis from MacColl (MacColl, 1998), which postulated the presence of the linker where two different compounds are assembled, will remain an open issue for the *A. marina* PBP in our investigation.

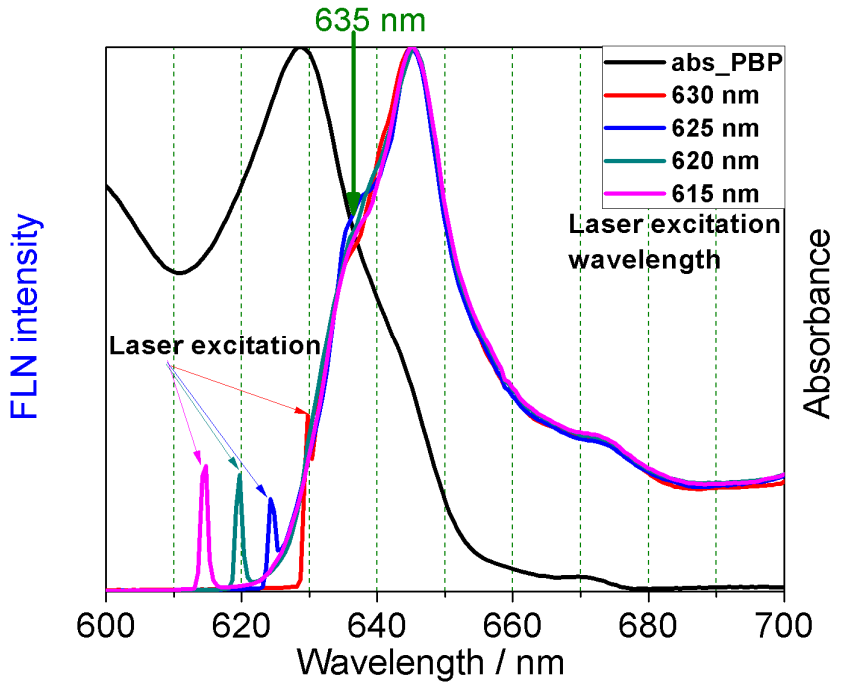

Figure 4 8 Comparison of FLN spectra after excitation at 615 nm, 620 nm, 625 nm, 630 nm at 4.5 K for the PBP of *A. marina*. The absorbance spectrum of the PBP of *A. marina* is shown in black.

Figure 4.8 shows the FLN spectra of the A. marina PBP after excitation at 615, 620, 625, 630 nm and the absorbance. Four sharp peaks induced by the laser excitation at the indicated positions as well as a shoulder between 630 nm and 640 nm are visible. The fluorescence spectra slightly differ at 635 nm. Thus, it is an indication of the small contribution of 635 nm in PC emission spectra. Furthermore, the PC emission spectra become selective at the red edge of PC, especially at 635 nm that we suggest to be the low state of PC. At longer wavelengths, no difference is observed on the vibration propagation.

One can see in Figure 4.8 that the broad absorption band of the PBP of *A. marina* contains more than one underlying band. Even at low temperature with a semi-order induced the amorphous phase system; the bands with different hole burning properties can overlap. The hole-burned spectra with a constant low fluency as a function of burn (excitation) wavelength can be used to monitor the sub-bands of the pigments absorbing at 635 nm as well as 660 nm. The burn intensity must be low enough to avoid saturation effects and to excite only the pigment absorbing at its specific wavelength. This is the 0-0 electronic transition of the pigment.

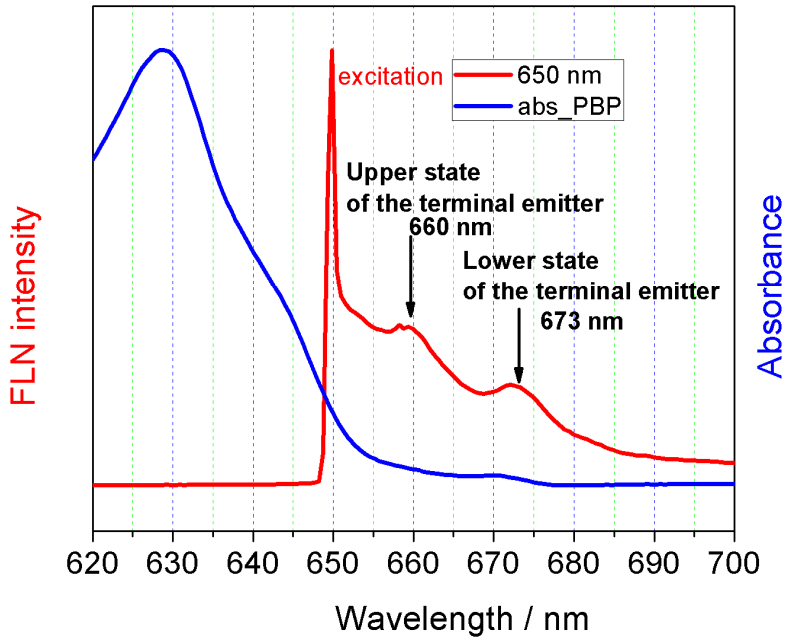

Figure 4 9 FLN intensity after excitation at 650 nm (red) and absorption of the PBP antenna system (blue)

Figure 4.9 shows the FLN spectrum after excitation at 650 nm. A steep peak in the FLN spectrum originates from the excitation at 650 nm. This latter is followed by two local maxima at 660 nm and 673 nm. These two maxima are in line with the Gaussian fit of the absorption of 0-0 electronic transition displays in figure 4.12. These two maxima can support two different hypotheses:

1. The terminal emitter exhibits two states at 660 nm and 673 nm.

2. The linker membrane can bind two different pigments. This second hypothesis can be supported by the spectral position of the maximum. The maximum at the 660 nm wavelength is typically associated with a site bound APC E, while the one at 673 nm are found in the binding pocket of APC B.

The two hypotheses are compatible with the conclusion that there is an upper energy state a 660 nm and the lower energy state at 673 nm, which are independent of the occupation sites of one form of the PBP chromophores. We proposed that, the upper energy state at 660 nm is a bridge for a fast energy transfer to a lower state. Because of the fluorescence of a fraction of excited lifetime in APC, which is coupled to the upper state of the linker at 660 nm, the fluorescence maximum at 660 nm appears in FLN. Based on the available data, a future biochemical preparation is necessary to address the site occupation as well as the functional role of the low energy site at 673 nm.

In the above section devoted to FLN the obtained result appears as follow: the identification of the low sate of PC at 635 nm and the 2 band of the linker membrane at 660 nm for the upper state and 673 for the low state. This technique did not give much information about the energy transfer to the successive low state of the PBP of the *A. marina*. Less is also know about pigment protein interaction. To have more insight to the aforementioned points we use in the following section spectral hole burning.

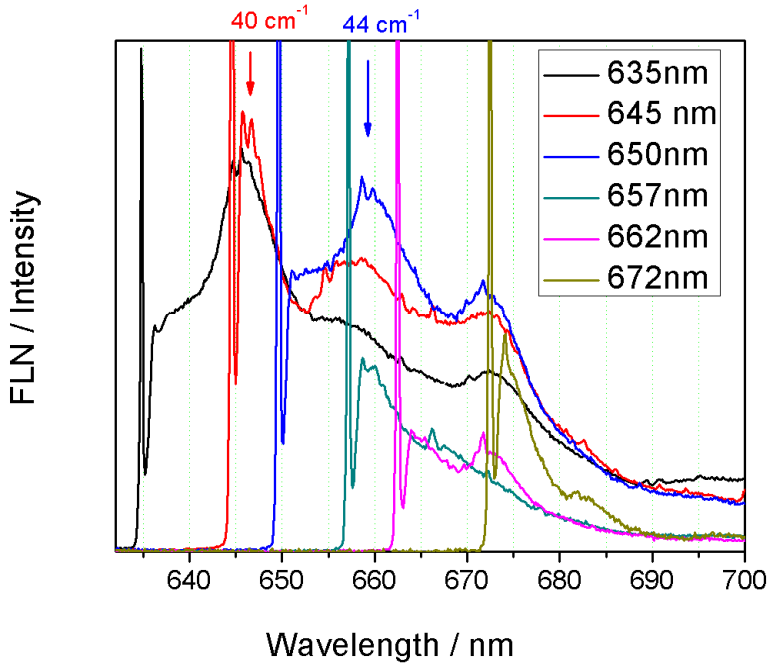

Figure 4.10 FLN intensity after a burn fluency of 0.6 J/cm² at 4.5 K.

Figure 4.10 portrays the FLN spectra after excitation at 635 nm, 645 nm, 650 nm, 657 nm, 662 nm and 672 nm. The zero phonon line appears with a sharp peak at the excitation wavelength. These peaks have been cut off to allow the visualisation of the phonon side-bands and different features on the one-phonon profiles. All the one-phonon profiles display a strong asymmetry in their maxima.

After excitation at 635 nm, the FLN spectrum shows a maximum at 645 nm, 660 nm and 673 nm. The 645 nm maximum appears with a double vibrational mode which is characteristic of the dimer pigments β_{84} and α_{84} originating from APC. The maximum at 660 nm is due to energy transfer from a fraction of APC, which is coupled to the upper energy state of the linker, which connects the antenna to the thylakoid membrane. The remained fraction of APC further transfers the energy to the lower state of the aforementioned linker at 673 nm.

The 645 nm excitation shows (of APC electronic states), on its phonon side-band, a double vibrational mode which originates from the 0-0 electronic transition of the dimer pigments β_{84} and α_{84} in APC. These vibrational modes are separated by an energy gap of 40 cm^{-1}. The APC electronic states (pigments) can transfer the energy to the upper energy state at 660 nm and also the lower one at 673 nm of the linker.

As result of the excitation at 650 nm, the energy is further transferred to the upper and lower energy states of the linker. The characteristic feature of the upper energy state is the appearance of double vibrational modes, which are characteristic of the dimer pigments found in APC. The energy gap of these modes is 44 cm^{-1}, which is close to the regular APC dimer. Because of its spectral position at 660 nm, we suggest that it is due to APC-E.

The red-shifted excitation at 657 nm and 662 nm of two different electronic states of the upper energy level of the linker displays different curve of the one-phonon profile. The 657 nm exhibits in its phonon side band the aforementioned double vibrational modes and energy transfer to 673 nm. For the 662 nm feature, it is equally likely that the double vibrational modes decreases in strength at the phonon side-band, or additional sub-electronic states are observed. The upper energy level of the linker membrane is likely to be organised in different sub-electronic states. The electronic state of the latter is well separated from the low energy level of the linker at 673 nm.

Finally, we observed an energy transfer to the terminal emitter at 673 nm. However, this energy originates from the residual population of the excited state in different sub-compounds, which are not coupled to each other, but rather to the low energy level of the linker membrane. The electronic state of the trimeric APC appears with a double vibrational mode separated by the energy gap of 40 cm^{-1}. Furthermore, the double vibrational modes with an energy gap of 44 cm^{-1} are characteristic to APC-E in the linker membrane. The low energy state of the linker is located at the same spectral position as for the APC-B, which is found in the linker core-membrane in other cyanobacteria and red algae.

4.5.2 Spectral hole burning

Figure 4.11 shows the absorbance of A. marina (blue) and the corresponding hole burning spectrum or the ΔA absorbance (red). This ΔA absorbance stands for the difference between the absorbance after excitation (burning) at λ = 620 nm (not shown) and the absorbance (blue). The spectrum reveals:

(a) A maximum absorbance at λ = 630 nm which corresponds to the well known β_{84} pigment;

(b) A vibrational mode at λ = 632 nm (not revealed in Figure. 4.12) which might be a delocalization between β_{84} pigment and the pigment newly discovered at 635 nm. The

localisation of the vibration mode at 632 nm might be due to the coupling between the mode at 630 nm and 635 nm.

(c) The dimer pigments bound at λ = 644 nm in APC; and,

(d) A terminal emitter at λ = 673 nm.

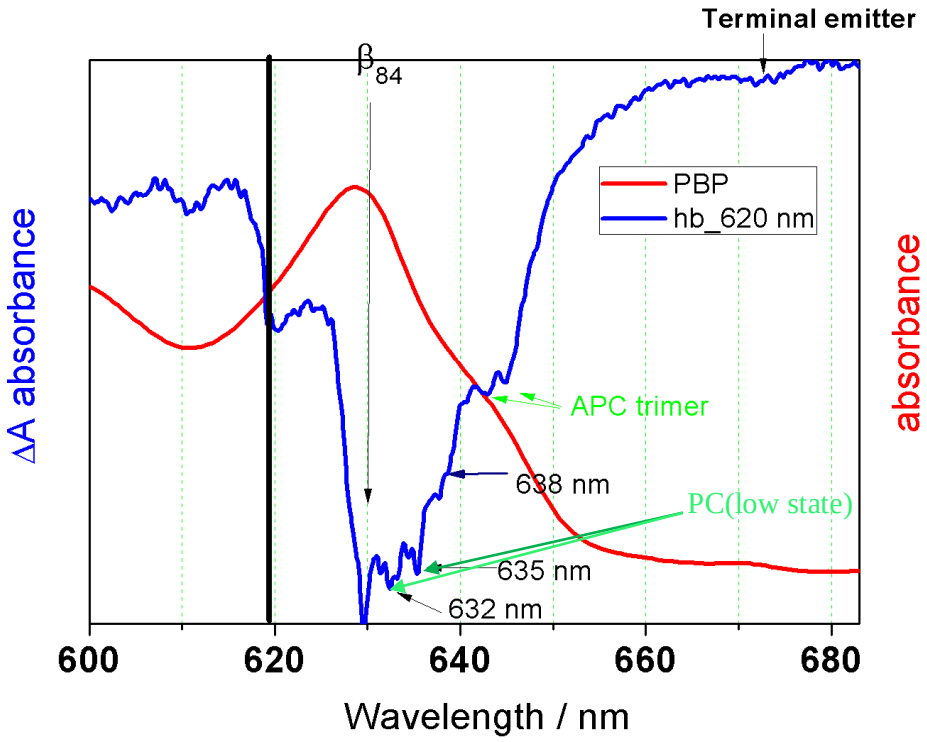

Figure 4.11: Hole burning spectra of the PBP of A. marina (red) after excitation at ~620 nm and the absorbance (blue) at 4.5 K. The burn fluence is 18.75 J/cm^2

However, the spectrum between the pigment at λ = 635 nm and the dimer bound in APC, precisely at 645 nm, seems to be showing the presence of another pigment at 638 nm which has in fact not been detected in Fig. 4.12. This signature of the pigment needs to be further investigated. The green line indicates the position of two intense vibrational lines at the characteristic wavelength of the pigments in the low absorption band of the PC and also the APC in the hetero-hexamer. The pigment composition of the PC low state will be studied further in order to explain the origin of the double vibrational modes. The two modes are the dimer pigments α_{84} and β_{84} of the APC due to their location at 645 nm. These features show that four different states of the pigments are attached to the protein membrane and can

provide EET to the core complex comparable to four strong oscillators. In addition, the broad hole of the terminal emitter is an indication that the excitation energy is funnelled to the terminal emitter.

We have certainly observed from the above result, that pigments embedded in the protein matrix interact with each other, when an excitation occurs, via a strong vibration. The vibrational line of individual chromophores is well observed, and the energy gap between the vibration modes gives an estimation of the coupling between these pigments. An energy gap of less than or equal to 60 cm^{-1} is due to a strong interaction with dimer pigments. Regarding the gap of the entire double vibrational, one can say that the interaction between APC pigments is stronger than that of the PC low state.

It is shown in Figure 4.16 that the broad absorption band of the PBP of *A. marina* contains more than one underlying band, which cannot be well resolved, by FLN and SHB at high fluency. Even at low temperature with a semi-order induced by the amorphous phase system, the bands with different hole burning properties can overlap. When this happens, the hole burned spectra with constant low fluency as function of burn wavelength can be used to monitor the sub-bands of the pigments absorbing at 635 nm as well as further sub-bands of the linker APC-membrane (mean: that connect the unique trimer of the hetero-hexamer to the thylakoid membrane). The burn intensity must be low enough to avoid saturation effects and to excite only the pigment absorbing resonantly at specific wavelength. This technique was applied to the following states:

(a) The low electronic state of the PC at 635 nm.

(b) The electronic state of APC at 645 nm.

(c) The upper electronic state of the linker connected the antenna system to the thylakoid membrane in two sub-bands: at 657 nm and 665 nm.

(d) The low electronic state of the linker at 670 nm.

(e) Figure 4.12 displays the evolution of the average position of the pigment absorbing resonantly at the applied wavelength labelled on the x axis, which are fitted with a sum of Gaussian functions. The successive centre obtained by the fit delivers peaks at 635.9 nm, 645 nm, 657 nm, 661 nm and 670 nm thereby determining estimated

positions of the different pigment state. We proposed that the 635.9 nm peak is in low electronic state of PC instead of the chromophore β_{84}, which is located at 630 nm.

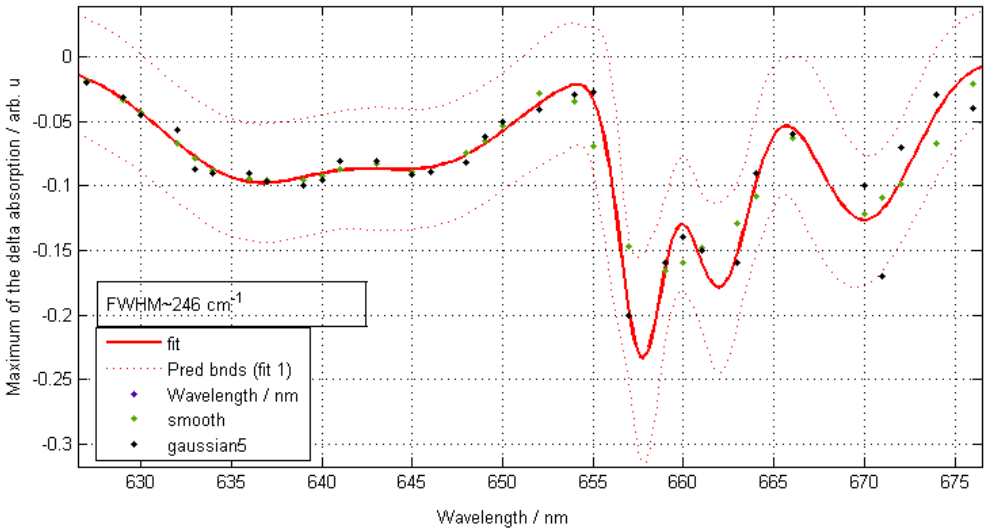

Figure 4.12 Constant-fluency of the maximum hole burned spectra of the PBP antenna system of *A. marina* between 626 – 676 nm. Typical burn condition 9.3 J/cm^2. The action spectra of the maximum absorption of the 0-0 electronic transition can be fitted with the sum of 5 Gaussian profiles (FWHM ~ 246 cm^{-1}). Black points represent the maximum absorption of the 0-0 electronic transition.

The above spectral hole burning section has portrayed the efficiency energy transfer funnelled to the terminal emitter at 673 nm. It also shows with action spectra the low state of PC, the APC and additional information on the sub-band of the linker APC membrane at 657 nm, 665 nm for the upper state and the 670 nm for the lower state. Further, the pigments attached to the protein matrices display a strong vibration. To get more in this vibration we present below a ΔFLN.

4.5.3 Delta fluorescence line narrowing

Figure 4.13 displays a comparison of ΔFLN spectra of selectively excited vibronic regions of the PBP antenna system of A. marina. The excitation wavelengths are labelled on the right side. The aforementioned ΔFLN stands for the difference between consecutive pre-burn (not shows) and post-burn (not shown). The ZPL has been cut off to allow a clear view of the phonon side-band labelled by Psb. The collected spectra reveal:

i. There are vibrational modes visible at 217 cm^{-1}, 273 cm^{-1},476 cm^{-1}, 510 cm^{-1}, 667 cm^{-1}, 822 cm^{-1} (HOOP), 1245 cm^{-1}, 1273 cm^{-1}(C-H), 1360 cm^{-1}(C-N), 1585 cm^{-1} and 1628 cm^{-1} (C=C) after excitation at 635 nm.

ii. Vibrational mode 250 cm^{-1} after excitation at 645 nm, which was in addition to the aforementioned mode after excitation at 635 nm.

iii. Interestingly, all the high frequency C=C 1585 cm^{-1} display a blue shift feature of the band at 1628 cm^{-1} . They are both shifted to the blue laser excitation while the low frequency torsion 250 cm^{-1} vibration shifts to the red.

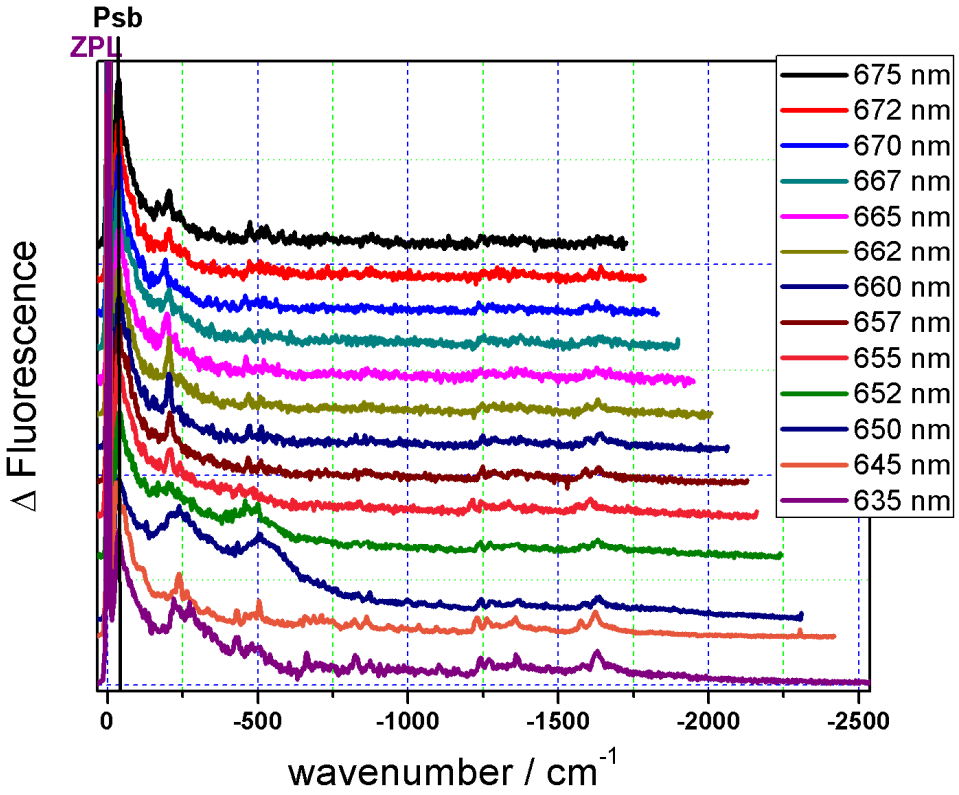

Figure 4.13 Vibronic region of the ΔFLN of the PBP antenna system of *A. marina* at 4.5 K. The Psb labels the phonon side-band while the ZPL is located at 0. (with a noise of 0.02)

This is an additional indication that the excited pigment at 635 nm induced a different vibration to the one of the other excitation wavelength (at 645 nm, 650 nm). The characteristic differenced at the 635 nm excitation is observed in the form of the symmetric double mode compose of 217 cm^{-1} , 273 cm^{-1} and the absence of 125 cm^{-1} and 250 cm^{-1}

while they are present at 645 nm excitation. Instead of the symmetric double vibration, a mode around 250 cm^{-1} is observed. Further observation at 645 nm is the energy gap of 40 cm^{-1} between 826 cm^{-1} and 866 cm^{-1} that is the characteristic energy gap of the dimer vibration of α_{84} and β_{84}. These bands of the HOOP mode are coupled with the low torsion mode of α_{84} and β_{84}. The excitations at 650 nm as well as 652 nm present a broad peak at 250 cm^{-1}, 500 cm^{-1} thereby reflecting a strongly coupled downhill EET of the 660 nm to 670 nm states, which affects the vibrational line of the mode at 250 cm^{-1} and 500 cm^{-1}. Further general observation supports a progressive blue shift of the 650 nm electronic transition towards the 675 nm excitation. In addition, the electronic transition of the 660 nm presents a double mode with energy gap 40 cm^{-1} that is characteristic of the low torsional dimer pigments of APC. Due to its spectral position it might be APC_E (APC_α_{84}) However, only a final comparison with the vibration of isolated APC_E can permit a final conclusion. Due to its spectral position, the final state at 675 nm is similar to APC_B (Bhalerao, 1995) and should be investigated further with the comparison of isolated APC_B. The vibration modes in figure 4.13 appear to be similar to the blue-shifted satellite holes which were seen using spectral hole burning. Some of these satellite holes have originated from the aforementioned C-H, C-N and C=C vibrational modes.

4.6 Insight the electronic structure of the phycobilisomes *Thermosynechoccocus Vulcanus*

4.6.1 Fluorescence Line narrowing

Figure 4.14 presents the absorbance of the *T. vulcanus* PBS (blue), the second derivative of the absorbance (black) and the fluorescence spectrum after excitation at 410 nm (red). In comparison to the PBP of *A. marina* different low states of the terminal emitter are observed from the PBS of T. vulcanus, while the upper state at 660 nm is similar. The fluorescence spectrum in red shows the presence of the new pigment near the rod core linker in addition to the one found by (David, 2011) at 635 nm. In comparison to the 635 nm pigment, this might be similar to the one found in the PBP antenna of *A. marina* as a low state of the PC. However the presence of a second state around 645 nm is an indication of a new pigment near the linker rod-core. The huge difference raises question about the PC low state inside the two systems, whether the linker is present or not. At first glance, it could be a monomer in the PBP case and the dimer in the PBS as well as two distinct pigments.

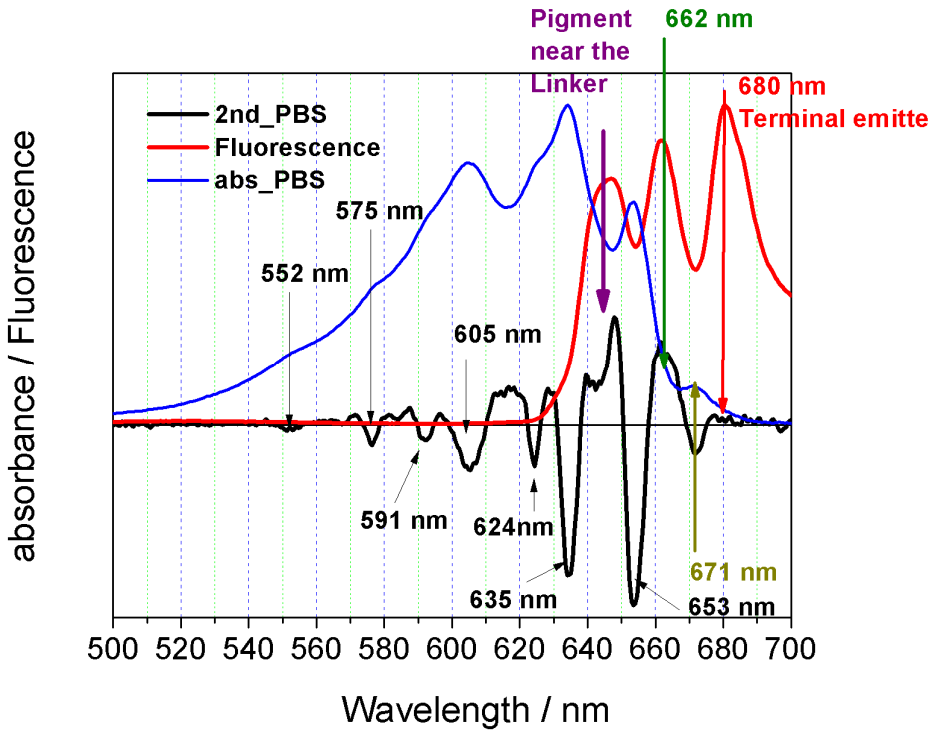

Figure 4.14 Inhomogeneously broadened absorption spectrum of Thermosynechoccocus vulcanus (blue) presents a more peaks of the aggregation states. The non-resonance fluorescence after excitation at 410 nm (red) shows strong and high peak absorption of the pigment at 645 nm as well as the asymmetric peak of the 662 nm and 680 nm pigment of the terminal emitter. The black curve is the second derivative of the absorbance.

Finally the FLN has hold the identification of the spectral position of the pigment near the core at 640-645 nm and the two states of the linker core membrane at 662 nm and 680 nm. By inspecting wile vibration can contribute in the excited state, we present below a ΔFLN after excitation at 630 nm.

4.6.2 Delta fluorescence line narrowing

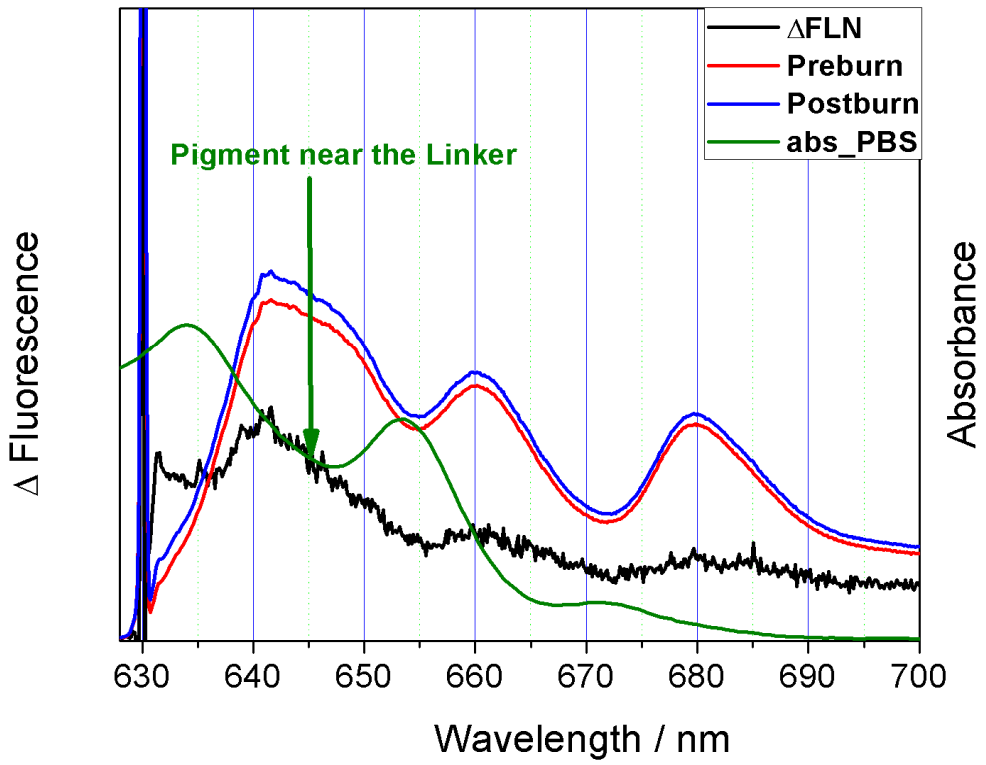

Figure 4.15 The inhomogeneously broadened absorption of the Thermosynechoccocus vulcanus (green). The fluorescence narrowing (FLN) for preborn (blue), post burn (red) and the delta fluorescence narrowing line (ΔFLN) (Black).

Figure 4.15 shows the inhomogeneously broadened absorption of the PBS *T. vulcanus*, while the blue and the red curves are fluorescence line narrowing (FLN) for pre-burn and post-burn, respectively. The ΔFLN spectrum is the black curve. The zero phonon line (ZPL) has been cut to allow a clear view of the phonon side band (PSB) at 631 nm. The strong asymmetry and the highly structured profile of one phonon are characterized by a weak peak at 631 nm for the ΔFLN spectrum, which is probably due to the non-resonant excitation of a pigment, which absorbs at this band. Further features are the inhomogeneously broad fluorescence peaks at the respective electronic site of the pigment near the core at 645 nm, the APC E at 660 nm and the APC B at 680 nm. Thus, these pigments show more fluorescence on the sub-compound electronic state than the terminal emitter at 680 nm. Interestingly, our observation comes with a near absence of double vibration modes on the ΔFLN spectrum in comparison

to the spectrum of the PBP antenna of A. marina. Thus, this is possibly due to stronger coupling between different compounds in accordance with the femtosecond absorption at RT.

4.7 Comparison of the electronic structure of the PBP of *Acaryochloris marina* and the PBS of *Thermosynechoccocus Vulcanus* by spectral hole burning.

4.7.1 Absorbance

Figure 4.16 provides a comparison between the PBP and PBS absorption at 4.5 K. Despite the different architectural organisation as well as the composition of the pigments, similarities were observed between the absorption spectra of the two antenna systems. These similarities are in particular the peak at 670 nm. This 670 nm peak is induced by the pigments in the L_{CM}. However, the PBS *T. vulcanus* in red displays a broader shoulder at 670 nm than the PBP of *A. marina*. Further similarity can be observed by the shoulder around 550 nm and 575 nm. The shoulder at 575 nm is a wavelength typically associated with phycoerythrocyanin, and it is suggested to be a high energy aggregated states in other cyanobacteria (MacColl, 1998).

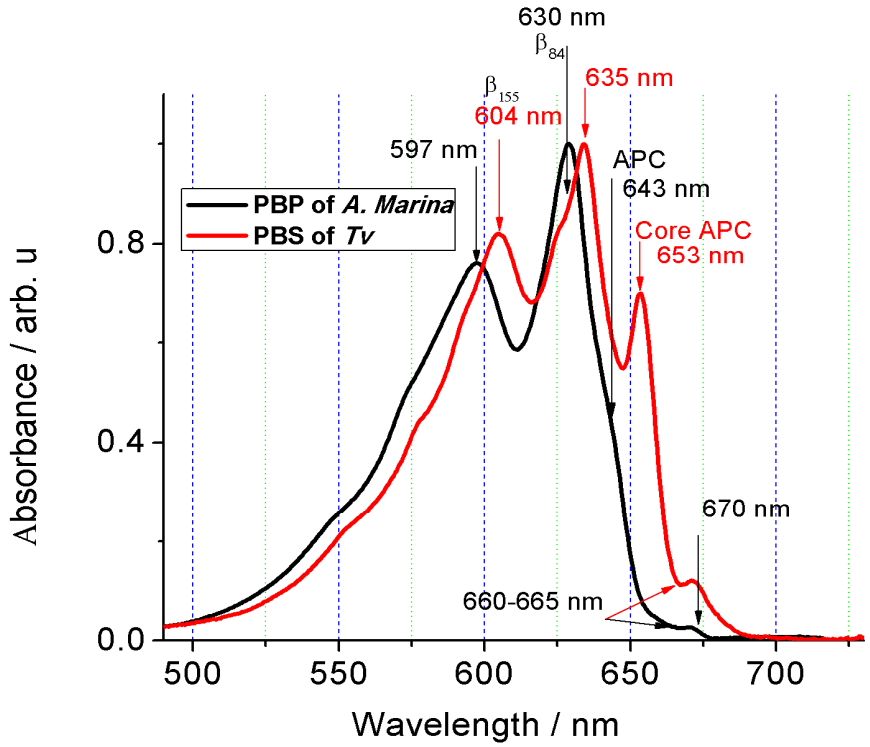

Figure 4.16 Comparison of the inhomogeneous absorption of the PBP antenna system of *A. marina* (black shaped) and the PBS of *Thermosynechococcus vulcanus* (red shaped) at 4.5 K.

The difference of the two absorption spectra is mainly the complete red shift of the spectrum of the *T.* vulcanus PBS probably induced by the presence of linker proteins inside the rod instead of the absence of those linker protein in *A. marina* PBP. Assignment of further features is directly labelled in the figure 4.16. A prominent shoulder between 630 - 635 nm highlights the effect of the linker proteins on the spectral shift in PBS of *T.* vulcanus in contrast to the PBP of *A. marina*.

4.7.2 Spectral hole burning comparison

Figure 4.17 shows a comparison of the hole burning at different wavelength between the PBS of *T. vulcanus* and the PBP of *A. marina*. The following conclusions specific to PBP of *A. marina* can be drawn:

(a) All the vibrations below 620 nm in the PBP of *A. marina* originate from trimer–trimer and hexamer–hexamer interactions. Some of these vibrations have been reported earlier (Debreczeny, 1992). These vibrations strongly depend on the excitation wavelength. Which has been seen to corroborate with the ΔFLN measurements (see Figure 4.13)?

(b) The upper region from 624 nm to the terminal state is strongly influenced by a strong coupling pigment that might lead to excitonic delocalisation, when an excitation occurs. The excitation at 634 nm, near or on the site of the low absorption state of PC, displays an anti-hole as re-absorption of the β_{84} and a hole on the maximum absorption of the α_{84} band. This is likely to be a fraction of the exciton that is delocalised on the site of the strongly coupled pigments, because of the disturbance of the 635 nm red-shifted pigment. This coupling has been observed in the anisotropy calculation after polarisation at 618 nm and probe at 630 nm for the PBP of *A. marina* in a high ionic strength environment.

A further product of the excited state formation after the excitation at 634 nm is also the downhill energy transfer to the APC band at 645 nm (labelled by the first arrow). In this APC band, a double vibrational mode of the dimer pigment β_{84} and α_{84} appears as result of the pigment protein coupling which was mentioned in Figure 4.10 and 4.11. As the energy is funnelled to the terminal emitter, two further double vibrational modes (labelled by the second arrow) appear to be delocalised between the APC band and the upper state of the linker at 660 nm. This suggests that the APC and the upper energy level are strongly coupled.

Hole burning PBS *T. vulcanus* **Hole burning PBP *A. marina***

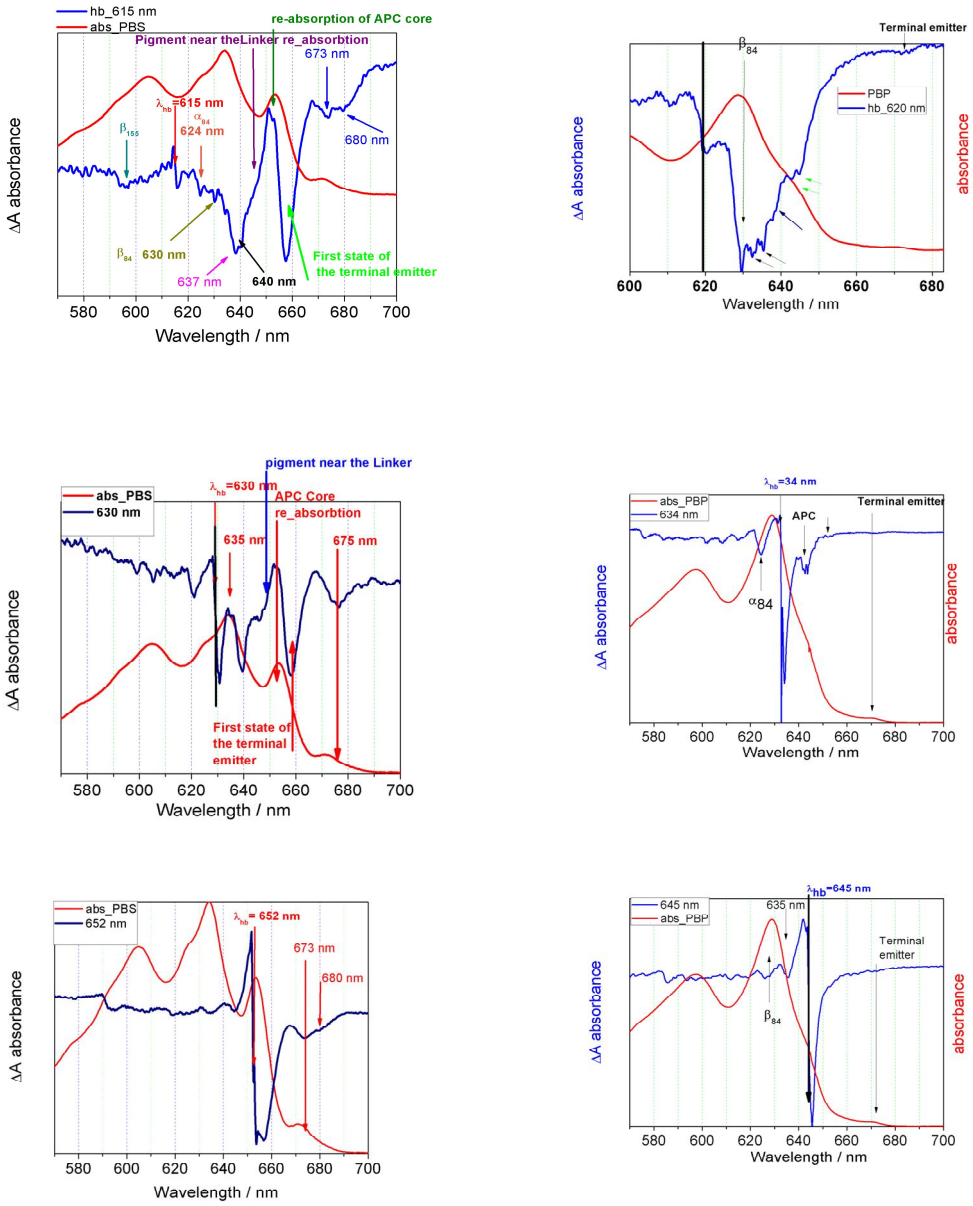

Figure 4 17 Comparison of the selective hole burning spectra between PBS *T. vulcanus* right side and PBP A. marina left side. The excitation wavelength and the future sub-band are labelled on each figure. The red curve represents the absorbance of each antenna system.

The 645 nm excitation induces a downhill energy transfer to the terminal emitter. Interestingly, it is the hole formation on the blue-shifted wavelength of an electronic state of PC at 635 nm and the β_{84} pigment. This supports the interpretation in point b. These electronic sites act as a trapping exciton site, which is strongly coupling with the 0-0

electronic transition of the APC. The 672 nm excitation displays a hole in an electronic upper state of the linker APC membrane. This also leads to the effect of a strong coupling between these states.

4.7.3 The PBS electronic structure

In this part devoted to the electronic structure of the PBP of *A. marina*, we suggest that the spectral band greater than 620 nm presents and electronic structure of strongly-coupled pigments. The PBS electronic structure is discussed as follows:

(a) The excitation at 615 nm induces a broad hole at the blue-shifted wavelength as a result of excitonic trapping which is probably induced by the β_{155}. The origin of the hole might be also due to the proximity of the adjacent rod. This proximity results in a strong interaction between the electronic sites of the β_{155} in the adjacent rod. The result of this interaction might be the formation of a delocalised exciton on the electronic site of these chromophores. As consequence of the excited state formation after the excitation at 615 nm, an absorption change is observed as a downhill energy transfer to the successively lower energies of the electronic states at 635 nm, 640-645 nm (pigment near the Core APC), 660 nm (the upper state of the linker core membrane) and 675 nm (near the lower state of the linker core membrane).

(b) The excitation of the electronic site of the β_{84} chromophore induces a downhill energy transfer to the terminal emitter at 675 nm. It is observed as a re-absorption of the maximum absorption band in PC at 635 nm. The latter appears with an asymmetric evolution of the absorption change in the electronic site of the pigment near the core. This is observed by a deep hole at 640 nm and shoulder at 645 nm. The energy is further transferred to the upper state of the linker core membrane at 660 nm.

(c) The 650 nm excitation of the Core APC displays in its hole burning spectrum a downhill energy transfer to the successive low energy states. The absorption of the upper state of the linker core membrane seems to be headed by the pseudo–PBS, while a broad hole is observed on the terminal emitter site at 672 nm. A slight shoulder indicates the site at 680 nm. In the blue-shifted wavelength different delocalised holes are observed. It is like located inside a broad cavity. This latter displays a clear edge cut-off in the region where a strongly-coupled electronic state seems to appear.

(d) When excited the at 670 nm (which is between the low state of the terminal emitter and its upper state), the energy flows to the low state at 680 nm and an additional state at 686 nm. As a consequence of strong coupling between the electronic states, different holes appear on the blue side of the spectrum. At the 662 nm we observed a hole due the coupling with the upper state of the linker core membrane. Moving a deeper into the blue end of the spectrum, one can see broader and deeper holes, which are evidence of the coupling with the Core and the pigment near the Core.

5.8 Concluding remarks

Based on the insight above, the PBS electronic structure of *T. vulcaus* and the one of the PBP of *A. marina*, some similarities appear on the electronic structure of the linker Core membrane in PBS in comparison to that of the linker APC membrane in the PBP of *A. marina*. Here are the conclusions:

i. The upper states of this linker are located around 660 nm, while the lower energy state seems to be located at a different spectral band.

ii. The electronic state of the linker seems to be more complex, as it has a different sub-band that will require further investigation

iii. The two antenna systems efficiently transfer the energy to the low state.

Finally, this section has shown many differences in the electronic structure between the PBP of *A. marina* and the PBS of *T. vulcanus.* The first strong contrast is the presence of an excitonic delocalised state around 600 nm – 615 nm in the PBS of *T. vulcanus* and its absence in the PBP of *A. marina*. All the electronic states of the PBS of *T. vulcanus* seem to be strongly coupled to the terminal emitter, while only the band greater than 620 nm in the PBP of *A. marina* is strongly coupled to the terminal emitter.

A Summary of the spectral comparison of these two systems is now presented. The spectral hole burning has been grouped for each species. In a) we have the entire spectral hole burning of the PBP of *A. marina* and in b) the one for PBS *T. vulcanus*. The important features have been labelled.

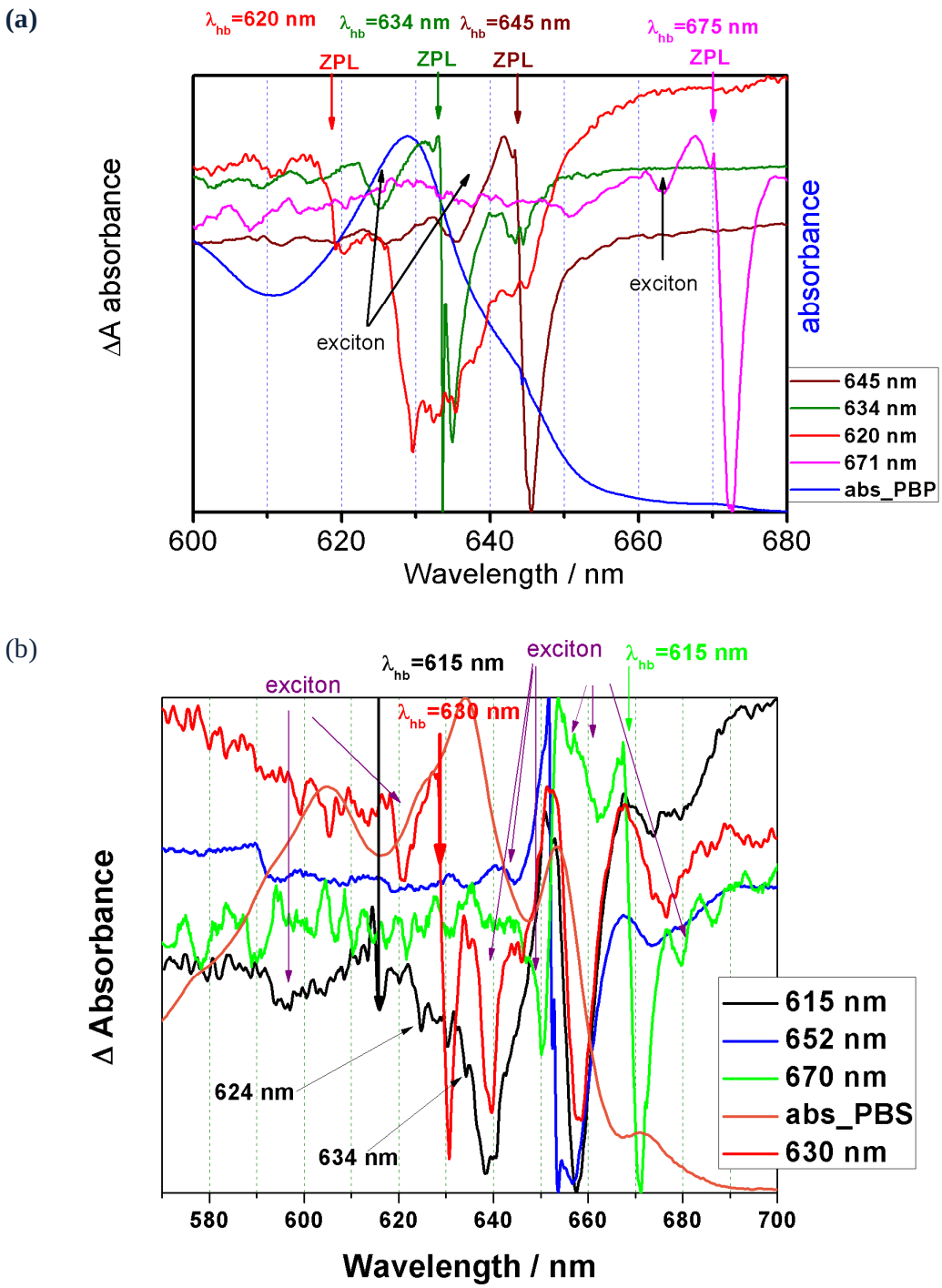

Figure 4.18 Resume of the hole burning spectra from (a) *A. marina* and (b) *T. vulcanus*

Figure 4.16 shows a resume of the hole burning at different wavelength. From this comparison resume, the following conclusion can be drawn:

a- The strong excitonically coupled pigments influence the energy transfer on the high energy state of PC in *T. vulcanus*. These strong coupling pigments originate to the proximity of the adjacent PC rod. This effect is absent in the high-energy PC band in *A. marina*.

b- In addition to the 635 nm pigment found by (David, 2011), the low electronic state of the PC between 639 – 645 nm is likely to have a different sub-bands. The first shoulder appears between 639 - 640 nm, the second between 640 – 641 nm and the third between 642 – 645 nm are all characteristic of different states, where the first and the second state seem to be more strongly coupled. These sub-bands of the pigment near the linker L_{RC} plays a key role in the fast kinetic of the EET (~900 fs) by changing its slope. This causes an accelerated EET kinetic. This pigment is strongly coupled to the L_{RC} and the first state of the terminal emitter through electrostatic interaction.

Having discussed the EET components in cyanobacteria using different technical analysis, we would like to turn attention in the next chapter to the high plant light harvesting LCH II.

5 The Influence of Aggregation on the Excitation Energy Transfer Processes in LHC II

It is well known that light-harvesting pigment-protein complexes (LHCs) in the thylakoid membrane serve as outer antennae to capture light energy and deliver it to photosynthetic reaction centres (Lokstein, 2007). LHC II contains a set of polypeptides and forms homo- and heterotrimers[6]. LHC II is found mostly in a trimeric form, but some monomers can also be found (Jansson, 1994). The LHC II trimer not only absorbs and transfers excitation energy, but also plays an important role in excess energy dissipation and regulation of energy distribution between the two systems (Lokstein, 1994). Its role in the formation of grand stacking is highly questionable (Lokstein, priv. comm). Its structures are shown in Figure 5.1 below.

It has been reported that the conformation of LHC II can be altered through the aggregate state, which can also lead to fluorescence quenching and is possibly related to photo-protection (Lokstein priv comm). Spectral analysis of pigment-protein complexes in relation to their aggregation size is of primary importance in understanding the mechanism of the EET in photosynthesis (V. Barzda, 2001).

The detergent n-dodecyl β-D_maltoside (β-DM) is a water soluble non-ionic detergent often used for isolation and stabilization of membrane proteins (Zouni,2001; Voigt, 2008; Barzda, 2001). In the literature, there is a wealth of studies on β-DM beyond the scope of this work, which shows the ability of β-DM to preserve protein activity by dual hydrophobic/hydrophilic properties. These properties allow lipid displacement and provide a lipid-like environment for membrane proteins.

[6] Homo come from homogeneous, which mean similar and heterogeneous which mean different. Homo-trimer therefore means only trimer, and hetero-trimer is a mixture between trimer and monomer.

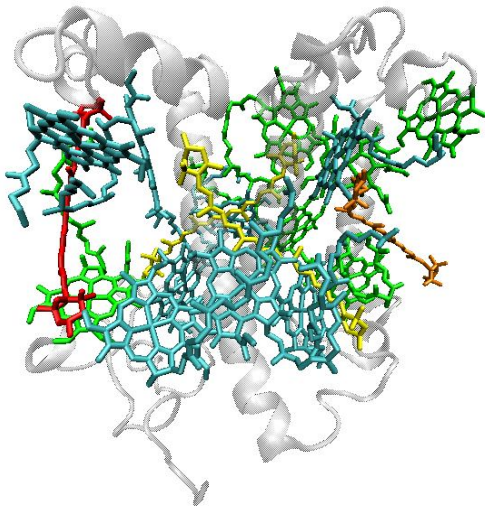

Monomer:

- 8 chlorophylls a
- 6 chlorophylls b
- 2 luteins
- 1 neoxanthin
- 1 violaxanthin
  (antheraxanthin. Zeaxanthin)

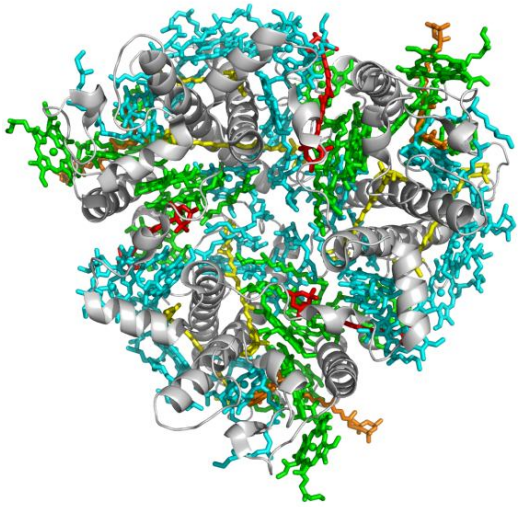

Trimer

Figure 5.1: Structure of trimeric LHC II and the monomeric subunit. Structures were drawn from the PDB data file 2BHW using VMD. The structure of trimeric LHC II was taken from Lokstein (H. Lokstein, 2007) and the structure of monomeric LHC II was taken from (Lokstein priv comm), with kind permission from H. Lokstein[7].

The control of LHC II terminal emitter by the aggregation state size leads to a challenging issue in the EET process. In the present work, β-DM has been used to influence the aggregation size of LHC II, especially affecting its excited state lifetimes (Voigt, 2008). The aggregation state of LHC II has been influenced by different amounts of the detergent β-DM in the buffer solution containing LHC II. The critical micelle concentration (CMC) is defined as the concentration of surfactants above which micelles are spontaneously formed caused by β-DM, which is 0,01% (Barzda, 2001). LHC II has been found to be completely trimeric at 0.06 % (Voigt, 2008).

The above-mentioned aim was achieved by flash induced absorption changes in the time domain of the EET in LHC II with different concentrations of β-DM, which were obtained by two-colour and multi-colour pump–probe techniques. This was done with the help of a lock-

[7] I would like to express my deep gratitude to H. Lokstein who provides me with the samples investigated in this chapter.

in-technique for better sensitivity as well as multi-colour pump-probe technique for the overall spectrum of different bands in time domain.

5.1 Spectral analysis of the LHC II with different β-DM concentrations

Figure 5.2 shows the absorption spectra of LHC II with different concentrations of β-DM. Only a weak difference appears at 472 nm whereas all the aggregates of LHC II seem to have the same absorption curve at 650 nm for a donor spectral band Chl b as well as all sub-bands of the acceptor Chl a wavelengths.

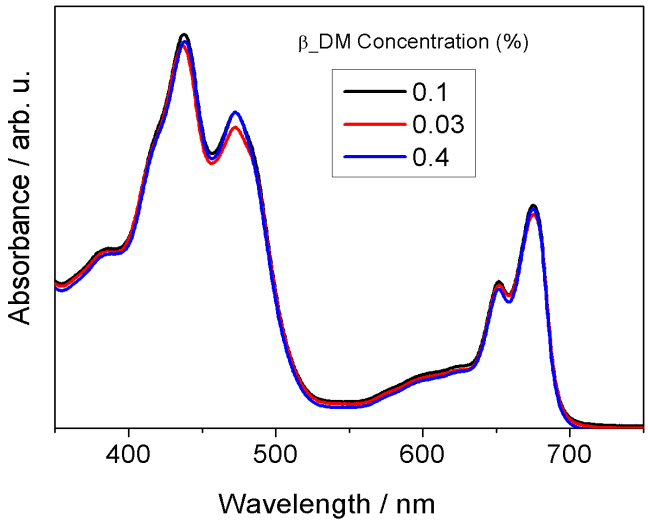

Figure 5.2: Absorption spectra of LHC II with different concentration of β-DM at RT.

The absorption of LHC II is relatively insensitive to different aggregation states (Voigt, 2008), which were varied by changing the concentration of β-DM.

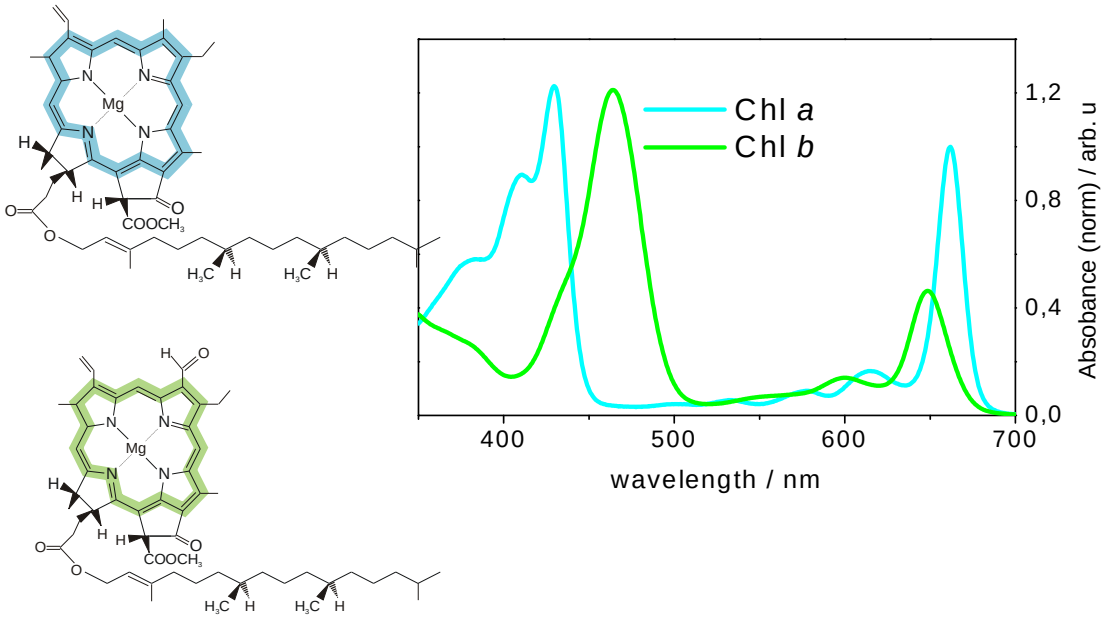

Figure 5.3: Chlorophyll a and b chemical structures and absorbance spectra, reproduced with courtesy of H. Lokstein.

Figure 5.3 shows the absorption band of Chl b and a. Comparing figure 5.3 with figure 5.2, we see that the spectral band of Chl b and a is preserved inside the LHC II complex independently of the aggregation state. We had excited the Chl b spectral band at RT and therefore expected the energy to be transferred to a different Chl a sub band. The ß-DM concentration influences the aggregation state size, so we would expect this to determine the terminal emitter sub-band of the Chl a.

5.2 Comparison of flash induced absorption changes spectra of LHC II within 0.03 % and 0.4 % of β-DM.

Figure 5.4 presents, at 650 nm excitation, the excited kinetic spectra of the donor pigment Chl b at 0.03 % and 0.4 % β-DM concentration in buffer with LHC II. No difference in the Chl b kinetics was observed at this wavelength, although the concentration of the β-DM was quite different. The relative amplitude (ΔA) of the acceptor sub-band Chl a shows, at 674 nm, a higher intensity at 0.03 % β-DM than at 0.4 % β-DM. This difference seems to be less at the lower sub-band energy of Chl a (682 nm).

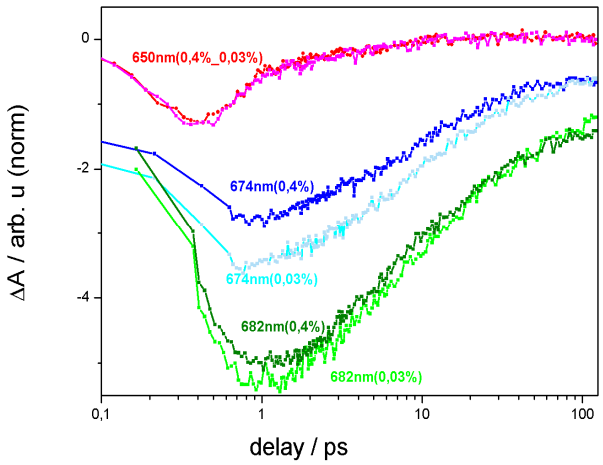

Figure 5.4: Comparison of flash induced absorption changes at different β-DM concentrations for different wavelengths in the Chl a spectral region. The percentage of the β-DM is given in parentheses. I_{pump} =50 nJ.

Figure 5.4 displays the absorption change trace at different probe wavelengths from the LHC II with different β-DM concentration.

a. The *Chl b* trace shows the same evolution of the amplitude independent of the β-DM concentration.

b. The *Chl a* trace at 674 nm displays a significant change in the amplitude. The larger aggregate size seems to harvest more light than the smaller, which is fully trimer. This is also weakly observed at 682 nm. The fully-recovered signal after 100 ps at 674 nm and 682 nm between *Chl a* in 0.03 % and 0.4 % β-DM may be due to singlet-singlet annihilation. Further investigations with different pump intensities are however needed to clarify this point.

To get more information on the influence of the β-DM on the aggregation sites, the sample was also probed with white light after excitation at the same wavelength of the donor Chl b spectral at 650 nm.

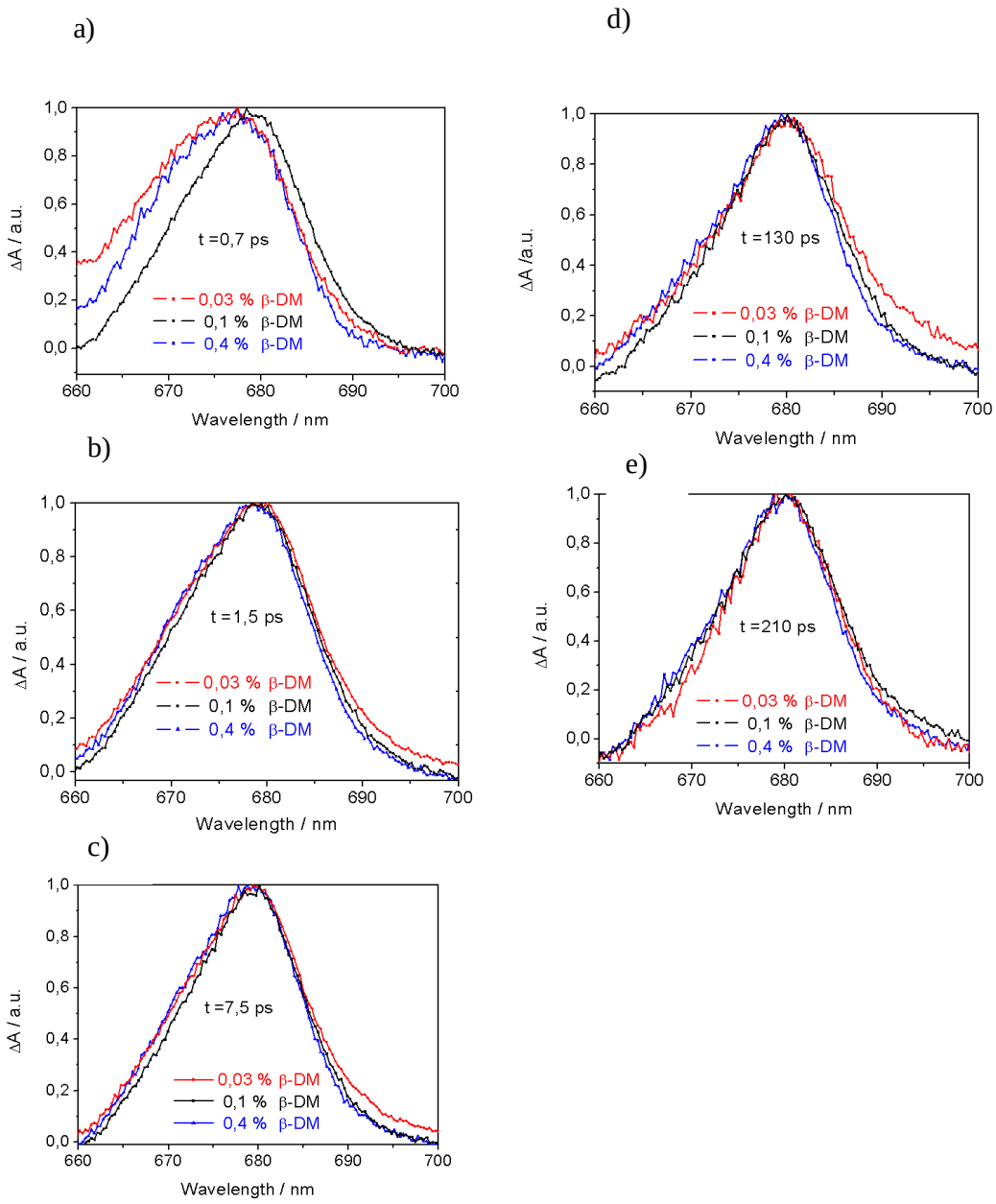

Figure 5.5: Transient absorption change trace of the acceptor sub-band at different β-DM concentrations are listed on each spectrum within a specific delay time a-e (this measurement has been recorded using the multicolour setup by Christoph Theiss.)[8]. All the traces are normalised to 1.

Figure 5.5 shows the influence of the β-DM concentration on the spectrum of the acceptor pigment at different wavelengths i.e. 660 nm – 700 nm, and different delay times after

[8] The author of the above transient absorption trace did not provided me with the experimental condition. Therefore, all assumptions on these results (figures 5.5 and 5.6) should be further verified.

excitation. The *Chl a* sub-bands seem to be dependent on the β-DM concentrations in figure 5.5 a. Comparing the 0.4 % and 0.1 % β-DM concentration, the curve width of the 0.4 % β-DM sample is lower than the 0.1% sample. However, between 674 nm and 700 nm the sample with 0.1% β-DM concentration at short wavelengths of the acceptor presents an inverse effect within a red end of ΔA curve. In addition, 0.4 % β-DM concentration exhibits slightly higher width than 0.03 % β-DM concentration between 685 nm and 700 nm.

In figure 5.5 b - d, the β-DM concentration changes the width of the absorption change trace. The high concentration of β-DM shows the same curve width while the 0.03 % shows a broader width of the amplitude curve, whereas at short wavelength between 660 nm and 674 nm, only a slight difference is observed between 0.03 %, 0.4 % and 0.1 % β-DM concentration.

Comparing the observation of the amplitude width at 130 ps, we can say that the width of the ΔA curve increases for a higher β-DM concentrations (see figure 5.5 d) than at 1.5 ps and 7.5 ps (see figure 5.5 b and c). Up to a time of 200 ps, the width of the ΔA curve recovers. It is likely the terminal emitter did not strongly depending on ß-DM. This is However, there is a slight difference for the protein pigment complex containing 0.1% ß-DM in the buffer (see figure 5.5 e). Furthermore, a pronounced shift in the absorption trace is not observed when compared to Voigt's work (Voigt, 2008).

Based on the spectral observation above, the time evolution of the terminal emitter, as influenced by the size of the aggregate states, cannot be properly evaluated. To have further insight the shift we compare the maxima shift of their absorption (see figure 5.6). Spectral analysis of flash induced absorption changes of LHC II within different concentrations of β-DM can be observed in figure 5.6. This Figure illustrates the maximum absorption in time of each LHC II within 0.03 %, 0.1 % and 0.4 % of the β-DM inside the buffer.

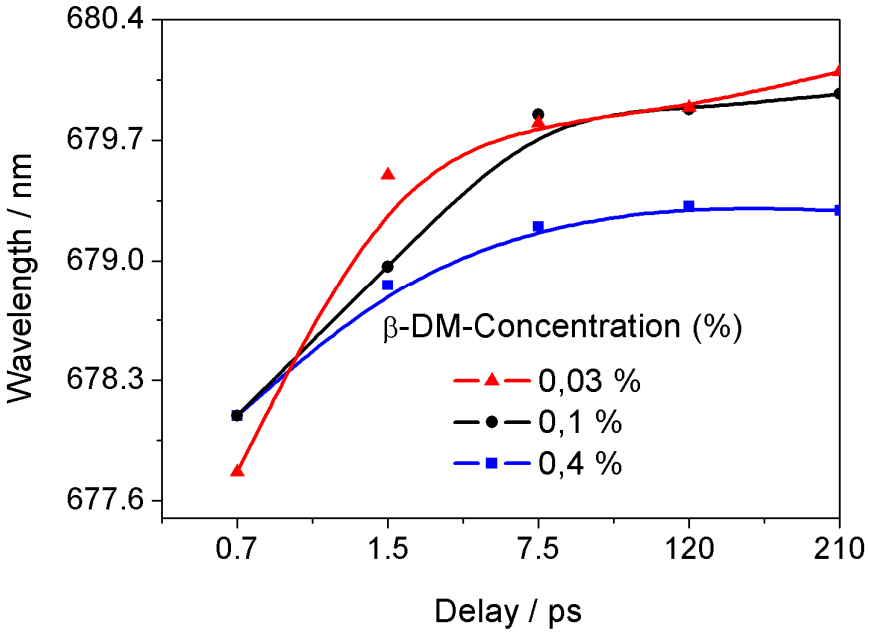

Figure 5.6: Maximum of the flash induced absorption changes depends on the delay time of the terminal emitter at different β-DM. Data obtained from the trace of Figure 5.5.

The terminal emitter absorption shows an increasingly divergent course in time for the various β-DM concentrations. The similarity observed on the largest aggregate size (0.03%) and the trimeric (0.1%) can be an indication of the fraction of the trimeric aggregate states present in the LHC II. A size of 0.03 % is high enough to induce quenching of the terminal emitter inside the mixture of monomer and trimer (Barzda,1998) (Barzda, 1994). The trimeric aggregate states are faster than the mixed aggregate states. Exact information about the EET components can however not be provided, as all exact experimental conditions are not known. To overcome this point, the experiment was repeated with a two-colour pump-probe system.

Figure 5.7 shows that flash-induced transient absorption changes the spectra of EET components after excitation at 650 nm. At 650 nm, no significant difference in the shape of the recovery kinetic of the donor is observed at different β-DM concentrations, although there is a slight difference in the amplitude ratio. Two fast components, 4.6 ps and 430 fs, of the kinetic might lead to excitonic coupling between Chl b. The faster 430 fs is 0.4% higher at 0.03 % β-DM concentration than 0.4% β-DM, while the 4.6 ps component of the EET show the inverse process, which is 2.1 % more ΔA in 0.4% of the β-DM concentration than 0.03%.

In the same figure (5.7), we observe a weak alteration profile of the Chl a sub-band at 674 nm, which is caused by a higher β-DM concentration. Three lifetimes 4.3 ps, 25.5 ps and a kinetic of more than 200 ps of the terminal emitter have been found. The kinetic greater than 200 ps is the lifetime of the Chl a, which is out of range of the measurement setup. The sample with a lower β-DM concentration of 0.03 % seems to have a longer lifetime than that with higher concentration of 0.4%. Therefore the largest aggregate states (0.03 %) show a dominant slow kinetic in comparison to the than their smaller size aggregate states (0.4 %).

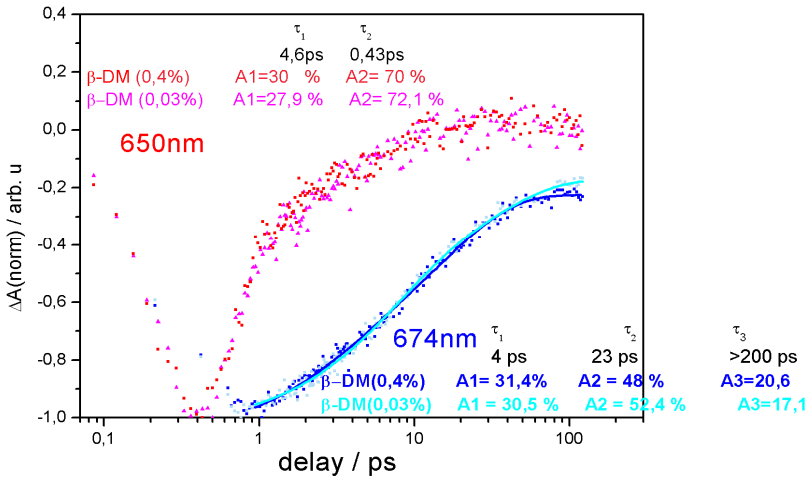

Figure 5.7: Comparison of the normalized flash induced absorption changes of LHC II at different concentrations of the β-DM in the buffer after excitation at 650 nm and probing at 674 nm.

Figure 5.8 shows the flash induced absorption changes of the EET component at 650 nm and at 682 nm after excitation at 650 nm of the LHC II pigment for the 0.03% and 0.4 % concentrations of the β-DM detergent inside the buffer. The kinetics 4.3 ps and 25.5 ps, and the kinetic of more than 200 ps of the EET energy transfer components at 682 nm were obtained by multi-exponential decay fit. Comparing the sub-band of Chl a (674 nm, 682 nm), we observed an increase of the amplitude of the fast component 4.3 ps for the reduced size of the aggregate states at 682 nm. The largest aggregate states are dominant for the 23 ps at 674 nm and 25.5 ps at 682 nm. This might be induced by the annihilation (exciton) that takes place in the inter trimer - trimer EET.

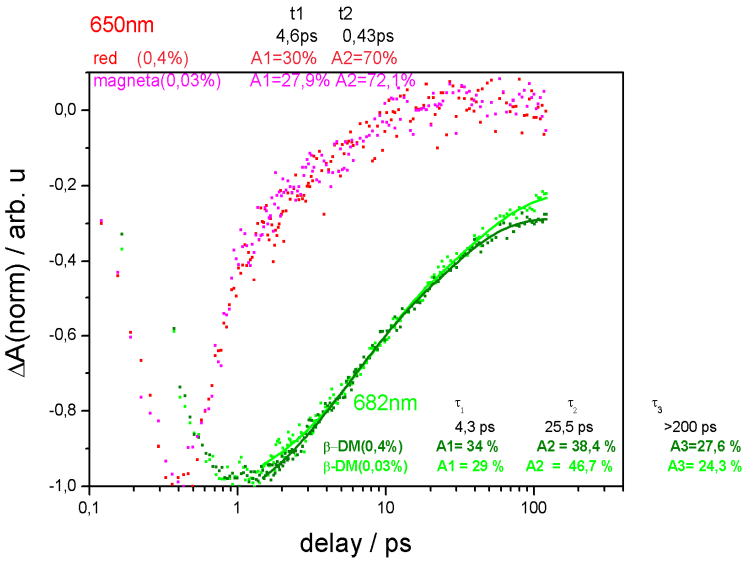

Figure 5.8: Comparison of the normalized flash induced absorption changes of LHC II at different concentration of the β-DM in the buffer after excitation at 650 nm and probe at 682 nm.

5.3 Discussion

The trimerisation of the LHC II aggregates controlled by the amount of the β-DM concentration (Voigt, 2008) certainly influences the size of their aggregate states. However, a weak influence of β-DM concentration in their dynamics is observed in contrast to that discussed by Barzda (Barzda, 2001). Barzda claimed that by decreasing the size of the LHC II aggregate states, trimerization slows down the kinetic of the acceptor and the largest aggregate state exhibits faster kinetics. The almost full-recovery of the kinetic after 100 ps between large and small aggregate sizes which is shown in figure 5.4 at 674 nm and 680 nm may support the latter assertion. However, a comparison of the excited state decay of large size (0.03% β-DM) and small size (0.4 % β-DM) aggregates does not show a significant change in the kinetic components to support faster decay of larger aggregate states instead of the smaller one. The annihilation that might be present in high pulse excitation might play a role of no less importance in the kinetic components. This issue needs further investigation.

Finally, we observed the energy transfer from *Chl b* to *Chl a* in LHC II, without a pronounced influence of the β-DM.

After having discussed the influence of β-DM on the size of the LHC II aggregate states, as well as their excited state decay components using time resolved pump-probe measurements,

we would like to direct the reader's attention to the next chapter that contains work on mimicking artificial photosynthesis reaction centre.

6. Evidence of Charge Transfer in an Artificial Photosynthesis System

Recently, the construction of protein-based artificial reaction centres has become a research topic field of highest relevance in the fields of artificial photosynthesis and new methods of energy conversion. The techniques start from a simple assembly between a donor-acceptor protein complex with electronic binding sites for pigments, as described by Collings in his book Artificial Photosynthesis (Collings, 2005) and they are applied in a recent study by Drori (Drori, 2010). How an artificial system for photosynthesis could be produced, is presented in Collings book (pg. 132) where he claimed, "*Much is known about how to create such a simple design from the structural analysis of natural systems*". He suggested an incorporate cofactors into a helical structure in order to modulate their redox properties and control their geometry (Hitoshi, 1998; Balaban, 2005). Directional ET can then be created by adjusting the location of the cofactors on the protein scaffold (Collings, 2005; D. Robertson, 1994).

Regardless of the specific chemical reactions that are coupled to the ET, all RCs are efficient solar energy converters. This is because the primary radical pair is stabilized by a series of fast and efficient short-range electron transfer steps (picoseconds to nanoseconds) that can lead to a stable charge separation across a distance (Holzwarth, 2006). This stable charge separation is a consequence of secondary electron transfer events that occur on the order of tens of micro- seconds and are unique to the protein environment (Holzwarth, 2006). The high quantum efficiency for charge separation and the synthetic peptide folded in the presence of the metalloporphyrin, which gives rise to a single conformation in solution and self assembly, has been a driving inspiration for creating artificial photosynthesis systems (Röger, 2006; Tamiaki, 1998).

The advantage of the helical bundle proteins can be readily modified without loss of their structural integrity, as shown by NMR spectroscopy (Gibney, 1999) in order to monitor the self-assembly in an efficient way (Balaban, 2005).

It has been demonstrated that the design thus allows the incorporation of organic cofactors or transition metals into structurally related variants to create artificial redox-active proteins. These proteins can be achieved in particular by heme maquettes through cytochrome where the redox potential spans over a range of 800 mV (Gibney, 1999; Collings, 2005).

The redox potential can be modulated by altering the electron-donating accepting the nature of the peripheral macrocycle substituent of the heme and the protonation/deprotonation state of neighbouring charged residues (Shifman, 2000; Jentzen, 1997). Furthermore, structural distortion of the porphyrin macrocycle may also play a role in tuning the ET. Besides, it has been shown that the modification on the π-π band cannot strongly increase the probability of ET (Starikow, 2009).

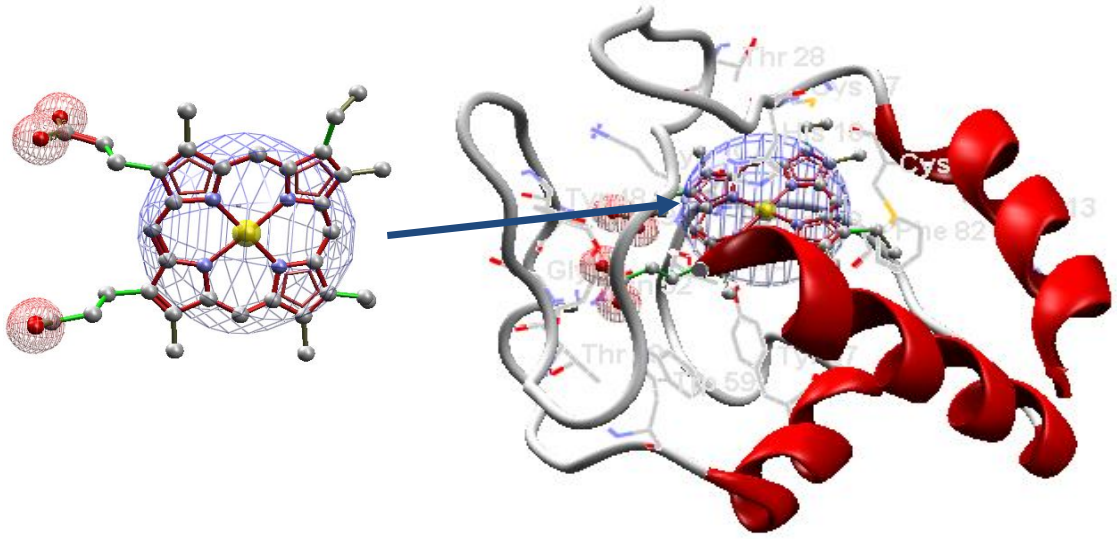

Figure 6.1: Left-side secondary structure of cytochrome c (Hem) with a charge distribution, and right-side cytochrome c (1hrc)

Figure 6.1 shows the interior pocket of the cytochrome c, which displays a dipole moment. The blue sphere of the Hem incorporates the positive charges, while the red spheres show the negative charge distribution. The entire protein matrix shows how the positive charge of the hem sequesters the negative interior pocket of the alpha helices by a strong electrostatic

interaction. The negative charge of the Hem remains free as well as the exterior pocket of the alpha helices, which are negatively charged. An assembly with any ligand would start by sequestering the negative pocket of the cytochrome c by its partner in the ligand. An example is PaCD. When this happens, a directional ET transfer can occur in the Hem band as result of a hem reduction.

A directional ET was reported between an N,N-dimethylaniline donor and a pyrene acceptor attached to two peptides that were different in the positions of the donor and acceptor with respect to the helix ends (Fox, 1997). It turns out that a PaCD can also bind the Hcc through an N bridge acceptor where directional ET can happen. The directional ET was ascribed to the helix dipole moment; however, such an effect was not observed when ET between polar metal complexes in a metallopeptide was studied (Fedorova, 2003). By varying the distance between two ruthenium ions attached to a three-helix bundle motif, strong distance dependence for the electron transfer rate was observed, indicating the structural integrity of the robustly designed protein.

Earlier work has shown that stable π-cation radical of Chl as well as a chlorine ring can undergo charge separation after excitation (Balaban, 2005), (Fajer, 1974), whereas self assembly of chlorine can drive the quenching rate (Lammi, 2001). Therefore, the synthesis of a novel ligand donor complex, which can efficiently harvest light and drive an electron, will be a challenging donor for an artificial photosynthesis RC. According to the functional flexibility of the natural system in employing various chlorophylls, even in the RC as the primary electron donors results from the fact that they all share the common chlorine ring, the PaCD seem to be a better derivative of chlorine ring for an electron donor.

The central metal ligation appears to be a decisive factor for the natural system choosing between a Chl or a Pheo molecule (Balaban, 2005). This implies that the binding site is actually tailored for Chl, with the entire ring and the phenyl tail buried inside the protein, thereby making contact with residues in distant helices. This complicated binding mode makes the design of small proteins with such a binding site very challenging and drive alternative binding issue through PaCD. Studies of PaCD binding can also be done with some relatively simple natural proteins to gain insight into the mode of PaCD-protein interaction and to construct a RC in these proteins by introducing electron acceptors and donors.

In this chapter, we first report a new functional artificial reaction centre based on the chlorine dendron–oxidized horse heart cytochrome c. Here the chlorine dendrone derivative of

pheophityn a (Pheo a) serves as an energy trap. Subsequently, as an electron donor for oxidized cytochrome c, and the novel self-assembly of an artificial RC might be also a better stabilizer of the excess EET when ET occurs at the same time.

Regardless of the ET that can occur via an overall hopping process inside the protein membrane as well as an intra-binding residue site through a polypeptide chain, we will first present the absorbance site of our donor-acceptor protein complex. Then the dynamics of the pigments involved inside the complex will be discussed, and the evidence of the charge transfer will be addressed.

6.1 Mimicking the Electron Transfer through an Artificial Reaction Centre of Photosynthesis system

In cooperation with (Schmilinsky, 2010) from the Fraunhofer Institute for Biomedical Engineering (IBMT) in Potsdam, we obtained samples that could mimic the electron transfer through an artificial photosynthesis system. We wanted to investigate the possibility of a charge separation in a special chlorine-cytochrome complex. This complex, contains a pheophytin a (Pheo a) derivate (referred to as PaCD) and a horse heart cytochrome c (referred to as HCC). Judging from steady state absorption and fluorescence spectra the group at the Fraunhofer Institute considered this PaCD-HCC complex as a possible donor-acceptor couple which could be used as the reaction centre in an artificial photosynthetic system. The aim was to investigate the possibility of flash-induced electron transfer from the donor PaCD to the acceptor HCC. The results obtained are as follows: the absorbance spectrum of donor-acceptor protein complex, and the flash induced transient absorption changes in the time domain.

6.2 Absorbance spectrum of the ligand – oxidized receptor protein complex

Figure 6.2 shows the absorption spectrum of the sample of pure PaCD with different concentrations of the oxidized HCC. The sample of zero concentration (PaCD) shows a dominant peak at 667 nm and three others at 520 nm, 550 nm, 620 nm. By adding progressively different concentrations of HCC from 0.08 mM to 0.8 mM one observes two important phenomena. The peaks at 520 nm, 620 nm and 667 nm are 10 nm, 2 nm and 5 nm red shifted respectively, while the one at 550 nm is 3 nm blue shifted to the Q-band of oxidized HCC. Apart from the maximum peak at 667 nm, which remains almost constant, the

other peaks grow. To get more insights into the absorbance spectra, we present in figure 6.3 the difference between the absorption of the ligand and the receptor, as function of the wavelength.

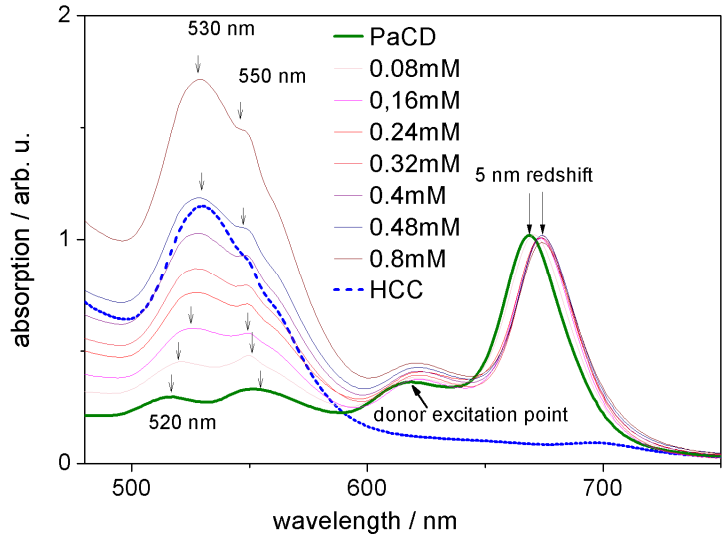

Figure 6.2: Absorption of PaCD with different oxidized Cytochrome c concentration[9]

Figure 6.3 confirms the disappearance of the 520 nm spectral band of the ligand (PaCD) towards the creation of a 530 nm Q-band of the acceptor protein HCCox (oxidized HCC), and the remaining 550 nm spectral band of the ligand is an indication of the formation of the complex protein PaCD-HCCox (HCCox is the oxidized HCC receptor). The 667 nm spectral band of the complex protein ligand – receptor shows the influence of the water dipole moment on the ligand's spectral band. The increased concentration of the receptor decreases the influence of the water towards the complete annihilation of the effect of the water dipole moment due to the absorption of the water by the complex protein ligand – acceptor. The 21 nm minimum-maximum is characteristic of the interaction between water molecule and the protein complex.

[9] Point stands here for absorption band

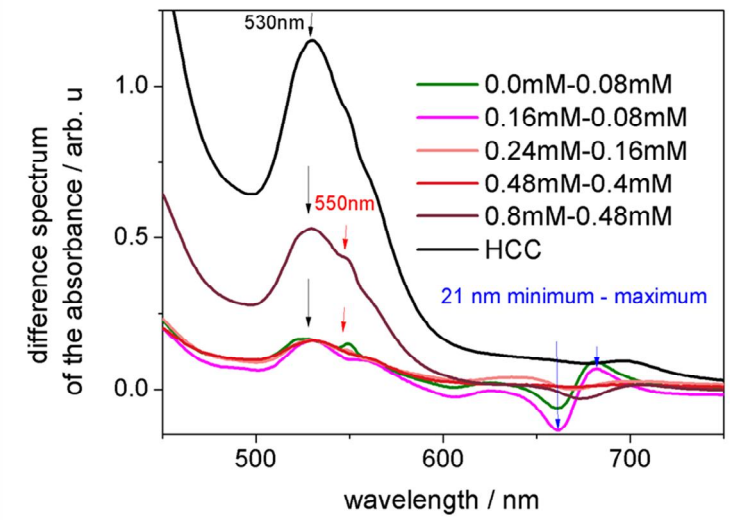

Figure 6.3: Difference spectrum of the absorption of the ligand – oxidized receptor. The subtractions are labelled on the figure.

In the interval concentration of 0.24 mM to 0.48 mM, the effect of water on the 667 nm spectral band disappears. It may be that the entire water molecule is absorbed. This can be an indication for an optimal concentration of the acceptor for efficient charge transfer in the protein complex formation. The hole observed at 662 nm, which shifted to the 667 nm spectral band at high concentration of 0.8 mM leads to another interpretation of the dipole moment of the protein complex at this wavelength.

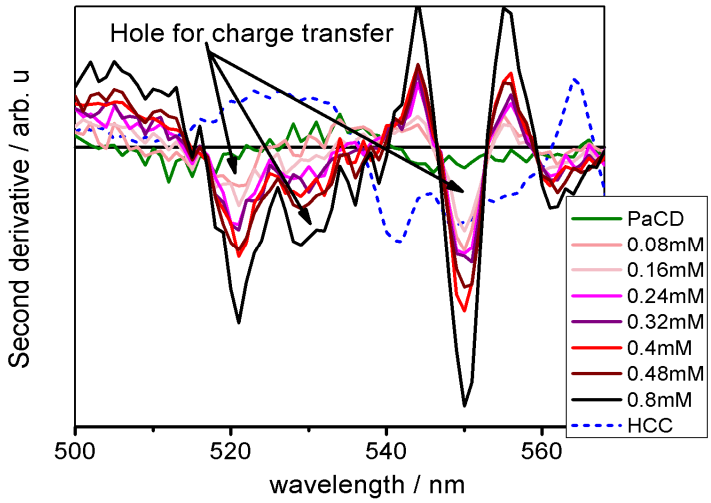

Figure 6.4: Second derivative of the absorption spectrum of the PaCD at different concentrations of the oxidized HCC in the range of 500 nm to 580 nm. (Hole for charge transfer means possible trapping electronic site)[10]

Figure 6.4 shows inhomogeneous electronic trapping states for charge or transfer where the dominant one is located at 550 nm. The depth of the hole strongly depends on the concentration thereabouts for the size of the protein complex. The first accession to be made from 6.5 is the spectral homogenization of the PaCD band into an all-protein complex formation, and the second one is the spectral shift at 667 nm to the pure PaCD and a lower concentration of the protein complex PaCD – HCCox towards a high-aggregation state, which is induced by a high concentration of HCCox. This spectral wavelength will later give us information about the stabilization of the excess excitation energy transfer (EET).

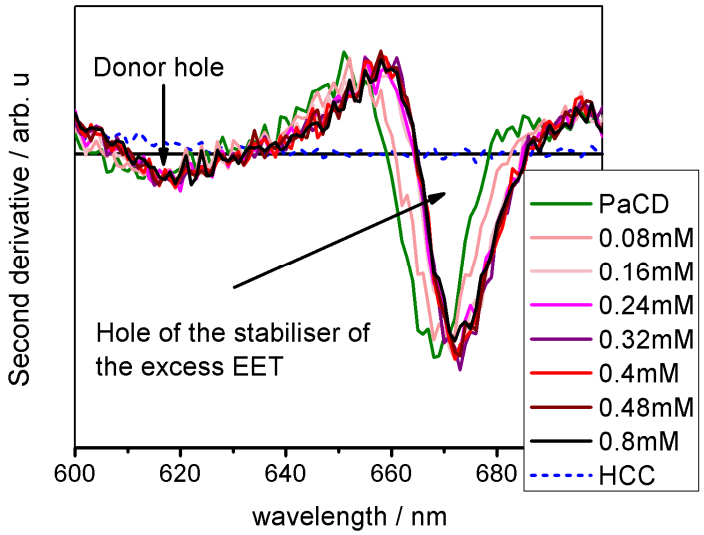

Figure 6.5: Second derivative of the absorption spectrum of the PaCD at different concentrations of the oxidized HCC in the range from 600 nm to 700 nm. (Donor hole means electronic site of the donor)

In comparison to the different spectra of the absorbance (figure 6.3), the 520 nm, 550 nm bands of the PaCD rise for the increased concentration. This means these electronic states of the PaCD are coupled with the Q-band of HCCox. In order to have comparative information about the complex protein formation between PaCD and the reduced heart horse cytochrome

[10] Hole stands in this chapter for absorption band.

c (HCC), we present below the absorption spectrum at a lower HCC, optimal HCC (the disappearance of the dipole moment of the water molecules) and a higher HCC concentration.

6.3 Absorbance spectrum of the ligand – reduced protein complex.

In comparison to the ligand–oxidized receptor protein complex, figure 6.6, which shows the absorbance of a protein complex PaCD-reduced Hcc, does not have 530 nm absorption peak. The two spectral bands of the ligand (PaCD) are preserved whereas the broadening form shifts to the sharp form. The 667 nm spectral range preserved the 5 nm red shift, which is an indication that the expected physical effect into this spectral range might be independent of the oxidized or reduced from of HCC.

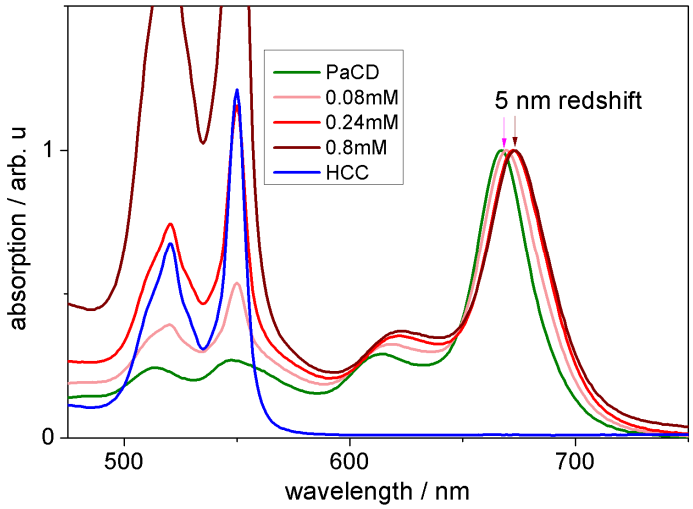

Figure 6.6: Absorption of PaCD with several reduced Cytochrome c concentrations.

In order to get more insight into the absorption spectrum we present below the second derivative of the absorbance in the following ranges: 500 – 580 nm, 600 – 700 nm, and the different spectrum of the related ligand–receptor protein complex.

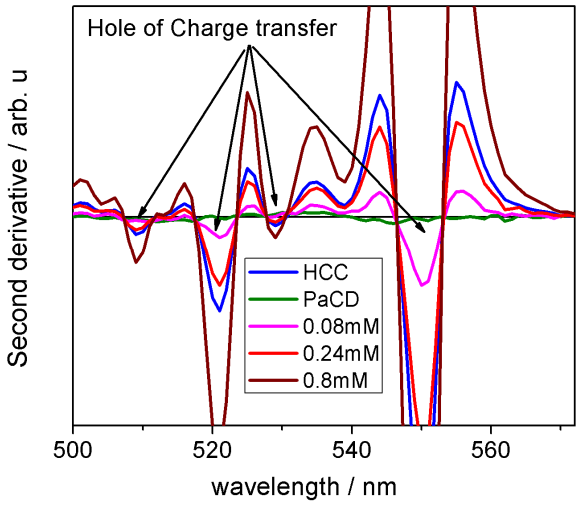

Figure 6.7: Second derivative of the absorption spectrum of the PaCD at different concentrations of the reduced HCC in the range 500 nm to 570 nm. (Hole for charge transfer means possible trapping electronic site)

In comparison to the ligand–oxidized acceptor protein complex, the reduced form also shows an inhomogeneous trapping sites at 520 nm, 550 nm, whereas the 530 nm is very weak. No difference is observed between figure 6.8 of the ligand–reduced acceptor protein complex and figure 6.5 of the ligand–oxidized acceptor protein complex.

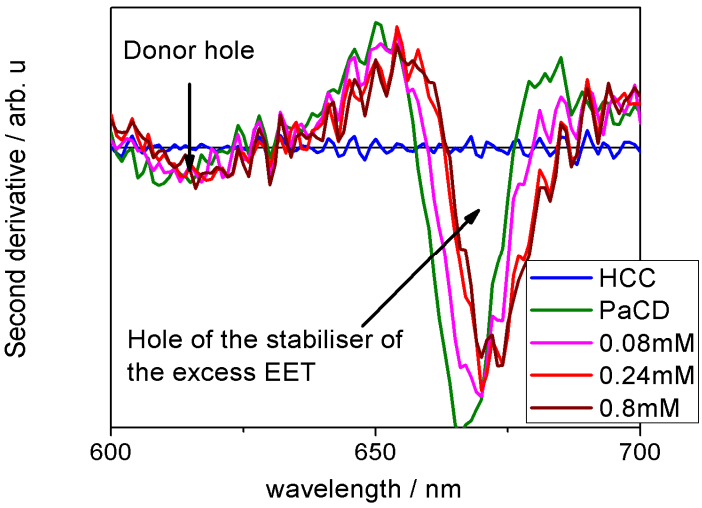

Figure 6.8: Second derivative of the absorption spectrum of the PaCD at different concentrations of the reduced HCC in range 600 nm to 700 nm. (Donor hole means electronic site of the donor)

Upon comparing to the difference spectrum of the absorption of the ligand–oxidized acceptor protein complex in figure 6.3 with the ligand–reduced acceptor protein complex in figure 6.9, the influence of the water dipole moment at 667 nm is conserved independently of whether the form of the receptor is oxidised or reduced. The spectral band of the reduced receptor protein complex is conserved while the spectral band of the ligand protein complex at 620 nm is also conserved. Between 0.24 – 0.8 mM, all the water molecules seem to be absorbed and a trapping site is therefore created. As we will see later, this trapping site will induce quenching of the excess EET after a fast charge transfer between the ligand–acceptor protein complexes.

Upon comparing the two systems, the PaCD with oxidised and the one with reduced HCC, we observed that the Q-band of the HCC is coupled with the 550 nm and the 520 nm band of the PaCD. These electronic sites can undergo ET, when the reduction of the Hem occurs by an absorbing electron that originates from the 550 nm band of the PaCD.

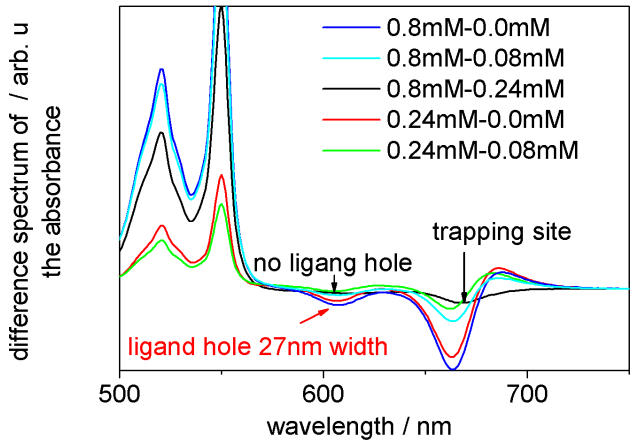

Figure 6.9: Difference spectrum of the absorption of the ligand–reduced receptor. The subtracted spectra are labelled on the figure.

After assigning spectral features to the absorbance of the ligand–oxidized acceptor and ligand–reduced acceptor protein complex, we present how at a stable concentration of the ligand PaCD, the absorbance of the ligand– acceptor protein complex is more strongly influenced by the concentration of the acceptor protein, independent of the reduced or oxidized form. We therefore, present below the dynamics of these proteins complexes by

exciting the ligand protein spectral band at 620 nm and probing at different wavelength where the influence of the acceptor protein is expected.

6.4 Photo induced transient absorption change of the ligand–oxidized receptor protein complex

In order to follow the course of the kinetic components inside the ligand-oxidized acceptor protein complex, measurements of the transient absorption change of PaCD-HCC excited at 620 nm and probed at 667 nm were carried out. The results obtained were fitted with a common lifetime kinetic linked model, and an amplitude dependent concentration of the oxidized acceptor as free parameter.

$$A(t, concentration) = \sum_{i=1}^{n} a_i(\text{concentration(i)})e^{\left(-\frac{t}{\tau_i}\right)} \qquad (6.1)$$

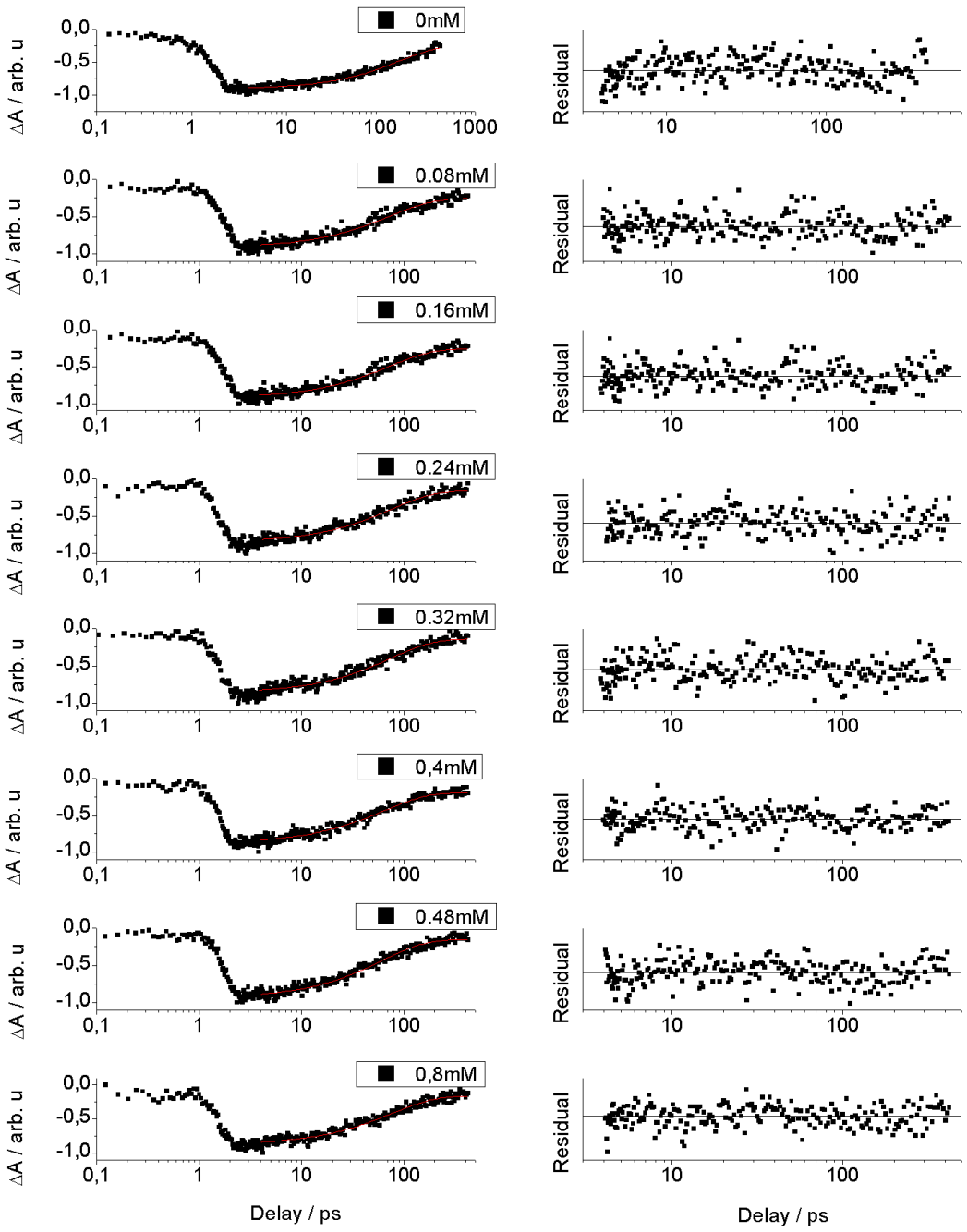

Figure 6.10: Photo-induced absorption changes of PaCD with different concentration of Hcc after excitation at 620 nm and probe at 667 nm (left). Residuals after fitting the kinetic model (right).

Typical traces of the absorption change at 667 nm for different concentrations of HCC are shown in Figure 6.10. The observed transient bleaching is caused by the photo-induced depletion of the ground state of PaCD and formation of the excited singlet state of PaCD (PaCD*).

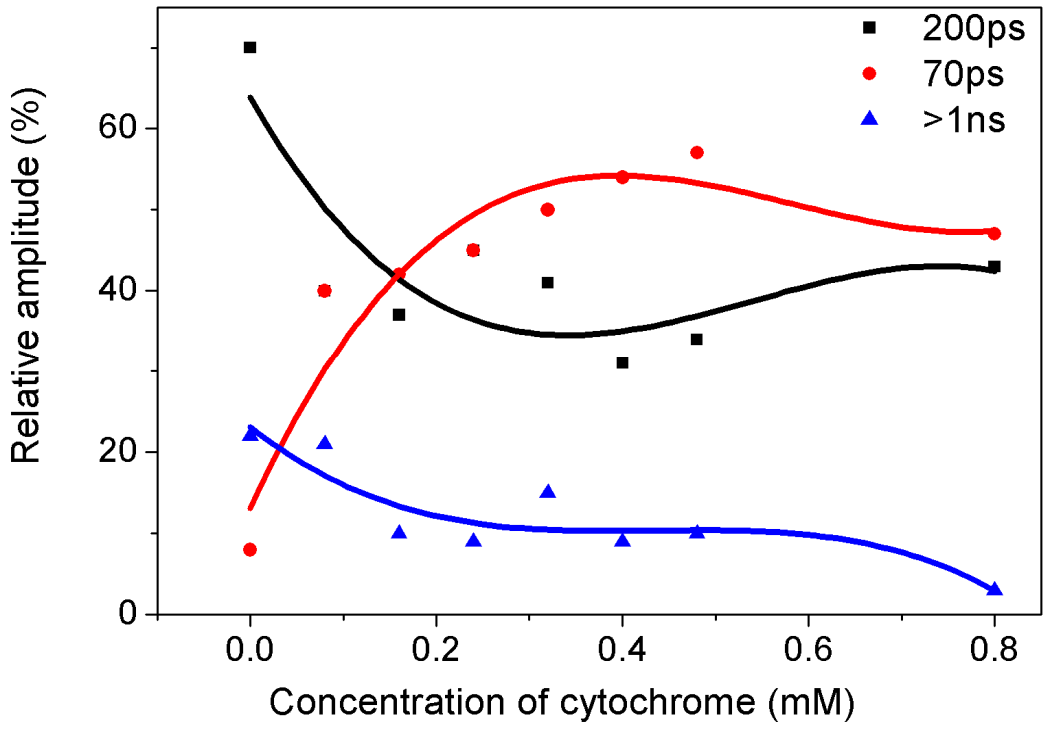

Figure 6.11: Decay associated spectra (DAS) gathered from the data analysis of the transient absorption changes spectra in figure 6.10 and the corresponding residual for a 2-component fit for different oxidized HCC acceptor protein complex concentration with a constant concentration of the ligand PaCD protein complex after excitation at 620 nm and probe at 667 nm. The pure PaCD indicates 0 mM of the oxidized HCC concentration.

Figure 6.11 displays the effect of HCC on the kinetic components of the excitation energy transfer (EET) of the donor protein complex PaCD spectral band at 620 nm to its higher absorption band at 667 nm (see figure 6.2) within the increased concentration of the acceptor protein complex HCC. Three components of the lifetime kinetic of the EET have been found: 70 ps, 200 ps and a component of more than 1 ns.

In the absence of the HCC the decay of PaCD* is dominated by two exponential decay components:

i. One with a very long lifetime above 1 ns

ii. Another with a lifetime of about 200 ps.

Within increasing the HCC concentration a third component appears with a lifetime of 70 ps, which becomes dominant, until, the combined relative contribution of the two slower components (τ= 200 ps and τ > 1 ns) decreases to about 50 %. According to the course of these different lifetime components, the asymptotic convergence we observed in figure 6.11 leads to two quenching channels of the EET, which can have different origin as:

i. Collision quenching involves collisions with other molecules that result in the loss of excitation energy as heat instead of as emitted light. This process is always present to some extent in solution samples. Species that are particularly efficient in inducing this process are referred to as collision quenchers (e.g. the nitroxide radical that is present on the PaCD donor protein).
ii. Static quenching: Interaction of the donor with the quencher (acceptor) forms a stable non-fluorescent complex. Since this complex typically has a different absorption spectrum from the donor at 667 nm, presence of an absorption change is a diagnostic of this type of quenching (by comparison, collision quenching is a transient excited state interaction and so does not affect the absorption spectrum). This might be induced by the HCC concentration around 0.2 micro molar inside a stable PaCD concentration of 135 µM. At this HCC concentration, we have observed a spectral red-shift in the absorbance spectrum (see figure 6.2 and 6.6) which is conserved in the flash induced absorption changes at 667 nm in the time domain.
iii. Resonance energy transfer: Like collision quenching, this is an excited state interaction but the two participating molecules do not have to collide - it can occur over distances of 100 Å or more. One dye (the donor PaCD) is excited by the absorption of a photon, but instead of emitting a fluorescence photon, the excitation is transferred by electronic coupling to an acceptor molecule (HCC) or to redshift electronic state of the PaCD. The result of this exchange is an excited acceptor and a ground state donor. In terms of measured signals, the result is either/or bleaching at longer wavelengths (compared to the spectrum of the donor alone) depending on whether the acceptor is itself bleached or not.

Base on the absorbance spectra (figure 6.2;6.6), the flash induced absorption changes (figure 6.5; 6.8) and the DAS (figure 6.11), we can conclude that the concentration of the acceptor (HCC) drives the energy quenching inside the system, around a concentration up to 0.2 micro Molar of HCC in 70 ps time scale, while the non-photochemical quenching is induced by the donor protein complex PaCD. Therefore, the artificial photosynthetic reaction centre can be

stabilized and protected from excess light harvesting by increasing the concentration of the acceptor protein. The information on the EET quenching alone cannot be taken as evidence of the charge transfer into the artificial reaction centre. In order to further into the charge transfer of the system PaCD-HCC, the measurement of the flash-induced absorption changes have been performed for the same condition on five different samples:

i. PaCD is the donor ligand alone

ii. CoxPa is the donor ligand + the oxidized acceptor protein complex

iii. CredPa is the donor ligand + the reduced acceptor protein complex

iv. Hccox is the oxidized acceptor protein complex alone

v. Hccred is the reduced acceptor protein complex alone

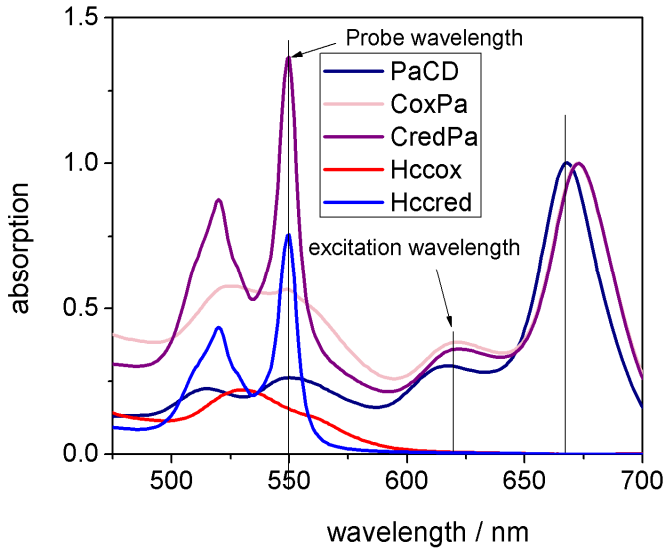

Figure 6.12: Absorption band of the chlorine dendron (PaCD) navy colour, the PaCD binding complex to oxide horse heart cytochrome c (CoxPa) in magenta colour, the PaCD binding complex to reduced horse heart cytochrome c (CredPa) in violet, the oxide horse heart cytochrome c (Hccox) without the PaCD in red colour and the reduced one without the PaCD in blue colour

The absorbance spectra in figure 6.12 reveal that the absorption of the donor PaCD presents an inhomogeneous absorption curve with two lower absorption spectral bands at 520 nm and 550 nm, and a slightly higher absorption band at 620 nm, and a higher one at 667 nm. In the same figure 6.12, it is shown that the reduced HCC and the oxidized HCC (Hccred and

Hccox) do not absorb at the choose excitation wavelength 620 nm of the donor PaCD. However a higher absorption band is observed at 550 nm for the ligand-oxidized acceptor (CoxPa) and ligand-reduced acceptor (CredPa). The second derivative of the CoxPa shows three trapping sites of a possible charge at 565 nm, 550 nm and 520 nm; where the higher in strength of trap seems to be the 550 nm (see figure 6.13).

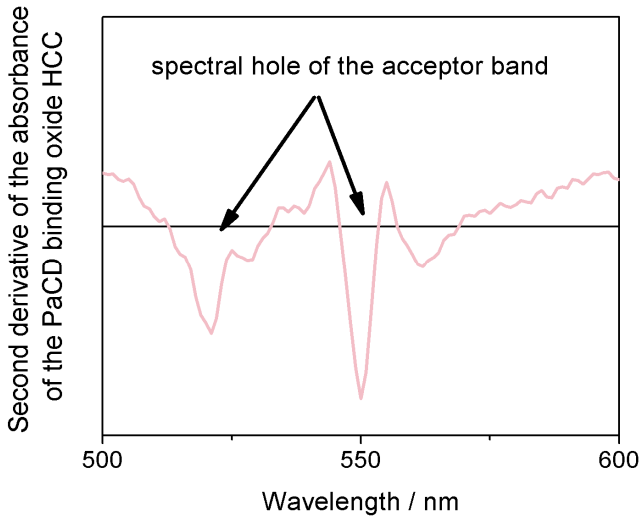

Figure 6.13: The second derivative of the CoxPa between 500 nm - 600 nm shows two inhomogeneous trapping sites of the acceptor band at 520 nm and 550 nm. (spectral hole of the acceptor means possible trapping electronic site of the acceptor)

Figure 6.14 shows the excited state absorption of the ligand PaCD alone as a function of time for short (3 ps) and long time scales (> 100 ps). The ligand PaCD exhibits alone an excited-state absorption at 550 nm. While the figure 6.15 below shows that the oxidized Hccox alone and the reduced Hccred alone after excitation at 620 nm does not absorb at 550 nm. We can conclude that within excitation at 620 nm of the PaCD alone, for Hccox alone and Hccred alone, no charge transfer is induced.

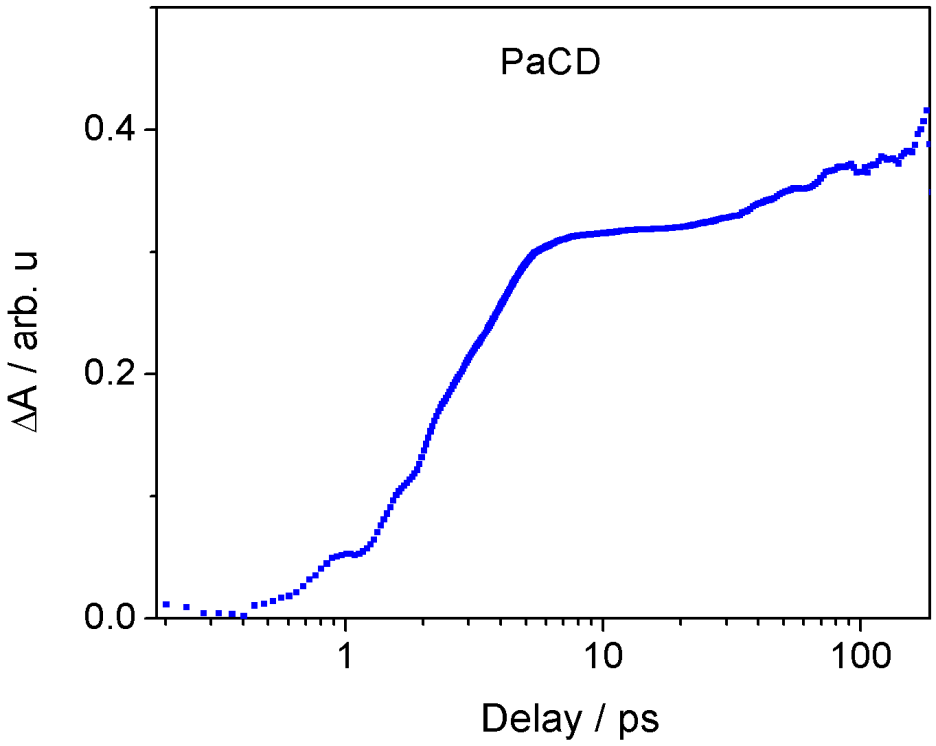

Figure 6.14: The photo-induced absorption change of PaCD after excitation at 620 nm does not exhibit a bleaching at 550 nm probe wavelength

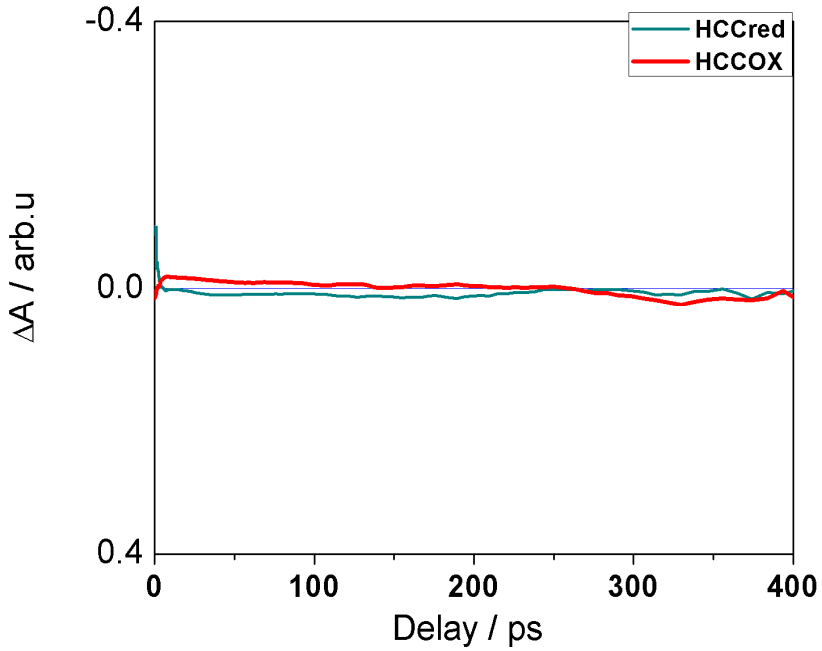

Figure 6 15: The photo-induced absorption change of HCCOX and HCCred after excitation at 620 nm does not show an appreciable change in absorption at the 550 nm probe wavelength.

After characterizing the donor ligand alone, the acceptor alone, and showing that the charge transfer cannot occur in these cases we found that the HCC could not absorb above 600 nm. We therefore performed a flash induced absorption change in the time domain on a donor-acceptor protein complex with the oxidized Hccox inside the donor ligand solution, and the same with the reduced form. The CoxPa was renamed as HccoxPaCD and the CredPa as HccredPaCD. After excitation at 620 nm and a probe at 550 nm, we observed in figure 6.16 that the flash induced absorption changes for HccoxPaCD appeared within 3 ps to 30 ps. The trace was fitted by two exponential decays with different signs of the exponential. The fast kinetic component which decays within 3 ps is attributed to the excited state absorption of the PaCD, while the logarithmic course of the delay bleaching within 30 ps is attributed to the charge transfer of the ligand donor PaCD* to the acceptor protein complex Hccox.

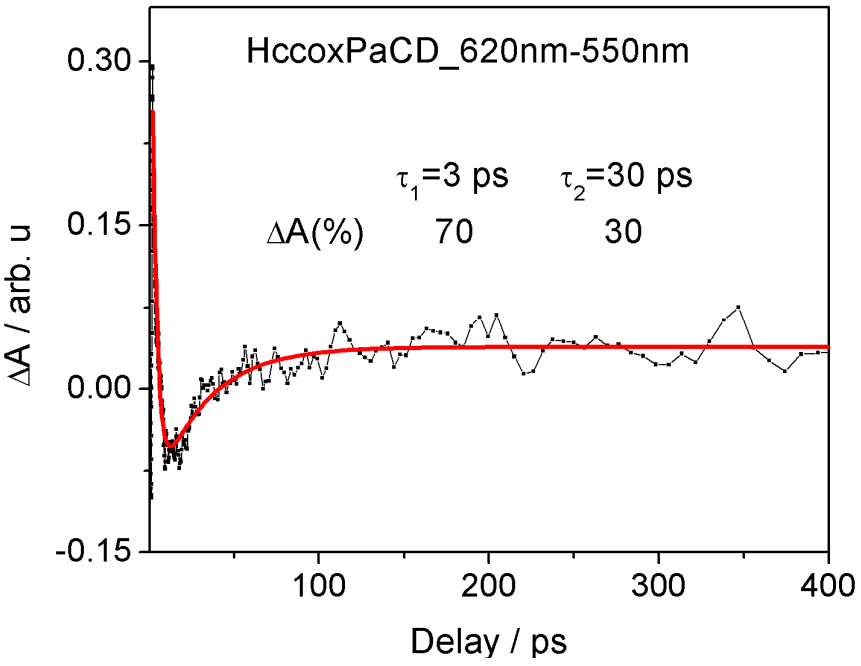

Figure 6.16: The photo-induced absorption change of the PaCD binding oxidant Hccox after excitation at 620 nm shows a bi-exponential decay at the 550 nm probe wavelength. The 3 ps time constant is assumed to be the ESA of the ligand while 30 ps is devoted to the acceptor Hccox.

In order to verify that, the charge transfer occurs in 30 ps, we performed the same experiment with the reduced acceptor inside the ligand solution (see figure 6.17). The excited state of the PaCD appears on 2 ps with lower amplitude than in oxidized case, and a better fit has been obtained with an exponential decay. The logarithmic delayed bleaching exhibits two components 20 ps and 30 ps. All the independent fits are free parameters in the oxidized as well as in the reduced donor-acceptor protein complex system. Almost the same time constant of 30 ps is found, and the 20 ps can also be due to some other fast channel on the charge transfer process.

Finally, the present section has shown the inhomogeneous electronic sites on the Q-band of the oxidized Hccox and reduced Hccred. When the complex PaCD-Hccox is formed, the band 520 nm of the PaCD disappears, and the Q-band of the Hccox at 530 nm becomes dominant with a shoulder at 550 nm. This 550 nm is also a sub-band of a Q-band of the Hccox as well as the PaCD. Because the PaCD band at 550 nm would rise in the present of HCC, the trapping electronic state of the PaCD and the HCC would be coupled. This 550 nm is characteristic for the Hem band in Hccox and Hccred. The excited state formation after excitation of the PaCD band at 620 nm would induce the following effects:

- A fraction of the exciton formation would be observed as an energy transfer to the high absorption electronic state of the PaCD at 667 nm.
- Another fraction of the exciton would interact with the Q-band of the Hccox. There, the PaCD would be promoted to an excited state within a time constant of 3 ps ($PaCD^*$). During this time constant, the $PaCD^*$ would transfer a charge to HCCox, and the Hem would be reduced from Fe^{3+} to Fe^{2+}. The consequence of this reduction would be an observed electron transfer in 30 ps.

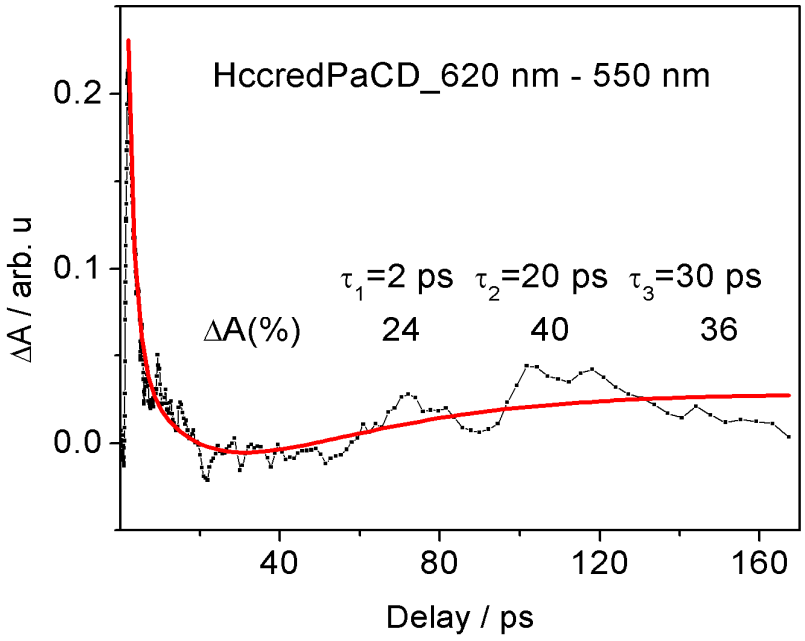

Figure 6.17: The photo-induced absorption change of the PaCD binding oxidant Hccred after excitation at 620 nm shows a tri-exponential decay at the 550 nm probe wavelength. The 2 ps component is assumed to be the ESA of the ligand while the 20 ps and 30 ps components are devoted to the acceptor Hccred.

This evidence of charge transfer (see figure 6.16 and 6.17) that occurs on time scales faster than the observed inhomogeneously bidirectional quenching, for the donor within a time scale up to 1 ns and the acceptor on a time scale of 70 ps respectively, is an indication that the system PaCD-Hcc can be a better donor acceptor for an artificial photosynthesis system, as well as an excellent quencher for the stabilization of the excess EET.

Thus, system protein design can now become a powerful tool to create synthetic peptides with catalytic activities by incorporating active pigments and redox cofactors. As this is a constructive approach, self-assembly can gradually introduce the biological complexity into the design to make functional complexes. The creation of these complexes not only provides valuable information on how the protein environment controls the redox activity, but also gives an opportunity to construct membrane assemblies as mimics of natural systems. Progress towards the construction of synthetic reaction centres is a step forward in creating artificial photosynthesis membranes.

7 Concluding remarks

7.1 General Conclusion

In this thesis, I mainly examined photon harvesting by the outer antenna system PBP of the *A. marina*, and the PBS of the *T. vulcanus*. The protein antenna system of A. marina is folding in low ionic strength and in high ionic strength in order to address the nature of the intervening pigment on the pigment-pigment coupling when energy transfer takes place. The *T. vulcanus* antenna system contains the un-pigmented linker protein in its PC rod. These linker proteins will change the environment of the covalently bound pigments in the protein matrices of antenna system. This change will be coupled with the electronic state of the pigments making the PBS as well as the coupling between those pigments. The investigation of the above sample will lead to a better understanding of the EET mechanism in cyanobacteria.

Our experimental method include the time resolved pump-probe technique for the examination of dynamic of the pigment-pigment coupling in time domain, the spectral hole burning, fluorescence line narrowing and delta fluorescence line narrowing. The three last techniques are site selective technique necessary for the study of the electronic site of the pigment inside the protein matrices and their tuning role in the energy. The Delta fluorescence line narrowing is useful for the 0-0 electronic transition vibrational modes.

In Chapter 3, we uncovered the existence of a new energy transfer pathway with a time constant of 14 ps component inside the PC band of the PBP antenna system of *A. marina*, which has never been reported before. This was revealed through observed spectral differences between intact (low ionic strength) and disrupted (high ionic strength) PBP antenna systems of *A. marina* using an accurate global analysis, and which were confirmed by anisotropy calculations using absorption changes and polarized traces in the spectral range of PC. Furthermore, the results present a more accurate non-deconvoluted anisotropy than the majority of which have been most reported in earlier studies by (Edington, 1995). The anisotropy showed that, the redshift of the femtosecond spectrum (of the pigment in PC spectral range 600-630 nm) was due to the downhill EET to the successive lower electronic states in PC hexamer toward a higher absorption electronic state of the β_{84} pigment. We

therefore suggest that, the aforementioned shift is not the occurrence of inter-exciton state relaxation at RT.

Due to the high disorder induced by the Brownian motion in the liquid state, the constructive propagation of an excitonic wave can be considered as sub-dominant. Consequently, the excitonic coupling can be regarded weak at RT, and so did not contribute to the excitation energy transfer inside the PBP antenna system at RT, in the spectral range below 625 nm. Our revised pathway model is presented below:

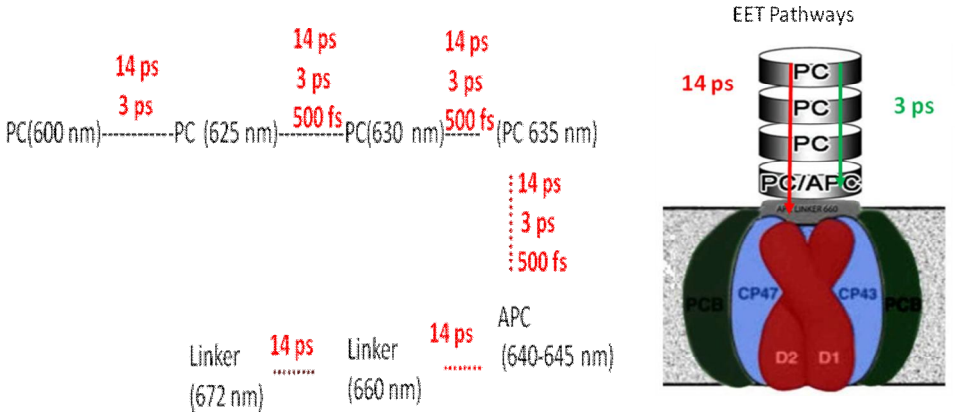

Figure 7.1 Our new model of the excitation energy transfer pathway in the PBP antenna system of *A. marina* at RT.

The investigation of *T. vulcanus* at RT, which were presented in chapter 4, revealed an ultrafast 888 fs kinetic along the rod-PC domain (containing linker proteins) to the APC core domain in the PBS antenna system. Because of this ultrafast kinetic we were led to propose a new design of the EET inside the PBS of T. Vulcanus (see figure 7.2):

A1. The EET transfer from the rod PC domain to the APC core domain occurs via two channels. The faster channel operates with a 888 fs component, which suggests an ultrafast transfer of the energy along the PC rod to the APC core only. The ultrafast time scale of the EET raises the question of a possible exciton delocalisation along the rod PC at RT. The second channel exhibits a component with a 17 ps time constant. This kinetic is the EET from the APC core domain to the $L_{CM,}$ which is the terminal emitter electronic state of the PBS. This was a slower component in comparison to the 14 ps component of the EET from APC to linker membrane in the PBP antenna system of *A. marina*.

A2. The EET to the terminal emitter and between different L_{CM} sub-bands occurred via two channels. The first kinetics component around 450 fs was dominant at 670 nm, which suggests a very fast excitonic coupling between these two states. The second channel with a 13 ps kinetic component was also dominant for the 680 nm. The latter kinetic might be an indication that the EET between the terminal emitter of the PBS antenna system to the Chl a in the RC of PS II of *T. vulcanus* can occur at a faster time-scale than ever reported for any cyanobacterium. This observation needs to be investigated in further detail, as well as the absorption band of the terminal emitter because of two different linkers Which can then folding to form dimer for various APC.

Finally we report and suggest that the simple rod-shaped architecture of the outer antenna system of *A. marina*, which involves fewer pigment units than in PBS of *T. Vulcanus*, did not show the PBP protein of *A. marina* to be a better harvester of light energy than PBS, where the linker strongly influences the kinetic of the EET. However, niche adaptation to the habitat may have induced the specificity of the architecture, which might explain the assembly of the pigments for better harvesting. This explanation may lead to more surprising insight and may be a piece of for the existence of another pigment in the rod of PBP, when the latter is well purified.

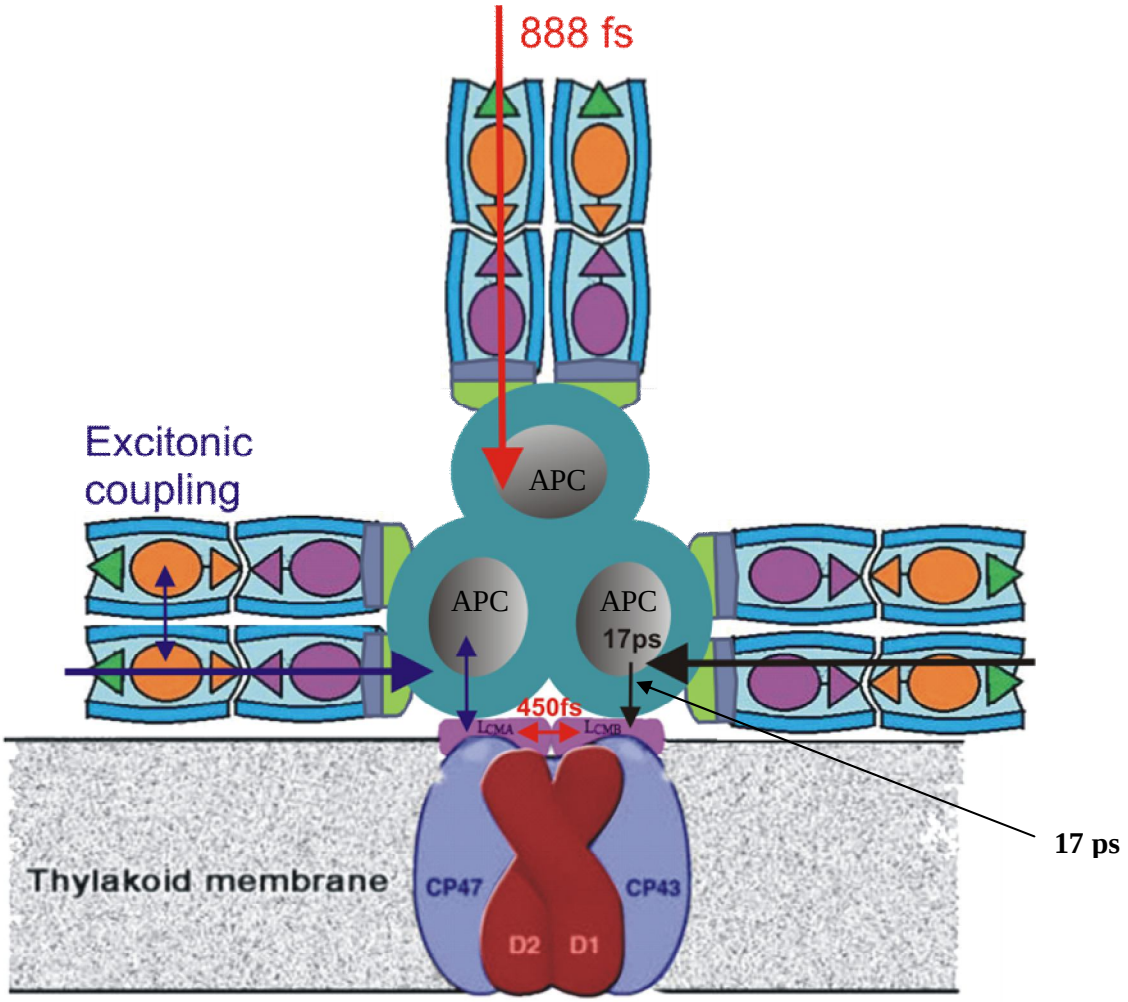

Figure7.2: Proposed new model of the excitation energy transfer pathway in the PBS antenna system of *T. vulcanus*.

In addition to the measurements at RT, the measurements at 4,5 K reveals a rich contribution of vibronic transitions inside the PBP, which were interesting for future theoretical comparisons, as well as gaining new insights into the spectral composition of the PBP antenna system of *A. marina*. Evidence of a pigment absorbing at 635 nm as a low state of PC has already been show by (David, 2011) in the case of the PBS of *T. Vulcanus*, but was here demonstrated for *A. marina*. The double vibrational mode indicates that this pigment is strongly coupled with the β_{84} chromophore. The intermediate vibrational mode at 632 nm is in fair agreement with an observed delocalised exciton between the 635 nm absorption component and the β_{84} at 630 nm. No evidence of an attached linker protein PC/APC inside

the last hetero-hexamer of the PBP rod of *A. marina* could be shown. The vibrational mode of the trimeric APC inside the rod of PBP present a propagation of two modes which originated from the dimer chromophores α_{84} and $\beta_{84,}$ and which are separated by the energy gap of 40 cm^{-1}. While the vibrational mode of the pigment absorbing at 635 nm and the delocalised mode at 632 nm is separated by the energy gap of 60 cm^{-1}. The first energy gap of 40 cm^{-1} which is in accordance with Womick (Womick, 2010) is found at 660 nm where two vibrational states are separated by the same energy gap of 40 cm^{-1}. Thus, it is an indication that the 660 nm state of the terminal emitter is an APC which contains dimer pigments α_{84} and β_{84}, and which is blue shifted in the first vibrational mode by 161 cm^{-1} relative to 675 nm. However further investigation of the latter is necessary.

At low temperature (4.5 K) the PBS antenna system reveals a pigment at 645 nm near the linker rod core, which is in addition to the one outlined by (David, 2011). The latter is the true lowest state of the PC in *T. vulcanus*. However, the question of how of the pigments are buried in the terminal emitter of the PC from the PBS cannot be fully resolved given the absence of vibronic modes induced by the high coupling strength between the chromophores. Further investigations are necessary, for example, the characterisation of the different absorption state of the terminal emitter, where some similarities to the rod of the PBP antenna of *A. marina* can be drawn at 660 nm and ~670 nm. An additional similarity at higher energy levels is evident, where a shoulder in the inhomogeneous broadened absorption was observed for both systems around 575 nm. This is a surprising result, given the absence of evidence of encoding for PE in the genes of the both antenna systems. As such, investigation may open up towards finding the origin of the blue-shift in satellite holes, which were observed along the PC bands of both systems.

In addition to cyanobacteria, we were also interested on the high plant light harvesting complex II, named LHC II. Chapter five addresses new insights into the EET in LHC II by controlling their aggregation states with the concentration of the detergent β-DM. This finding reveals that small aggregated states induce a geometry for efficient energy transfer that is better than the hetero-mixture of large aggregates. Therefore, it is evident that inside the trimeric LHC II, the EET is much faster than the largest aggregates with hetero-population. The trimer might be the optimal configuration of the LHC II for an efficient energy transfer pathway as well as an excess of EET quenching that avoids photo-damage in higher plants.

Finally, Chapter 6 shows how one can overcome the challenging task of creating artificial reaction centres with an efficient charge transfer that has a 30 ps component, as well as having efficient quenching of the excess excitation energy transfer. The latter occurs through a two scales convergence process inside the mechanism of the artificial nano-machine (chlorine dendrone/oxidized cytochrome c) where the donor chlorine Dendron is quenched in time scale up to 1 ns. After charge transfer, the second quenching of the excess excitation energy occurs in time scale 40 -70 ps.

7.2 Synopsis

Our major findings on the PBP antenna system of *A. marina* are listed below:

i. The PBP rod showed two different pathways inside the PC spectral band by which the energy is funnelled to APC with characteristic times of 3 ps and 14 ps. From APC the energy is transferred to the terminal emitter with a typical time constant of 14 ps.

ii. A pigment absorbing at 635 nm mediates the EET from PC to APC. This pigment is assumed to represent the terminal emitter of the PC rod and is involved in the efficient energy transfer to the APC. Thus, the lower state of PC at 635 nm plays a key role in mediating the energy transfer kinetics to APC.

iii. The state at 660-665 nm is part of the linker membrane containing an APC gene, which most probably binds the dimer chromophores α_{84} and β_{84} (apcE).

iv. The state at 670-675 nm, which differed in its first vibrational mode but had a similar spectral position to the apcB electronic site (Koyama, 2006), could play a role in burying this latter pigment.

v. Once identified, the ΔFLN spectrum of the PBP rod derived a considerable amount of information that can be used for future theoretical modelling and model comparison. It shows a site-selective insight into the electronic structure of the PBP. Some examples are:

   - The energy gap of the double vibrational mode at 635 nm, which is 20 cm-1 more than the gap for the APC dimer, pigments at 645 nm

- The energy gap of the double vibrational modes at 645 nm and 660 nm display the same gap of 40 cm^{-1}.

- The 660 nm state of the terminal emitter is an APC which contains the dimer pigments α_{84} and β_{84}, and which is blue-shifted in the first vibrational mode by 161 cm^{-1} in comparison to vibrational modes observed at 675 nm.

- Upon comparison of the complementary methods ΔFLN and spectral hole burning it was found that there exist at least four long wavelength states that are distinguishable by way of the site-selective method, but that they are distinguishable, in general, by their broadened spectra.

vi. A blue-shift in different excitonic satellite holes was presented at low temperatures (along the PC assembly), which is an indication of partial excitonic coupling that contributes to the energy transfer at low temperatures via the excitonically coupled states that determine the energy transfer in the band (624 nm -675 nm).

In the case of the PBS *T. vulcanus*, the major findings are the following:

i. An additional new pigment, which is different from the 635 nm pigment found by David (David, 2011), was identified by way of absorption and ΔFLN spectroscopy at 645 nm. This latter finding is supported by a shoulder of the characteristic 888 fs component identified in the global analysis. This pigment shows three different states of the absorption at 639-640 nm, 641 -642 nm, 642 -645 nm.

ii. The linker proteins (along the rod of the PC hexamer) inside PBS of *T. vulcanus* induce an ultrafast EET transfer which is faster than 888 fs, i.e. more than three times faster than the supposed 3 ps kinetic found along the rod of the PBP of *A. marina*.

iii. The coupling strength of the pigment in the PC rod was found to be higher than inside the PBP of *A. Marina*

iv. The terminal emitter absorption bands at 670 nm and 680 nm were strongly coupled by two channels of 13 ps and 430 fs. Therefore, the energy flow from 670 nm to 680 nm via two channels 13 ps and 430 fs.

v. Two prominent absorption bands of the terminal emitter are located at 660 nm and 680 nm. The 660 nm might involve the APC_E while the 680 nm might be due to the red shifted APC_B.

vi. Excitons might be delocalised along the PBS and the rod.

However, some major similarities between the rod PBP antenna of *A. marina* and the one of PBS *T. vulcanus* were found, and they are listed here below:

i. The two systems contain a pigment absorbing at 635 nm (as terminal emitter of PC in the PBP of *A. marina*).

ii. In addition, the absorption of the electronic states of the linker membrane at 660 nm and ~670 nm seem to be similar in both systems.

For LHC II of higher plant the major findings are:

i. Higher plants containing LHC II need a trimeric configuration of the outer antenna for better photo-protection (quenching of excess light harvesting).

ii. In addition, higher plants can adjust the aggregation state of the outer LHC antenna to adapt to changing environmental light conditions.

For artificial photosynthetic reaction centre, it was observed that Chlorindendrone–cytochrome c function as an artificial reaction centre that undergoes charge transfer. This can be of use in a novel system for photovoltaic solar cells due to the efficiency of the charge transfer with a time constant of 30 ps, as well as due to the existence of a photo-protection system.

7.3 Perspectives and outlook

(i) What do we learn from the study and where can it be applied?

Many studies have been carried out to establish the structural model of different cyanobacteria. Most of these were based on new insights about the architectural organisation of some compounds, where the functional role of the available linker proteins were addressed (Liu et al., 2005).

To get a better understanding of the EET route to the reaction centre of the cyanobacteria, further studies with an isolated APC disc containing one of the linkers necessary. By gaining knowledge of the variety of cyanobacteria in their living environments, as well as by mimicking their function in artificial photosynthesis to create new photovoltaic devices or function as data storage devices, one will be contributing to the challenging task of efficiently harnessing the pure energy of the sun.

(ii) What could be some key features to be established by such studies?

One challenging issue still stands out: The linker in the different samples needs to be intensively investigated and some functional roles need to be pointed out. Up to date, its presence and its functional role in many cyanobacteria remain an open issue. In this study, it is pointed out that less is known about the structural organisation of the linker, their location as well as the gene composition in many organisms. One example is the linker protein near the core of PBS and the pigment covalently bound to it. The gene of this unknown pigment in PBS *T. vulcanus* at 645 nm and the pigment absorbing at 635 nm in both systems remain a mystery to be clarified as well as the characterisation of all the sub-absorption bands of the terminal emitter in the two systems.

Let us consider the question above. The linker proteins in the rod of PBS *T. vulcanus* induce a complete red shift in the spectral band absorption of the PBS of *T. vulcanus* in comparison to that of *A. marina*, where the maximum absorption of PC at RT is located around 621 nm. The effect of the linker on the energy transfer has been shown to enhance existing fast energy transfer kinetics. This observation might suggest that bilinchromophores are spatially displaced / structured by the linkers. If this is true, how may this affect the funnelled pathway of the energy and the excitonic contribution? Is it the open-chain tetrapyrole structure that makes bilinchromophores flexible to any change and modify the distance between its nearest neighbours as well as the spectral shift? How can this influence the conformational change in the protein matrices when the energy is transfer to the terminal emitter?

Bibliography

A. Fedorova A.C., M. Ogawa. (2003) Photoinduced electron-transfer along alpha-helical and coiled-coil metal-lopeptides. J. Am. Chem. Soc. 125:357–362.

A. Zouni H.-T.W., J. Kern, P. Fromme, N. Krauss, W. Saenger, P. Orth. (2001) Crystal structure of photosystem II from Synechococcus elongatus at 3.8 Å resolution. Nature 409:739-743.

A.R. Holzwarth M.G.M.ü.l., M Reus , M. Nowaczyk , J. Sander , M. R ö gner. (2006) Kinetics and mechanism of electron transfer in intact photosystem II and in the isolated reaction center: pheophytin is the primary electron acceptor. Proceedings of the National Academy of Sciences of the United States of America 103: 6895 – 900.

Adir N. (2005) Elucidation of the molecular structures of components of the phycobilisome: reconstructing a giant. Photosynthesis Research 85:15-32. DOI: 10.1007/s11120-004-2143-y.

Adir N., Dobrovetsky Y., Lerner N. (2001) Structure of c-phycocyanin from the thermophilic cyanobacterium Synechococcus vulcanus at 2.5 Å: structural implications for thermal stability in phycobilisome assembly. Journal of Molecular Biology 313:71-81.

Akiyama. (2001) Detection of Chlorophyll d′ and Pheophytin a in a Chlorophyll d-Dominating Oxygenic Photosynthetic Prokaryote Acaryochloris marina. Analytical Sciences 17:205.

Andrei V. Sharkov I.V.K., Eugeny V. Khoroshilov, Piotr G. Kryukov, Richard Fischer, Hugo Scheer, Tomas Gillbro. (1994) Femtosecond spectral and anisotropy study of excitation energy transfer between neighbouring α-80 and β-81 chromophores of allophycocyanin trimers. Biochimica et Biophysica Acta (BBA) - Bioenergetics 1188:349 - 356.

B. Starikow C.N., G. CUNIBERTI, W. WENZEL. (2009)

Single-molecule DNA conductance in water solutions: Role of explicit water-counterion sheath and chemical modification of nucleobases Biophysical Reviews and Letters 4:231.

B. Voigt M.K., H. Lokstein. (2008) Influence of detergent concentration on aggregation and the spectroscopic properties of light-harvesting complex II. Photosynthesis Research 95:317-325.

B.R Gibney F.R., J.J. Skalicky, A. J. Wand, L.P Dutton. (1999) Iteratiprotein design. J. Am. Chem. Soc. 121:4952–4960.

Bhalerao P.R., Gillbro T., Gustafsson P. (1995) Functional phycobilisome core structures in a phycocyanin-less mutant of cyanobacterium Synechococcus sp. PCC 7942. Photosynthesis Research 45:61-70.

Chen M., Bibby T. (2005) Photosynthetic Apparatus of Antenna-reaction Centres Supercomplexes in Oxyphotobacteria: Insight through Significance of Pcb/IsiA Proteins. Photosynthesis Research 86:165-173. DOI: 10.1007/s11120-005-1330-9.

Chen M., Floetenmeyer M., Bibby T.S. (2009) Supramolecular organization of phycobiliproteins in the chlorophyll d-containing cyanobacterium Acaryochloris marina. FEBS letters 583:2535-2539.

Chen M., Schliep M., Willows R.D., Cai Z.-L., Neilan B.A., Scheer H. (2010) A Red-Shifted Chlorophyll. Science 329:1318-1319. DOI: 10.1126/science.1191127.

Collings A.F., Critchley C. (2005) Artificial Photosynthesis.

Cornelia Röger M.G.M., Marina Lysetska, Yulia Miloslavina, Alfred R. Holzwarth, Frank Würthner. . (2006) Efficient Energy Transfer from Peripheral Chromophores to the Self-Assembled Zinc Chlorin Rod Antenna: A Bioinspired Light-Harvesting System to Bridge the “Green Gap”. J. AM. CHEM. SOC.9.128 NO. 20:6542-6543.

D. Robertson R.F., C. Moser, J. Urbauer, S. Mulholland, R. Pidikiti, J. Lear, A. Wand, W. DeGrado, P. Dutton,P (1994) Design and synthesis of multi-Haem proteins. Nature:425–431.

David. (2011) High-resolution Crystal Structure of Trimeric and Rod Phycocyanin. Journal of Molecular Biology 405:201 - 213.

Debreczeny M., Gombos Z., Szalontai B. (1992) Surface-enhanced resonance Raman spectroscopy of phycocyanin. European Biophysics Journal 21:193-198.

Debreczeny M.P., Sauer K., Zhou J., Bryant D.A. (1993) Monomeric C-phycocyanin at room temperature and 77 K: resolution of the absorption and fluorescence spectra of the individual chromophores and the energy-transfer rate constants. The Journal of Physical Chemistry 97:9852-9862. DOI: 10.1021/j100140a050.

Dexter D.L.J. (1953). Chem. Phys. 21:836 - 850.

Diels. (2006) Ultrashort Laser Pulse Phenomena.

Edington M.D., Riter R.E., Beck W.F. (1995) Evidence for Coherent Energy Transfer in Allophycocyanin Trimers. The Journal of Physical Chemistry 99:15699-15704. DOI: 10.1021/j100043a001.

G R. (1992) "Energy transfer and trapping in photosystem II", in: The photosystems: Structure, Function and Molecular Biology Elsevier Science

Gantt E., Lipschultz C.A., Grabowski J., Zimmerman B.K. (1979) Phycobilisomes from Blue-Green and Red Algae: Isolation Criteria and Dissociation Characteristics. Plant Physiology 63:615-620. DOI: 10.1104/pp.63.4.615.

Gillbro T., Sandström Å., Sundström V., Wendler J., Holzwarth A.R. (1985) Picosecond study of energy-transfer kinetics in phycobilisomes of Synechococcus 6301 and the mutant AN 112. Biochimica et Biophysica Acta (BBA) - Bioenergetics 808:52-65.

Gillbro T., Sharkov A.V., Kryukov I.V., Khoroshilov E.V., Kryukov P.G., Fischer R., Scheer H. (1993) Förster energy transfer between neighbouring chromophores in C-phycocyanin trimers. Biochimica et Biophysica Acta (BBA) - Bioenergetics 1140:321-326.

Govindjee. (2001) Photosynthesis, New York.

H. Lokstein B.G. (2007) Chlorophyll binding proteins, in: K. Roberts (ed.) Handbook of Plant Science.

H. Lokstein H.H., P. Hoffmann, P. Woitke, G. Renger. (1994) The role of light-harvesting complex II in excess excitation dissipation: an in -vivo fluorescence study on the origin of high-energy quenching. J. Photichem. Photobiol. B:Biol 26:175-184.

Hitoshi Tamiaki S.T., Seiichi Tsudzuki, Tomohiro Miyatake, Rikuhei Tanikaga. . (1998) Self-Aggregation of Synthetic Zinc Chlorins with a Chiral 1-Hydroxyethyl roup as a Model for in vivo Epimeric Bacteriochlorophyll-c and d Aggregates. Tetrahedron 54:6699-6718.

Holzwarth A.R., Wendler J., Suter G.W. (1987) Studies on Chromophore Coupling in Isolated Phycobiliproteins: II. Picosecond Energy Transfer Kinetics and Time-Resolved Fluorescence Spectra of C-Phycocyanin from Synechococcus 6301 as a Function of the Aggregation State. Biophysical journal 51:1-12.

Holzwarth A.R., Bittersmann E., Reuter W., Wehrmeyer W. (1990) Studies on chromophore coupling in isolated phycobiliproteins: III. Picosecond excited state kinetics and time-resolved fluorescence spectra of different allophycocyanins from Mastigocladus laminosus. Biophysical journal 57:133-145.

Hu. (1999) Molecular structure, localization and function of biliproteins in the chlorophyll a/d containing oxygenic photosynthetic prokaryote Acaryochloris marina. Biochimica et Biophysica Acta (BBA) - Bioenergetics 1412:250.

Hu Q., Marquardt J., Iwasaki I., Miyashita H., Kurano N., Morschel E., Miyachi S. (1999) Molecular structure, localization and function of biliproteins in the chlorophyll a/d containing oxygenic photosynthetic prokaryote Acaryochloris marina. Biochimica et Biophysica Acta-Bioenergetics 1412:250-261.

Irene Schmilinsky K.P.S., Nenad Gajovic-Eichelmann, Marco Vitali, Han-Jörg Eckert, Peter Hildebrandt, Martin Katterle (2010) Photoinduced Electron Transfer from a new pheophytin a - derivative to cytochrom c - a Biomimetic Reaction Center Model., Sixth International Conference on Porphyrins and Phthalocyanines (ICPP-6 / S05-037) New Mexico, USA.

J. Fajer D.C.B., A. Forman, R. H. Felton, D. Dolphin, L. Vegh. (1974) The Cation Radicals of Free Base and Zinc Bacteriochlorin, Bacteriochlorophyll, and Bacteriopheophytin. Proc Natl Acad Sci 71(3): 994–998.

J.M. Shifman B.R.G., R.E Sharp,P.L Dutton. (2000) Heme redox potential control in de novo designed four- a-helix bundle proteins. Biochemistry 39: 14813–14821.

Jansson. (1994) The Light-harvesting chlorophyll a/b-binding proteins. Biochimica and Biophysica ACTA 1184:1-19.

Jodan. M. Womick S.A.M., Andrew M. Moran. (2010) Toward the origin of exciton electronic structure in phycobiliproteins. The Journal of l Chemical Physics 133:024507.

Jovanovic I. (2010) Chirped-Pulse Amplification.

Lakowicz J.R. (2006) Principles of fluorescence spectroscopy. Springer ed.

Larkum A.W.D., Kühl M. (2005) Chlorophyll d: the puzzle resolved. Trends in Plant Science 10:355-357.

Liron David A.M.a.N.A. (2011) High-resolution Crystal Structure of Trimeric and Rod Phycocyanin. Journal of Molecular Biology 405:201 - 213.

Liu L.-N., Chen X.-L., Zhang Y.-Z., Zhou B.-C. (2005) Characterization, structure and function of linker polypeptides in phycobilisomes of cyanobacteria and red algae: An overview. Biochimica et Biophysica Acta (BBA) - Bioenergetics 1708:133-142.

Lobo R.P.S.M., LaVeigne J.D., Reitze D.H., Tanner D.B., Carr G.L. (2002) Subnanosecond, time-resolved, broadband infrared spectroscopy

using synchrotron radiation. REVIEW OF SCIENTIFIC INSTRUMENTS VOLUME 73: NUMBER 1.

Lundell D.J., Glayer A.N. (1981) Allophycocyanin B. The Journal of Biological Chemistry 256:12600-12606.

Lundell D.J., Glazer A.N. (1983) Molecular architecture of a light-harvesting antenna. Quaternary interactions in the Synechococcus 6301 phycobilisome core as revealed by partial tryptic digestion and circular dichroism studies. Journal of Biological Chemistry 258:8708-8713.

M. A. Fox E.G. (1997) Electricfield effects on electron transfer rates in dichromophoric peptides: the effect of helix unfolding. J. Am. Chem. Soc. . 119:5277–5285.

MacColl R. (1998) Cyanobacterial Phycobilisomes. Journal of Structural Biology 124:311-334.

MacColl R. (2004) Allophycocyanin and energy transfer. Biochimica et Biophysica Acta (BBA) - Bioenergetics 1657:73 - 81.

May. (2005) Charge and Energy Transfer Dynamics in Molecular Systems Wiley-VCH.

Midwinter F.Z.a.J.E. (1973) Applied Nonlinear Optics John Wiley & Sons, Inc, New York / Sydney / Toronto / London.

Mimuro M., Lipschultz C., Gantt E. (1986) Energy flow in the phycobilisome core of Nostoc sp. (MAC): Two independent terminal pigments. Biochimica et Biophysica Acta (BBA) - Bioenergetics 852:126-132.

Miyashita H. (1996) Chlorophyll d as a major pigment. Nature 383:402.

Nelet A. (2007) Le façonnage d’impulsions ultracourtes

par amplification paramétrique optique à dérive de fréquence. , Université de Bordeaux, Bodeaux. pp. 203.

Petrasek Z., Schmitt F.-J., Theiss C., Huyer J., Chen M., Larkum A., Eichler H.J., Kemnitz K., Eckert H.-J. (2005) Excitation energy transfer from phycobiliprotein to chlorophyll d in intact cells of Acaryochloris marina studied by time- and wavelength-resolved fluorescence spectroscopy. Photochemical & Photobiological Sciences 4:1016-1022.

Post A.F., Bullerjahn G.S. (1994) The photosynthetic machinery in prochlorophytes: Structural properties and ecological significance. FEMS Microbiology Reviews 13:393-413.

Rätsep M., Freiberg A. (2007) Electron–phonon and vibronic couplings in the FMO

bacteriochlorophyll a antenna complex studied by difference

fluorescence line narrowing. Journal of Luminescence 127:251-259.

Renger G. (1999) Concepts in Photobiology: Photosynthesis and Photomorphogenesis, Dordrecht and Narosa Publishing Co.

Robin k. Lammi A.A., Richard W. Wagner, James R. Diers, David F. Bocian, Dewey Holten, Jonathan S. Lindsey. . (2001) Quenching of porphyrin excited states by adjacent or distant porphyrin cation radicals in molecular arrays. Chemical physics letters 341 35 – 44.

Rullière C. (2003) Femtosecond Laser Pulses. second ed. Springer, New York.

Sandström Å., Gillbro T., Sundström V., Fischer R., Scheer H. (1988) Picosecond time-resolved energy transfer within C-phycocyanin aggregates of Mastigocladus laminosus. Biochimica et Biophysica Acta (BBA) - Bioenergetics 933:42-53.

Sarcina M., Tobin M.J., Mullineaux C.W. (2001) Diffusion of Phycobilisomes on the Thylakoid Membranes of the Cyanobacterium Synechococcus 7942. Journal of Biological Chemistry 276:46830-46834. DOI: 10.1074/jbc.M107111200.

Sauer K., Scheer H. (1988) Excitation transfer in C-phycocyanin. Biochimica et Biophysica Acta (BBA) - Bioenergetics:157-170.

Schliep M., Crossett B., Willows R.D., Chen M. (2010) 18O Labeling of Chlorophyll d in Acaryochloris marina Reveals That Chlorophyll a and Molecular Oxygen Are Precursors. Journal of Biological Chemistry 285:28450-28456. DOI: 10.1074/jbc.M110.146753.

Scholes G.D., Jordanides X.J., Fleming G.R. (2001). J Phys Chem B 105:1640 - 1651.

Stokkum. (2004) Global and target analysis of time-resolved spectra. Biochimica et Biophysica Acta (BBA) - Bioenergetics 1657:82-104.

T. Drori J.H., Z. V. Vardeny. (2010) Optical studies of the charge transfer complex in polythiophene/fullerene blends for organic photovoltaic applications. PHYSICAL REVIEW B 82:075207

Teodor Silviu Balaban H.T., Alfred R. Holzwarth. (2005) Chlorins Programmed for Self-Assembly @Springer-Verlag Berlin, Heidelberg

Tetenkin V.L. (2003) Structural-functional organization of the main light harvesting complex and Photosystem 2 of higher plants. Biochemistry-Moscow 68:662-677.

Theiss C. (2006) Transiente Femtosekunden-Absorptionsspektroskopie des Anregungs-Energie transfers in isolierten Pigment-Proteinkomplexen des Photosynthese apparates TU Berlin, Berlin.

Theiss C., Schmitt F.-J., Pieper J., Nganou C., Grehn M., Vitali M., Olliges R., Eichler H.J., Eckert H.-J. (2011) Excitation energy transfer in intact cells and in the phycobiliprotein antennae of the chlorophyll d containing cyanobacterium Acaryochloris marina. Journal of Plant Physiology In Press, Corrected Proof.

Theiss C., Schmitt F.J., Andree S., Cardenas-Chavez C., Wache K., Fuesers J., Vitali M., Wess M., Kussin S., Eichler H.J., Eckert H.J. (2008) Excitation Energy Transfer in the Phycobiliprotein Antenna of <i>Acaryochloris marina</i> Studied by Transient fs Absorption and Fluorescence Spectroscopy, in: J. F. Allen, et al. (Eds.), Photosynthesis. Energy from the Sun, Springer Netherlands. pp. 339-342.

Tleugabulova D., Zhang Z., Chen Y., Brook M.A., Brennan* J.D. (2004) Fluorescence Anisotropy in Studies of Solute Interactions

with Covalently Modified Colloidal Silica Nanoparticles. Langmuir 20:848 - 854.

V. Barzda L.M., G. Garab. (1994) Size dependency of circular dichroism in macroaggregates of photosynthetic pigment-protein complexes. Biochemistry 33:10837-10841.

V. Barzda M.V.F.C., R. Van grondelle, H. Van Amerongen. (1998) Reversible light-induced fluorecence quenching- an inherent property of LHC II. In Photosysnthesis: Mechanisms and Effects, Kluwer Academic Publishers, The Netherlands. pp. 337-340.

V. Barzda V.G., R. Kananavicius, V. Cervinskas, H. Van Amerongen, R. Van grondelle, L. Valkunas. (2001) Singlet-Singlet Annihilation kinetics in Aggregates and trimers of LHCII. Biophysical 80:2409-2421.

W. Jentzen X.Z.S., J. A. Shelnutt (1997) Structural characterization of synthetic and protein-bound porphyrins in terms of the lowest-frequency normal coordinates of the macrocycle. J. Phys.Chem. B 101: 1684–1699.

Wehrmeyer. (1983a) Organisation and composition of cyanobacterial and rhodophycean phycobilisomes In: Parageorgiou GC and Packer L (eds) Photosynthetic Prokaryotes: Cell differentiation and Function. Elsevier Biomedical ed., New York.

WEINER A.M. (1995) FEMTOSECOND OPTICAL PULSE SHAPING AND PROCESSING Prog. Quant. Elecrr. 19: 161-237.

Weiner A.M. (2000) Femtosecond pulse shaping using spatial light modulators. Review of Scientific Instruments 71:1929-1960.

Witt H.T. (2004) Steps on the way to building blocks, topologies, crystals and X-ray structural analysis of Photosystems I and II of water-oxidizing photosynthesis. Photosynthesis Research 80:86-107.

Y.R.Shen. (1984) The principle of Nonlinear Optics, New York.

Zhang J.-m., Zhao J.-q., Jiang L.-j., Zheng X.-g., Zhao F.-l., Wang H.-z. (1997) Studies on the energy transfer among the rod-core complex from phycobilisome of Anabaena variabilis by time resolved fluorescence emission and anisotropy spectra. Biochimica et Biophysica Acta (BBA) - Bioenergetics 1320:285-296.

Zhao K.-H., Su P., Bfhm S., Song B., Zhou M., Bubenzer C., Scheer H. (2004) Reconstitution of phycobilisome core–membrane linker, LCM,

by autocatalytic chromophore binding to ApcE. Biochemical and Biophysical Acta 1706:81-87.